Kinetic Analyses of the Electron Transfer Mechanism of Cytochrome P450 Reductase and the Role of the Flavin Mononucleotide Semiquinone State

Honors Research Thesis

Presented in Partial Fulfillment of the Requirements for graduation "with Honors Research Distinction" in the undergraduate colleges of The Ohio State University

by
Michael Christopher Isfort

The Ohio State University
June 2011

Project Advisor: Professor Richard Swenson, Department of Biochemistry

Abstract

Cytochrome P450 reductase (CPR) is a mammalian enzyme that plays a crucial role in the metabolism of drugs and other xenobiotics. This diflavin reductase contains two essential flavin cofactors— flavin adenine dinucleotide (FAD) and flavin mononucleotide (FMN)— each bound to a separate protein domain. CPR transfers two electrons sequentially from NADPH to the heme-iron of the cytochrome to support its monooxygenase reaction. My research is focused on elucidating CPR's electron transport mechanism and the role of the FMN semiquinone (FMNsq, one-electron reduced species) in the process. Thus far, my efforts have focused on the Glycine-141 residue in the FMN-binding domain in CPR. This residue is thought to be a critical component in preserving a unique and stabilizing hydrogen bond with the N(5)H group of the neutral FMNsq state. Through the process of site-directed mutagenesis, Glycine-141 has been replaced by a threonine (G141T) and an alanine (G141A, which I personally generated). More recently, this residue has been deleted (G141del) from the loop it occupies in an attempt to alter the conformation of this loop and to disrupt this crucial interaction with the cofactor. Each Glycine-141 alteration is theorized to affect the stability of the FMN semiquinone, as evidenced primarily by changes in the electron transfer between the domains of CPR. The primary goal of my research project, therefore, is to characterize how the alterations in the mutant CPR varieties affect the kinetics of electron transfer.

Following the generation of each mutant, the protein was expressed in culture, purified (using affinity chromatography) and finally characterized (using SDS-PAGE analysis,

as well as high performance liquid chromatography (HPLC)). Additionally, a series of analytical assays were performed to gain insight into the effects of the Glycine-141 alteration. The first analytical experiments that were performed were steady-state turnover (SSTO) assays, which provide an overall rate of electron transfer through CPR (from the NADPH electron donor to a cytochrome c electron acceptor). Essentially these experiments assessed the activity of the proteins and confirmed, to a certain degree, that all CPR varieties were folded correctly and functioning properly. Upon analyzing the procured turnover data, it was determined that there were, at a cursory level, significant kinetic differences between the Glycine-141 altered mutant CPR variants and wild-type CPR (WT CPR). Oxidative titrations of the CPR varieties with ferricyanide were then performed to establish the level of FMN semiquinone formation among the CPR varieties. These experiments permit for the controlled removal of electron equivalents from the CPR system which allows specific observance of pre-identified redox species of CPR. Again there were significant differences in the amount of semiquinone formed in WT CPR, G141A, G141T, and G141del CPR. The focus of my research then became elucidating the specific mechanistic differences causing these changes in CPR characteristics and how the changes in stability in the FMNsq accounted for these kinetic discrepancies.

Two major methods were utilized to elucidate the mechanism of electron transfer in CPR: pre-steady state turnover (pre-SSTO) assays and using iterative exponential and global data fitting along with kinetics modeling software to acquaint our kinetic data to specific biochemical steps. Pre-steady state turnover assays are performed using a stopped-flow spectrophotometer, which allows for a reaction to be monitored within the first couple

milliseconds of mixing two solutions, and is therefore a valuable tool in characterizing CPR activity which occurs very quickly. The majority of my research effort is focused on establishing the inter-flavin electron transfer characterization of WT CPR, G141A CPR, G141T CPR and G141del CPR during reductive and oxidative half-reactions in these pre-steady-state turnover assays. Reductive half reactions consist on looking at the transfer of electrons from bound NADPH to the FAD domain of CPR and then from the FAD domain to the FMN domain of CPR. This absorbance plot of the reductive half reaction was observed to be triphasic. The first kinetic phase, which is the rate of hydride transfer from NADPH to the FAD, was not appreciably affected by alterations. However, the first observed species is the disemiquinoid form (each flavin contains one electron) indicating that inter-flavin electron transfer is more rapid. The second phase appears also to be associated with inter-flavin transfer and is dependent on $NADP^+$ and the alteration. In the deletion variant, this phase is associated with the more rapid loss of the disemiquinoid species, consistent with its instability. The third, previously unrecognized, phase was not appreciable affected by the Glycine-141 alterations and may be too slow to be catalytically relevant. The data supports our hypothesis that the unique FMN-binding loop in CPR plays a significant role in its electron-transferring activity and serves to help clarify the specific mechanistic steps in the electron transfer process in diflavin reductases. To complement this reductive half reaction data, oxidative half-reactions, which consist of watching electrons move from the FAD domain to the FMN domain of CPR and finally to a final cytochrome c electron acceptor, were be performed. Effectively, analysis of this oxidative half-reaction experiment allow us

to dissect the overall electron transfer from CPR to cytochrome c into individual steps, much like we did with the reductive half reaction.

The absorbance change plots from these pre-steady state turnover experiments are often difficult to understand. The most reasonable way to acquaint our kinetic data to specific biochemical events will be to model reaction mechanisms using kinetic simulation software, which allows for the fitting of experimentally acquired data to pre-constructed species-based models. This technique will allow us to make models of the reductive and oxidative half-reactions and relate observed absorbance changes to specific rates of electron transfer between redox species of CPR. After a prototypical model of electron transfer has been made for wild-type CPR, then application of the model to the data of the G141A, G141T and G141del CPR oxidative and reductive half-reactions will allow us to identify more precisely how the alteration in the FMN-binding domain is affecting the electron transfer in CPR. The effectiveness of this modeling software has been proven in our preliminary analysis of the reductive half-reaction data of all CPR varieties, which has generated a better understanding of the experimental data. Our original kinetic model (acquired from literature and experimental inference) for the reduction and interflavin electron transfer of CPR with stoichiometric amounts of NADPH consisted of five species and could account for only the initial reactionary phase in the triphasic reactionary curve seen in the pre-SSTO reductive half-reactions. From this initial construct, I worked methodically building in new species to create a model that would not only allow the KinTek software to fit the kinetics data for WT, G141A, G141T and G141del CPR, but also be able to account for varying reactionary conditions (in particular changing levels of $NADP^+$ in

solution, a variable which had been shown to affect the rate of reduction and shape for kinetics traces, presumably due to competitive binding with NADPH to CPR). After some time, we had developed a full model for the 2-election reduction of CPR with NADPH which consisted of nine species. To help fill out this mechanism, additional stopped-flow spectrophotometric pre-SSTO reductive assays were performed on WT CPR and G141del CPR with varying levels of $NADP^+$ and the model was modified to fit these data sets. Currently, our model for the electron transfer in CPR can accurately fit data sets from every CPR variety and could be called roughly complete. From the model, we have already acquired some new insights. Primarily, our model supports the idea that the first observed phase in the reductive half-reaction of CPR is the rate hydride transfer from NADPH. Secondly, the observed rate of the secondary phase of the reactionary trace seems not to be associated with a single electron transfer step, but rather is just the apparent rate of a number of steps and the product of several microscopic rate constants. This secondary phase seems to be the related release of $NADP^+$ from CPR species at varying degrees of flavin reduction (disemiquinoid and FMN fully reduced in particular). In essence, the release of $NADP^+$ creates multiple species which have the same absorption character, allowing for the appearance of a bi- or triphasic curve in the reductive process. Additionally, the rate release of $NADP^+$ appears to be somewhat correlated to the Glycine-141 alteration, an unexpected finding that I am currently investigating. Finally, the competitive binding of $NADP^+$ and NADPH seems to be a significant occurrence as demonstrated by the changes in reactionary trace at high $NADP^+$ concentrations.

Seeing the efficacy of the kinetic model and understanding the complex experimental data my current and future research efforts will be to continue working on the reductive half-reaction, as well as, to develop a similar model for the oxidative half-reaction. This process will undoubtedly involve a number of additional clarifying and exploratory experiment to confirm the validity of the theoretical mechanism under differing or untested reaction conditions. However, the final product of this data analysis is a thorough model of electron transfer in cytochrome P450 reductase and upon comparison of electron transfer rates between the CPR mutants; we will have a substantial understanding of the role of the Glycine-141 residue and the FMN semiquinone state in the electron transfer process.

The significance of this research project revolve around cytochrome P450 reductase's role in the oxidative metabolism drugs, xenobiotics, and endogenous compounds in the endoplasmic reticulum of cells. The metabolism of all of these molecules is actually performed by the monooxygenase activity of cytochromes P450, but for these proteins to be enzymatically active, they require the addition of two consecutive electrons. This reduction process is performed primarily by CPR and therefore the electron transfer mechanism that we are studying has implications in better understanding of pharmaceutical design and breakdown, cellular catabolism of toxins and vitamins, and physiological oxidative metabolism as a whole. Additionally, this project could have benefits to the specific biochemical field of flavoprotein research. Cytochrome P450 reductase is a prototypical diflavin reductase enzyme, so mechanistic understanding of this protein could help in the understanding of other diflavin reductases including nitric oxide synthase (NOS), a cancer cell protein (NR1), subunits of bacterial sulfite reductases (SiR), and the

flavoprotein domain of flavocytochrome P450BM-3 (which is a bacterial enzyme also studied in the Swenson lab). Although all of these enzymes are different in structure, their operating mechanism cannot be too varied because they electron transfer proceeds through the flavin cofactors. That said, understanding the kinetics of one of these diflavin reductases could augment understanding of this entire class of proteins.

Acknowledgements

My sincere thanks go to members of the Swenson Lab Group including, Matt Wohlever, Huai-Chun Chen, Amanda McKenna, Yicheng Long, and Jammi McClead. These individuals donated time, encouragement, and materials to make this project possible. Additionally, I would like to thank The Ohio State University Biochemistry Department and the College of Biological Sciences for their support and funding, which allowed me to fully pursue my research. Finally, I would like to acknowledge and express my deepest gratitude to Dr. Richard Swenson, my project advisor and friend for the past three years. With his constant guidance, teaching, and encouragement, I have been able to have a full research experience and complete this thesis.

Dedication

This work is dedicated to my friends and family, particularly my mother and father, who put me in position through their encouragement and support to complete this work. Also, my efforts are dedicated to the memory of William Burke Coleman, my Grandfather.

Table of Contents

Introduction

The physiological role of cytochrome P450 reductase: Cytochrome P450 reductase (CPR) serves as an electron donor to the microsomal cytochrome P450 dependent monooxygenase system [2]. The cytochrome P450 system is composed CPR and cytochrome P450 (CYP), both of which are integrated into the endoplasmic reticulum of liver cells primarily. The role of CPR in this system is to transfer two electrons from a bound NADPH molecule to a cytochrome P450 as the final electron acceptor. The transfer occurs in a sequential one-by-one fashion (see Figure 1). Overall, the cytochrome P450 system functions primarily to oxidize xenobiotic chemicals and, to a lesser degree, synthesize endogenous compounds [3,5].

Cytochrome P450s are common throughout nature, but their function varies depending on the enzymatic system they are a part of. CYP genes are present in many diverse eukaryotes and in different quantities. The prevalence of CYP genes is most extensive in higher order plant species like the thale cress (*Arabidopsis thaliana)* and the rice plant (*Oryza sativa)* which have 249 and 323 CYP genes, respectively. In addition, these higher order plants can have 2 or 3 isotypes of cytochrome P450 reductase which have differing reduction-oxidation (redox) properties and sub-cellular distribution. This accounts for the greater functionality of plant CYP systems in the areas of coloration, detoxification, and biosynthesis [5,7]. In contrast, animals have less extensive arrays of CYP genes. For example, whereas mice (*Mus musculus)* have 102 putatively functioning full length CYP genes, fruit flies (*Drosophila melanogaster)* have 84, humans have 57, and Baker's yeast (*Saccharomyces cerevisiae)* has a mere 3 CYP genes. There is only one isotype of cytochrome P450 reductase gene in animals which supports catalysis of many cytochrome P450s and, in microsomes, it has been shown that the molar ratio of CPR to

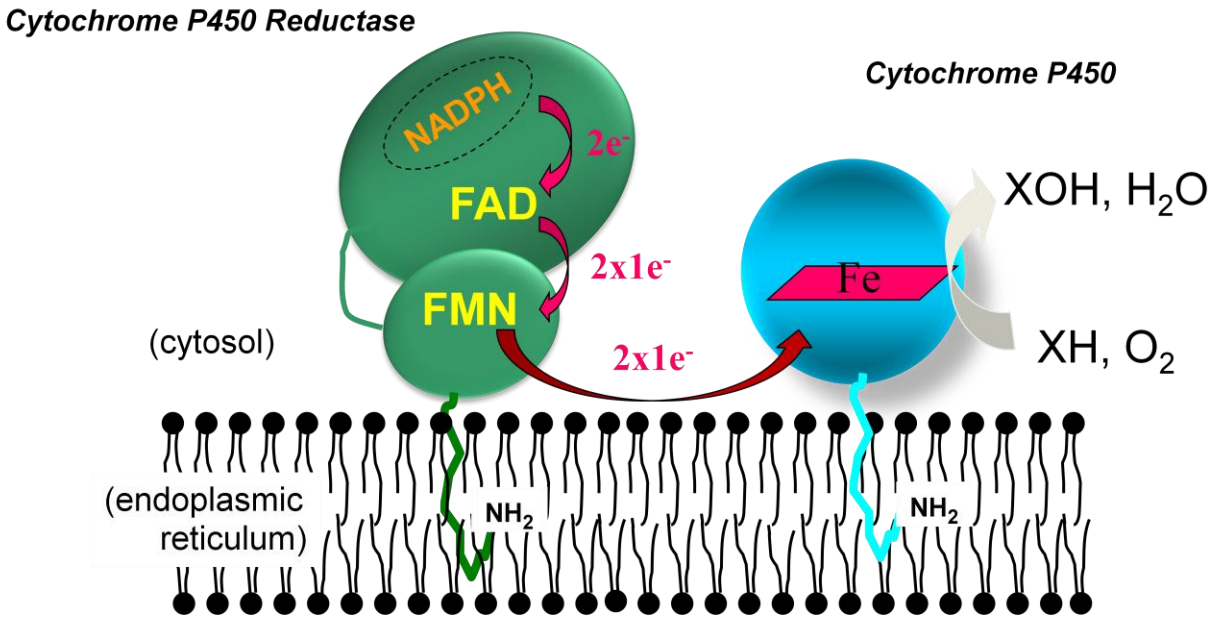

Figure 1 – This cartoon shows the general electron transfer mechanism from cytochrome P450 reductase (including transfer within CPR) to cytochrome P450.

CYP is about 5-10 to 1 [5,6,7]. CPR acts as the primary reductant of the cytochrome P450 system and, therefore, understanding of CPR activity has vast implications across a large variety of eukaryotic species.

Degradation of xenobiotics is the primary action of the cytochrome P450 system and to a lesser degree the synthesis of certain endogenous chemicals. In terms of synthesis, CYP has been implicated in the production of steroids, eicosanoids, bile acids, prostaglandins, and vitamins D3 [3,5]. The majority of the biochemical processes are performed by cytochrome P450 systems in the inner membrane of the endoplasmic reticulum of liver cells; however, there are a small number of CYP enzymes located in the mitochondria. It is also theorized that limited numbers of CYPs are transported to the plasma membrane where they are exposed extracellularly and can participate in immune response development caused by anti-microsomal autoantibodies [5,8]. Despite the cellular localization, the primary role of the cytochrome P450 system is to catalyze the oxidation of xenobiotic chemicals. Xenobiotics are, very generally, substances found in an organism which are not normally found there and either have some medicinal value or no functional value. Xenobiotics that are water-soluble can typically be excreted in feces or urine without chemical modification. Most xenobiotics, however, are hydrophobic (lipid-soluble) and therefore harder to excrete and these substances are toxic at high enough concentrations [3,5]. Therefore, complex systems to make xenobiotics water soluble have been evolved and the cytochrome P450 system is a prototypical example. CYP enzymes are involved in the metabolism of such substances as carcinogens, pesticides, fat-soluble vitamins, steroids, eicosanoids, alkaloids, and drugs; just to name a very few [5]. Drug metabolism by cytochrome P450 enzymes has been a topic of intense interest by

pharmaceutical companies for three reasons. First, P450 catalysis lowers the bioavailability of the drug in the plasma and at the target site (problems in bioavailability is one of the most prevalent reasons for failure in drug discovery). Secondly, cytochrome P450 monooxygenases can convert pro-drugs to their active form through oxidation activity. Such effects are being taken advantage of in the design of bioreductive drugs, which play off a predictable degradation patterns to activate drugs. Also, gene therapies can be used to insert cytochrome P450 genes into tumor cells to make them targets for anti-cancer pharmaceuticals. Finally, the P450 catalysis could degrade drugs to inactive forms or, conversely, degrade other xenobiotics which covalently bind to macromolecules or interact with an unintended molecular target to cause toxicity [3,4,5]. These actions of cytochrome P450 systems are crucial for understanding better pharmaceutical design and xenobiotic degradation in general.

The reaction performed by the cytochrome P450 (a heme-based monooxygenase reaction) can be generally classified as a mixed-function oxidation, which causes the insertion of one oxygen atom from molecular oxygen into the substrate with the byproduct of water derived from the other oxygen atom (equation 1) [3,5]:

(1) $NADPH + H^+ + O_2 + R \rightarrow NADP^+ + H_2O + RO$

The widely accepted catalytic cycle for cytochrome P450 can be seen in Figure 2. In particular for this thesis, it is of importance to look at the role of cytochrome P450 reductase. In step 1, the substrate binds to CYP, with the iron in the ferric state, then in step 2 CPR transfers a single electron (from NADPH to FAD to FMN) directly to the heme of CYP to take the iron to the ferrous state. Then ferrous CYP binds O_2 in step 3 and in step 4 CPR donates a second electron

into the system, but in some cases this electron may be transferred through a cytochrome b_5 intermediate. This is not that outlandish because CPR has been shown to reduce a multitude of other enzymes including squalene monooxygenase, heme oxygenase, and cytochrome b_5 in separate reactions [5,6,7]. Either way, it is important to note that the electrons are transferred from CPR to CYP in a sequential one-by-one fashion (this will be described later in more detail). Continuing, in step 5 a proton is added to CYP which leads to the formation of H_2O and ferric CYP in step 6 following the cleavage of the O-O bond. In step 7, a hydrogen atom or an electron is added into the system from the substrate and then this intermediate generates the product of step 8 which is released in step 9 [5]. The reaction of cytochrome P450 is technically only the first of three steps in the metabolism of xenobiotics, that is, the activation of the compound. Following activation of the compound, reactive groups are inactivated, and finally the product is conjugated with highly hydrophilic compounds to make the complex water soluble and able to be secreted [3].

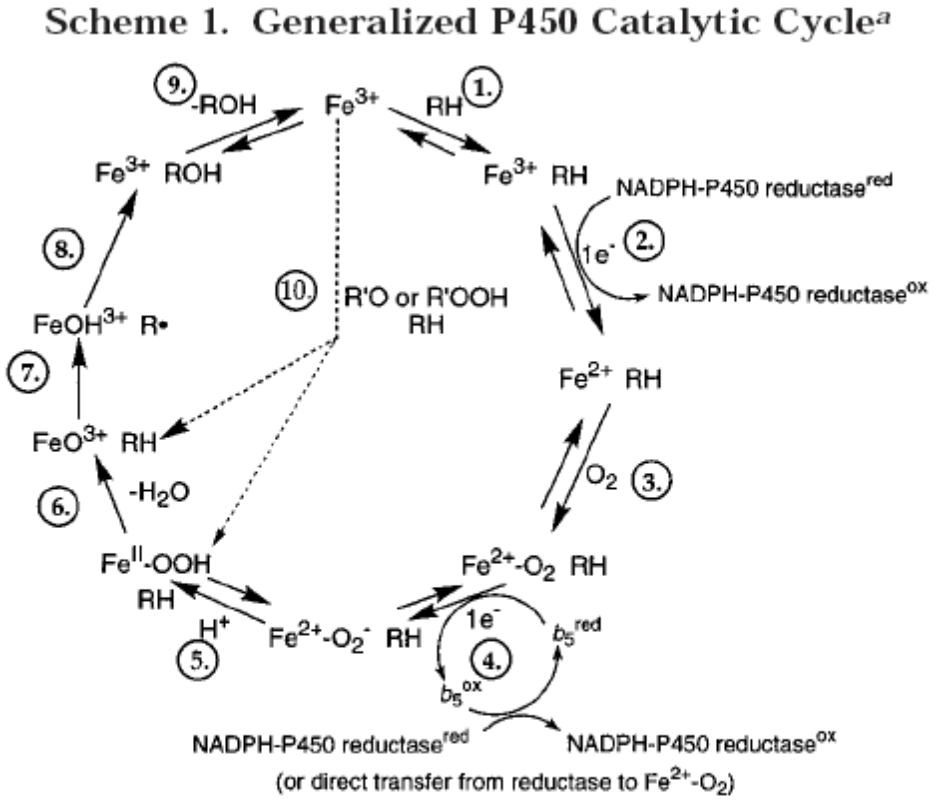

[a] Fe = iron atom in P450 heme, RH = substrate, ROH = product, ox and red indicate the reduced and (1-electron) oxidized states of the reductase involved in the electron transfers (see text).

Figure 2- Cytochrome P450 Catalytic Cycle.

Recreated from F.P. Guengerich (Reference 5).

The structure of cytochrome P450 reductase: The monooxygenase reaction of cytochrome P450 depends on the transfer of electrons, either directly or indirectly, from cytochrome P450 reductase, therefore understanding of the important structural features of CPR that are responsible for this efficient electron transfer is of importance. CPR is a prototypical diflavin reductase and contains two essential flavin cofactors—flavin adenine dinucleotide (FAD) and flavin mononucleotide (FMN)—each bound to a separate domain. Overall this 78 kilodalton (kDa) protein is comprised of four distinct structural domains which form two primary "functional" domains [1,10]. From the N-terminus to C-terminus: the single CPR polypeptide forms a 56-residue (6 kDa) hydrophobic anchor which secures the protein to the endoplasmic reticulum, followed by a FMN-binding domain, a short flexible linker region, and finally a FAD- and NADPH-binding domain (in this paper, the latter two structural domains will be referred to functionally as the FAD-binding domain) [9,10]. It is important to note that for the bulk of the discussion in this thesis "CPR" will refer to "solubilized CPR", representing the recombinant form of the protein without the hydrophobic membrane anchor. This 72 kDa form of CPR has very similar function to the natural form, but the truncated enzyme cannot transfer electrons to membrane-associated cytochrome P450s, although cytochrome c is able to serve as a final electron acceptor and is widely used and accepted as an expedient surrogate for experimental studies [6,10]. Cytochrome c (cyt c) is similar in structure and biochemical function to cytochrome P450 with the exception that it is a one-electron acceptor, whereas, the oxygen complex of cytochrome P450 is a two-electron acceptor. The FMN- and FAD-binding domains are the functional domains of the protein that allow for the transfer of electrons from the

bound NADPH to the final electron acceptor. Electron transfer occurs from the NADPH to the FAD cofactor and then the FMN which serves as the electron donor to the cytochrome.

The FMN-binding domain forms a canonical flavodoxin-like motif consisting of a five–stranded parallel β-sheet sandwiched between α-helices [1,10,25]. The FMN cofactor is bound in a mainly hydrophobic pocket at the C-terminal of the domain. This binding site is comprised of the polypeptide fragments ^{139}TYGEGPD and ^{175}NKTYEHFN with the isoalloxazine ring of the FMN forming a π- π stacking interactions with the aromatic resides Tyr140 and Tyr178 on the *re*-side and *si*-side, respectively [6,10]. Additionally, the FMN-binding domain contains a "bowl" provided by β4-α6 and β5-α7 peptide loops, which allow for maximal contact between the positively charged cytochrome c surface and the negatively charged FMN surface, presumably holding the cytochrome c (or cytochrome P450) in proper place for electron transfer [16]. After the FMN-binding domain, there is a connection mainly composed of α-helices, which couples the FMN- and FAD-binding domains and is also responsible, along with a 117 residue α-helical insertion in the FAD-binding domain, for bringing the two isoalloxazine rings of the flavin cofactors into a "continuous ribbon" conformation that is about 3.5 Å apart with an angle of about 150° to each other. This proximity allows for effective and direct electron transfer (see Figure 3) [6,10,11]. Another critical action of this connection domain is the formation of a "hinge" between this connection domain and the FMN-binding domain of CPR which, judging from the lack of resolution in crystallographic studies, allows the FMN-binding domain, and the FMN cofactor, a substantial amount of conformational motility assumed to aid in electron transfer [10]. Following this connector sequence is the FAD- and NADPH-binding domains. The FAD-binding domain is a flattened anti-parallel β-barrel and, furthest C-terminal, the NADPH-

binding domain is another parallel five-stranded β-sheet sandwiched between α-helices (see Figure 4 for full CPR structure) [6,10]. The FAD cofactor is bound, in extended confirmation, by polypeptide fragments ^{455}YYSIAS and ^{471}ICAVAV with the isoalloxazine inserted in the boundary of the FAD- and NADPH-binding domains and the remainder of the FAD molecule bound between the FAD-binding domain and the connecting domain. Like in the FMN cofactor, the isoalloxazine ring forms π- π stacking interactions, on the *re*-side with the indole ring of the Trp677 residue and on the *si*-side with the Tyr456 residue [10,25]. The nicotinamide portion of $NADP^+$ molecule, bound to the NADPH-binding domain does not show high resolution in crystallographic studies, demonstrating that there are possible multiple conformations based on 120° rotations around the pyrophosphate bond in bound $NADP^+$. The finding of conformational changes has lead to the hypothesis that the binding of NADPH and rotation around the pyrophosphate (P_n-O-P_a) bond would allow the reduced nicotinamide to displace the Trp677 residue on the re-side of the FAD cofactor allowing direct hydride transfer from NADPH to N5 position of the FAD [6].

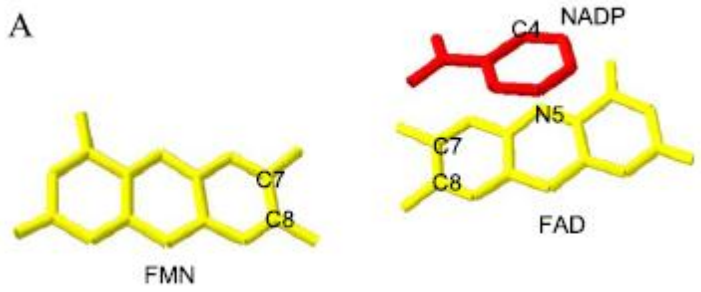

Figure 3- Orientation of CPR cofactors FMN (flavin mononucleotide) and FAD (flavin adenine dinucleotide) and the CPR coenzyme NADP (nicotinamide adenine dinucleotide phosphate).

Recreated from M.B. Murataliev *et al.* (reference 6).

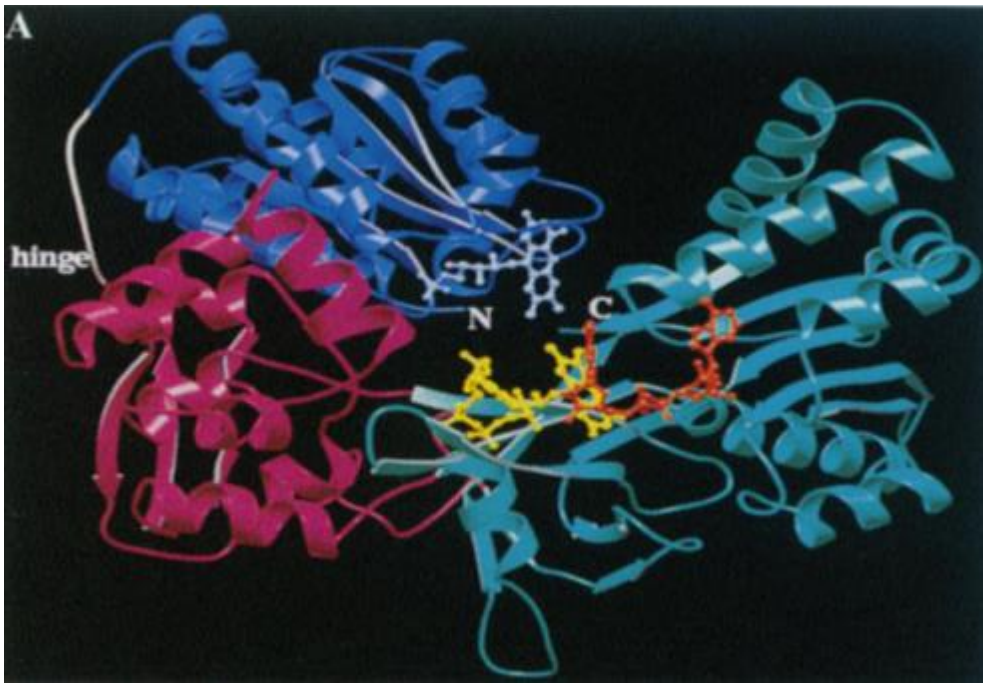

Figure 4- Ribbon diagram showing the structure of CPR. The FMN-binding domain is in blue, the connecting-domain is shown in maroon, and the FAD- and NADPH-binding domains are shown in green. The disordered hinge region is in pink and labeled “hinge”. Enzyme cofactors are in ball-and-stick form and FMN is blue, FAD is yellow and $NADP^+$ is in orange.

Recreated from M. Wang *et al.* (reference 10)

Cytochrome P450 reductase is a typical diflavin reductase, as can be seen in the structure, because the fused two functional domains of electron transfer are integrated with the flavin cofactors FAD and FMN. Besides CPR, there is an entire family of diflavin reductases including: bacterial sulfite reductase (SR), methionine synthase reductase (MSR), nitric oxide synthase (NOS), and human novel reductase 1 (NR1) [6,22,25]. Related to this family are further evolved complex multi-domain enzymes which have incorporated the heme-containing oxygenase component with the diflavin reductase. These include the bacterial flavocytochrome P450BM-3 (BM-3) and the P450 fatty acid hydroxylases [11,12,22]. The relatedness of these proteins provides a motivation for studying CPR because although all of these enzymes are different in structure, their electron transfer mechanisms are likely to share similarities as they all involve two flavin cofactors. That said, understanding the kinetics of one of these diflavin reductases could augment understanding of this entire class of proteins.

The evolution of cytochrome P450 reductase has been a topic of interest, most probably, due to the fact that understanding the formative components of this fusion enzyme could help elucidate the mechanism of the whole enzyme. Through sequence and structural studies it has been suggested that CPR and other diflavin reductases are the result of a fusion between the ancestral genes of a ferrodoxin-$NADP^+$ reductase (FNR) and a flavodoxin. The FMN-binding domain is homologous to the *Desulfovibrio vulgaris* flavodoxin, which is a well-characterized FMN-dependent low potential electron transferase involved in the catalysis of electron transfer in many systems [1,6]. This flavodoxin displays considerable structural homology to the FMN-binding domains of several diflavin reductase and CPR in particular. FNR is an example of a transhydrogenase-type flavoprotein, which catalyze electron transfer

between a nicotinamide cofactor and a one-electron acceptor or donor protein [2,21]. Comparison of the FAD-binding domain of CPR to FNR shows a great deal similarity (especially if a 117-residue insert is added in the middle of the FAD-binding domain). Also, structural and sequence comparison of the FAD-binding domain to other transhydrogenase-type flavoproteins such as cytochrome b_5 reductase (b_5R) and glutathione reductase (GR) show that FNR, b_5R, GR, and CPR's FAD domain are homologous [1,2]. The similarity of these proteins suggest that flavodoxin and FNR genes may have been arranged in the same operon, or in close genomic position, and an alteration event eventually linked the two protein into an ancestral form of CPR (see Figure 5). A similar fusion event could even be seen happening between CPR and cytochrome P450 genes to create cytochromes P450BM-3 and P450 fatty acid hydroxylases.

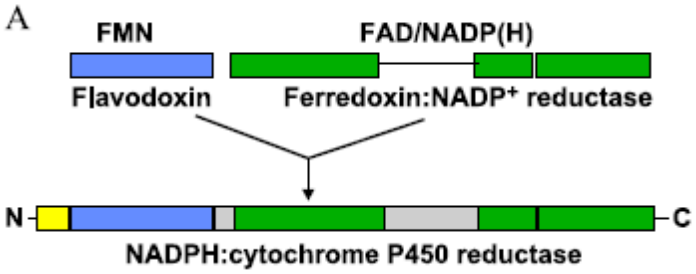

Figure 5- A cartoon of the gene fusion of *D.sulfibrio* flavodoxin and ferrodoxin-$NADP^+$ reductase into a single polypeptide of cytochrome P450 reductase

Recreated from M.B. Murataliev *et al.* (Reference 6)

Mechanism of electron transfer in CPR: The basic mechanism for electron transfer in cytochrome P450 reductase is pretty well understood; a molecule of NADPH binds to the FAD-binding domain of CPR, followed by an obligatory two electron hydride transfer to the FAD. The two electrons are then thought to be transferred in two sequential one-electron steps to the cytochrome P450 via the FMN domain (see Figure 1). The reaction catalyzed by CPR is shown by equation 2 [6,14]:

(2) $NADPH + 2A_o \rightarrow NADP^+ + 2A_r + H^+$

where A_o and A_r represent the electron acceptor in the oxidized and reduced forms, respectively. And, as was previously mentioned, the physiological final electron acceptor is most often cytochrome P450 or cytochrome *b5*, where electron transfer supports monooxygenase reactions. Other "artificial" electron acceptors are commonly used and accepted for *in vitro* studies such as cytochrome c and potassium ferricyanide.

Looking more specifically at the mechanism of CPR, the reductase has two substrates, NADPH and the terminal electron acceptor, and two products, $NADP^+$ and the reduced electron acceptor. Both Ping-Pong and sequential Bi-Bi mechanisms have been used to classify two-substrate enzymes [6]. In the Ping-Pong mechanism, the first product is released from the modified enzyme before a second substrate binds (see Figure 6a). Typically, enzymes that proceed by Ping-Pong mechanisms have two substrates binding at the same site or overlapping sites. However, inspection of the structure of CPR casts doubt on this mechanism because NADPH binds to the FAD-binding domain and oxidized cytochrome c or cytochrome P450 very likely binds to the FMN-binding domain given that this domain is essential for electron transfer

to the cytochrome. Therefore, a more appealing mechanism is a sequential Bi-Bi mechanism, in which the enzyme typically has separate and independent binding sites where both substrates can bind to the enzyme to form a ternary complex. At this point, there have been considerable observations made and subsequently confirmed by kinetics analysis to determine that CPR proceeds by a sequential random Bi-Bi mechanism (see Figure 6b).

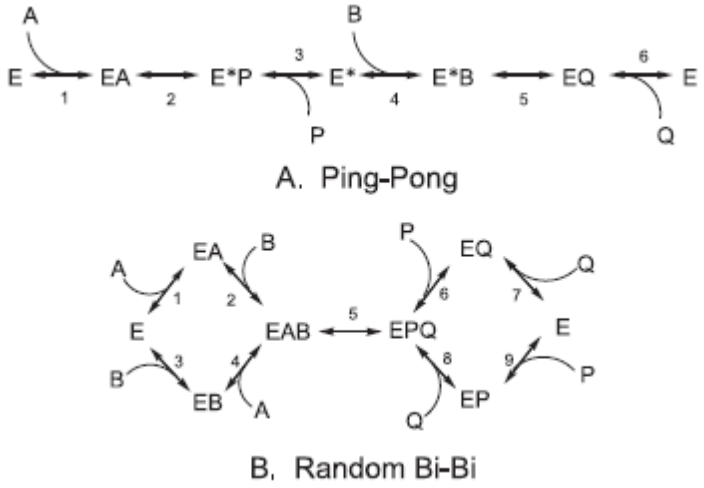

Figure 6- This is a cartoon of the Ping-Pong mechanism and the Sequential Random Bi-Bi mechanism. A and B species represent substrates and P and Q represent products.

Recreated from M.B. Murataliev *et al.* (Reference 6)

The mechanism of electron transfer in CPR has many unique characteristics which make its study quite interesting. The architecture of CPR allows for very close interaction of the flavin cofactors and the NADPH coenzyme. This intimacy permits direct electron transfer from NADPH to the FAD cofactor and then from the FAD cofactor to the FMN cofactor, without the participation of any protein residues [16,25]. The bound NADPH, specifically the nicotinamide ring portion, can change from a planar to "boat" configuration which effectively moves the hydrogen of the C4 atom close enough to the N5 of the FAD cofactor, about 3.5 Å in distance, so that the rapid direct hydride transfer can occur [6,15]. Similarly, the very close and "continuous ribbon" orientation of the isoalloxazine rings if FAD and FMN allow for direct transfer of electrons between the two flavins. It has been shown that substantial movements of the FMN- and FAD-binding domains contribute to bringing the cofactors and substrate in close enough orientation for direct transfer. The relative positions of the FAD- and FMN-binding domains have been determined to have a large effect on the biological redox properties. Several models of domain movement have been suggested. The primary player in domain movement is the α-helical "hinge" domain between the FAD-binding domain and the FMN-binding domain, which allows for the FMN-binding domain to "swing" into and out of position to allow electron transfer from the reduced FAD, through the FMN, to the heme of cytochrome [10,13,15]. The binding of the NADPH, particularly the adenine portion of the coenzyme, has been shown to move the flavins from a distance of 20Å to a mere 4Å, increasing favorability upon NADPH binding of intermolecular and intramolecular electron transfer in CPR [15]. The NADPH binding represents another domain movement in an overall system which is likely many conformational changes in coordination.

Another important aspect in the mechanism of electron transfer within CPR is the formation of the semiquinone (SQ) of the flavin cofactors, particularly the FMN. Flavin cofactors have three redox states: oxidized, semiquinone (one-electron reduced), and hydroquinone (two-electron reduced). A unique feature (and application in some biological processes) of the flavin cofactor is its ability to participate in both two- and one-electron transfer processes, occasionally sequentially as with CPR and other diflavin reductases. The flavin semiquinone state can be in the cationic, neutral, or anionic forms, however, in flavoproteins only the neutral and anionic forms are found. The neutral and anionic forms of the flavin semiquinones are readily distinguished by their electronic absorption properties and are often classified as "blue" or "red" for the neutral or anionic semiquinone, respectively (see Figure 7) [17]. The major difference between the two is the protonation state of the N5 of the isoalloxazine ring (H^+ present in neutral form). More specifically, both the CPR flavin cofactors readily and exclusively form an "air-stable" blue, neutral radical. This is of interest due to the fact that the neutral FMNsq is not usually stabilized and if so only transiently, in most other enzymes except for flavodoxins and diflavin reductases [18]. The neutral FMNsq has been shown to be the state that transfers the electron to the terminal electron acceptor and this fact demonstrates that the reductive cycle of CPR most like proceeds through a 0-2-1-0 mechanism, where the numbers represent the number of electrons collectively on both the flavins. The widely accepted and holistic turnover mechanism for electron transfer in CPR, and many other diflavin reductases, can be seen in Figure 8 and is described as follows: (1) NADPH binds to CPR, (2) then NADPH transfers a hydride to the FAD cofactor taking FADox to FADhq (this step is theorized to be the rate limiting step), (3) then FADhq transfers a single electron to FMNox

taking CPR to the disemiquinoid state with both cofactors in neutral SQ state, (4) FMNsq transfers its electron to the terminal electron acceptor taking FMN to the oxidized form (binding of the oxidized terminal electron acceptor can occur at any time in steps 1, 2, or 3 and most likely binds to CPR after NADPH has bound and transferred electrons), (5) the reduced electron acceptor is released from the enzyme and another oxidized electron acceptor binds to the enzyme, meanwhile, FADsq transfers its electron to FMNox to take it to FMNsq, (6) following this the FMNsq transfers its electron to the oxidized electron receptor to reduce it, and finally (7) the second reduced electron receptor is released along with $NADP^+$ [6,18,19].

This mechanism demonstrates the central role and importance of the FMN semiquinone state in the intermolecular and intramolecular electron transfer process. Because of this, the molecular basis for the formation, stabilization, and utilization of this redox state forms the fundamental basis and significance of the study described herein and those previously and currently addressed in the Swenson laboratory among others.

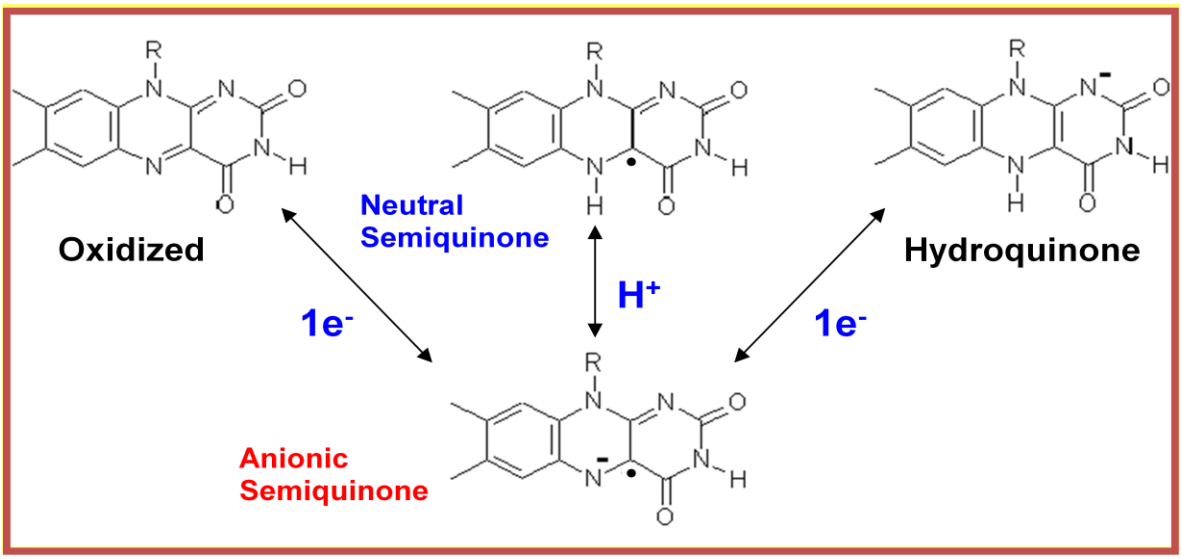

Figure 7- This diagram shows the multiple reduction-oxidation states of the flavin cofactor

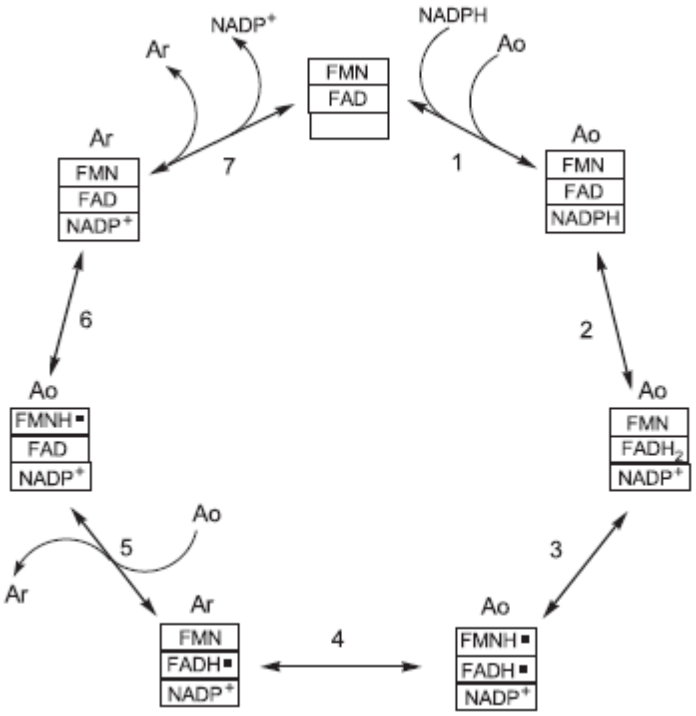

Figure 8- This figure is a cartoon of the overall electron transfer in CPR (and diflavin reductases in general). A_o represents an oxidized electron acceptor and A_r represents a reduced terminal electron acceptor.

Recreated from M.B. Murataliev *et al.* (Reference 6)

Background of Thesis Project: The premise for this thesis project is centered on a few unique characteristics of flavodoxin proteins, as they are related to many of the diflavin reductases. The first is that flavodoxin proteins, and the homologous FMN-binding domain in CPR and other diflavin reductases, are able to stabilize the neutral form of the FMN semiquinone, a radical species which is typically only transiently or not at all formed in other enzymes [17,18]. The second characteristic of interest is that in many different flavodoxins, the FMN-binding loop has been shown to facilitate hydrogen bonding between the backbone carbonyl oxygen of a glycine and the N(5)H of the FMN isoalloxazine ring, an interaction that has now been established to stabilize this redox state. Additionally, this glycine is conserved in the FMN binding loop of many diflavin reductases (see Figure 9), but absent in flavocytochrome P450BM-3; this is unique because the FMN semiquinone is not thermodynamically stabilized, but only transiently forms the red anionic form. In flavodoxins from *Clostridium beijerinckii* and *Desulfovibrio vulgaris,* it has been shown that there is a conformational change associated with the reduction of the FMN characterized by the "flipping" of the carbonyl group of the conserved glycine residue (within the FMN-binding loop) into a position favorable for the glycine-N(5)H hydrogen bond formation [20,21].

To study the importance of this conserved glycine and the conformational change in the stabilization of the neutral FMN semiquinone and its role in the overall electron transfer process, site-directed mutagenesis was used to replace the conserved Glycine-141 in CPR with alanine and threonine. This approach was used based on the results of previous studies of the *C. beijerinckii* and *D. vulgaris* flavodoxins [20,21]. The conformational energetics of the Gly57-Asp58 peptide bend in the *C. beijerinckii* flavodoxin has been shown to correlate with the

stability of the reduced states of the FMN cofactor. With oxidized FMN, the Gly57-Asp58 peptides accept an "O-down" confirmation (with *cis* isomerization) in which the carbonyl oxygen of Gly57 (O57) points away from the flavin. Thus, there is no apparent hydrogen bonding with the N5 of the FMN in this redox state. As discussed below, this differs from the situation in the flavocytochrome P450BM-3 system. However, in the semiquinone and hydroquinone states, the Gly57-Asp58 peptide bond adopts a *trans "*O-up" formation with O57 pointing towards FMN, forming a strong hydrogen bond with the N(5)H [20]. Evidence for the importance of this conformational change and resulting hydrogen bonding interaction was indirectly demonstrated by the replacement of Glycine-57 with four different amino acids with differing sidechain properties: alanine (G57A), aspartic acid (G57D), asparagine (G57N) and threonine (G57T) [20].The basic premise for those studies was that the unique structural propensities of the glycine residue lacking, of course, any sidechain is essential for the conformational change and associated interactions. The presence of any sidechain, even one as small as the methyl group of alanine, was expected to interfere with these changes. Of particular interest to this thesis are the G57A and G57T site-directed variants, which served as a guide for the corresponding substitutions introduced in CPR. Alanine was introduced as the simplest sidechain substitution whereas threonine was utilized to introduce the much more conformationally restricting β-branched sidechain. G57A showed almost stoichiometric formation of FMNsq (nearly equal to wild-type flavodoxin) with two observable separate electron transfer steps. Also similar to wild-type, x-ray crystallography indicated that the O57 of the G57A mutant flavodoxin was in *cis* O-down position with FMNox and *trans* O-up position for the FMNsq and FMNhq states. Contrastingly, G57T showed all three oxidation states of FMN

throughout the reduction with only about 52% of stoichiometric FMNsq production. The backbone conformation of G57T with FMNox was *trans* O-down and although with FMNsq and FMNhq state the O57 is in the *trans* O-up position, there were "subtle" changes in geometry of the protein/cofactor orientation. In addition, there is evidence to indicate that the energy gap between *trans* O-down and *trans* O-up in G57T is close to locking the molecule in the O-down position [20]. The value of this study was to highlight, for our own project, two amino acids which could be substituted for the Glycine-141 in the FMN-binding loop of CPR: alanine with potentially minimal effect to kinetics, redox, and conformational changes; and threonine with potentially major effect to kinetic, redox, and conformational changes. Our studies, then, would serve two purposes. First, the introduction of similar amino acid substitutions might confirm the generality of the role of a similar conserved glycine residue in CPR, shedding further light on a shared function of hydrogen bond formation and associated conformational changes to orient the glycine correctly to stabilize and promote the stabilization of the neutral FMNsq. Second, unlike for the flavodoxin where electron transfer involves separate and often not well known redox partners, similar modifications in CPR will much more effectively allow for the detailed study of the influence and role of the formation of the FMNsq on optimal electron transport.

The conserved glycine residue seen in flavodoxins and most diflavin reductases is missing from the FMN-binding loop of flavocytochrome P450BM-3 from *Bacillus megaterium* (see Figure 9). The result of this absence is a shorter and less flexible flavin-binding loop. The loss of this residue in BM-3 may be the reason for the formation of a hydrogen bond with the backbone amide NH group of Asn537 and the N5 of the flavin [22,24]. This change in binding

may be responsible for the unique redox and electron transfer properties of BM-3 compared to other diflavin reductases, exemplified by the inability of BM-3 to stabilize neutral FMNsq. Instead, the anionic form of FMNsq forms, but only transiently during reduction. To address the role of the absence of the equivalent glycine in this protein, studies were performed to reinsert the glycine residue into equivalent position in the FMN-binding loop (after Tyr536) in both the FMN domain and the diflavin reductase portion of BM-3 to determine the overall effect of glycine-N(5)H bonding on semiquinone stability and reductase activity. It was found that the insertion variant was able to accumulate the neutral form of FMNsq like flavodoxin and CPR, although not to the same extent, and based on NMR studies that the Asn537-N5 interaction was disrupted in the oxidized state. The results seem consistent with the newly inserted glycine carbonyl forming the hydrogen bond with N(5)H in the reduced state [22]. As a converse to that study and as part of the work presented here, the Glycine-141 residue of CPR, was deleted in an attempt to make a FMN-binding loop more like that of flavocytochrome P450BM-3. Theoretically, this should have significant changes in the amount of neutral FMNsq being formed and the mechanism of electron transfer in the Glycine-141 deletion CPR.

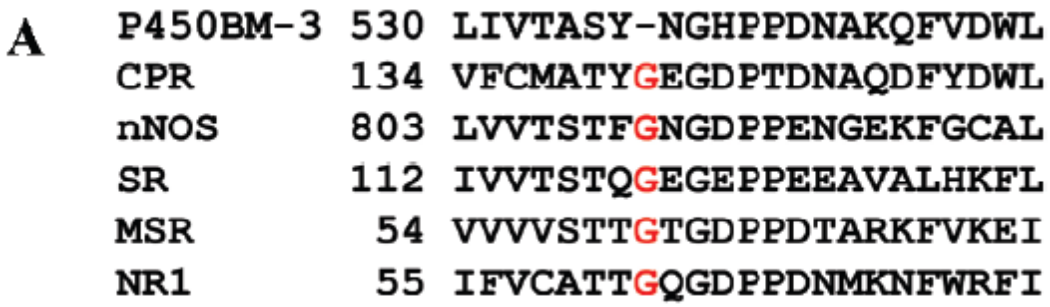

Figure 9- The amino acid sequence alignment for the binding region flanking the *re*-face of the FMN cofactor for six members of the diflavin reductase family, note the conserved glycine residue in red. Flavocytochrome P450BM-3 (P450BM-3), human cytochrome P450 reductase (CPR), rat neuronal nitric oxide synthase (nNOS), *E. coli* sulfite reductase (SR), human methionine synthase reductase (MSR) and human novel reductase 1 (NR1).

Recreated from H.C. Chen and R.P. Swenson (Reference 22).

Thesis project objectives: The primary objective of this project, then, is to determine the role of the flavin mononucleotide cofactor and, more specifically, the role of the conserved glycine residue in the FMN-binding loop in the electron transfer of CPR. To this end, Glycine-141 was replaced by amino acids with increasingly large sidechains, *i.e.* alanine and a β-branched threonine. Additionally, the Glycine-141 residue was deleted, which is thought not only to disrupt the N(5)H interaction, but also to reduce flexibility in the FMN-binding loop. The primary focus of this project was to obtain significant quantities of the purified Glycine-141 variants, to characterize them initially, to establish the redox properties of the G141A CPR variant, establish their reductase activities relative to wild-type CPR, and to characterize in detail the pre-steady-state kinetics associated with both the reductive and oxidative half-reactions. By doing so, the role of Glycine-141 in establishing both the redox properties of the reductase, as well as, its electron transfer mechanism will have been more thoroughly determined. The overall objectives of this project are, therefore, as follows:

(1) Transform cells with the G141A CPR containing plasmid.

(2) Perform cell growths to preferentially express G141A CPR.

(3) Harvest and purify G141A CPR.

(4) To analyze flavin content of G141A CPR, with and without FMN incubation, by HPLC analysis and compare results to those of WT and G141del CPR.

(5) Perform a steady-state turnover assay with NADPH and cytochrome c to establish activity of G141A CPR and compare this activity to that of WT, G141T, and G141del CPR.

(6) Perform a FAD-dependent electron transferase assay with ferricyanide on G141A CPR and compare this activity to that of WT, G141T, and G141del CPR.

(6) Perform an FMN-dependent oxidative titration with sodium dithionite and potassium ferricyanide on G141A CPR and compare this activity to that of WT, G141T CPR, and G141del FBD.

(8) Perform pre-steady state turnover, reductive half-reaction assays on G141A CPR and fit the reaction traces.

a. Perform in standard conditions

b. Perform with varying concentrations of $NADP^+$ to observe competitive binding

(9) Perform pre-steady state turnover, reductive half-reaction assays on WT CPR and fit the reaction traces.

a. Perform in standard conditions

b. Perform with varying concentrations of $NADP^+$ to observe competitive binding

(10) Perform pre-steady state turnover, reductive half-reaction assays on G141T CPR and fit the reaction traces.

a. Perform in standard conditions

b. Perform with varying concentrations of $NADP^+$ to observe competitive binding

(11) Perform pre-steady state turnover, reductive half-reaction assays on G141del CPR and fit the reaction traces.

a. Perform in standard conditions

b. Perform with varying concentrations of $NADP^+$ to observe competitive binding

(12) Use reaction trace fittings and kinetics modeling software to model the reductive half-reaction for WT, G141A, G141T, and G141del CPR.

a. With stoichiometric amounts of NADPH

b. With $NADP^+$ added to solution

(13) Perform pre-steady state turnover, oxidative half-reaction assays on G141A CPR and fit the reaction traces.

(14) Perform pre-steady state turnover, oxidative half-reaction assays on Wt CPR and fit the reaction traces.

(15) Perform pre-steady state turnover, oxidative half-reaction assays on G141T CPR and fit the reaction traces.

(16) Perform pre-steady state turnover, oxidative half-reaction assays on G141del CPR and fit the reaction traces.

(17) Use reaction trace fittings and kinetics modeling software to model the oxidative half-reaction for WT, G141A, G141T, and G141del CPR.

Materials and Methods

Materials: The QuikChange® Site-Directed Mutagenesis Kit was purchased from Stratagene. *Escherichia coli* stain DH5α Max Efficiency competent cells were obtained from Invitrogen and BL21 (DE3) Rosetta strain cells were purchased from Novagen. Sodium dithionite was purchased from JT Baker. Ampicillin was purchased from Amresco. Chloramphenicol, horse heart cytochrome c, NADPH, $NADP^+$, FMN, FAD, and potassium ferricyanide were all purchased from Sigma. All other chemicals used were analytical reagent grade.

Mutagenesis, transformation, and expression of G141A CPR: Three CPR variants were generated for studied in this thesis. Included those in which Glycine-141 was replace by threonine (G141T CPR), by alanine (G141A CPR), and in which this residue was deleted (G141del CPR). The primary focus of my thesis research was initially on the mutagenesis, expression, purification, and characterization of the G141A CPR variant. The G141T CPR variant was generated, expressed, purified, and characterized by Matthew Wohlever. The G141del CPR mutant was generated, expressed, and purified by Amanda McKenna, while the same deletion was introduced in the isolated recombinant FMN-binding domain of CPR by Yicheng Long.

The G141A variant was generated in soluble form (lacking the N-terminal membrane anchor region) of recombinant rat cytochrome P450 reductase using the QuikChange® site-directed mutagenesis protocol. The complementary oligonucleotides used for generating the glycine to alanine substitution were (with the altered nucleotides underlined),

5’-GCCACATACG<u>CA</u>GAGGGCGACC-3’ and 5’-GGTCGCCCTC<u>TG</u>CGTATGTGGC-3’.

The open reading frame obtained from a cDNA clone for soluble rat CPR previously prepared and recloned in the T7-7 expression plasmid (Stratagene) was used as the template for mutagenesis. The altered plasmid preparation obtained from the QuikChange procedure was used to transform competent *E. coli* strain DH5α Max Efficiency cells. Several colonies from cells grown on LB agar plates containing ampicillin for selection were selected, cultured separately, and the pT7-7/G141A CPR plasmids purified via Qiaprep® Spin columns using prescribed protocol. The plasmid DNA was sequenced by the Plant Microbe Genomics Facility at the Ohio State University to confirm the site-specific mutations as well as to insure the integrity of the entire coding region. A positive confirmed G141A CPR mutant plasmid was then used to transform the BL21 (DE3) Rosetta *E. coli* strain which was cultured in LB media containing ampicillin (100 μg/ml) and chloramphenicol (35 μg/ml). The Rosetta strain was required for the expression of this eukaryotic protein in *E. coli* cells to improve yields due to the codon usage differences. Expression of G141A CPR was induced by IPTG, in methods described by Chen and Swenson [24].

Purification of G141A CPR: The *E. coli* cells were harvested by centrifugation and the pellets were resuspended in 50 mM Tris, pH 7.7 buffer containing 0.1 mM EDTA, 0.05 mM dithiothreitol and 10% glycerol (designated as "Buffer A"). Cells were lysed using a French press cell at an effective cell pressure of 12,000 psi followed by centrifugation to remove cellular debris. G141A CPR was purified from the cell extracts by affinity chromatography on agarose resin contained covalently bound 2',5'-ADP (Sigma Chemicals) by the procedure described by Rock *et al.* [26], except using a slightly different buffer compositions. The 2',5'-ADP represents an analog for $NADP^+$, one of the products of CPR. Cell lysates were loaded onto the column and

washed with Buffer A. G141A CPR was eluted with Buffer A containing 20 mM 2'(3')-AMP and 100 mM NaCl. Fractions were collected during elution and flavin content was monitored using an Agilent Model 8453 photodiode array spectrophotometer. Fractions containing a typical flavin absorbance spectrum associated with CPR and with A274:A450nm ratios less than 10 were pooled and concentrated using Amicon® 10kDa NMWL Ultra Centrifugal Filter Devices (Centricon-10). Three rounds of solvent exchange with Buffer A using the Centricon-10 ultrafiltration device was performed to remove the 2'(3')-AMP and NaCl prior to storage at -80°C. Purity of the G141A CPR preparations was established by standard SDS polyacrylamide gel electrophoresis methods. Purity estimated to exceed 95% was routinely achieved.

Flavin content analysis of CPR variants: The flavin cofactor content (FAD and FMN) of the CPR variants was determined by high performance liquid chromatography (HPLC) using a LKB Bromma 2150-2152 HPLC system and a procedure similar to Marohnic *et al.* [29], with the exceptions that 450 nm was the observed wavelength and flavin standards were at 40 µM for FAD and 60 µM for FMN. In addition, for the variants a number of trials were done to examine the FMN reconstitution. In these experiments, the enzyme was incubated in 5-fold excess of added FMN in the dark at 4°C for one hour.

Spectral analyses and steady-state turnover (SSTO) assay of CPR: All ultraviolet-visible absorbance spectra were recorded on Agilent Model 8453 photodiode array spectrophotometer at 25°C. The cytochrome c reductase activity of CPR was measured under saturating substrate concentrations with NADPH used as the electron donor essentially as described by Shen *et al.* and Klein and Fulco [16,27]. Assay solutions contained 270 mM

potassium phosphate buffer, pH 7.7, 100 µM NADPH, 65 µM cytochrome c, and CPR concentrations of 0, 2.5, 5.0, 7.5, and 10 nM. Cytochrome c reduction was monitored at 550nm with $\Delta\varepsilon = 21\ mM^{-1}cm^{-1}$.

FAD-dependent electron transferase assay with ferricyanide: Ferricyanide reductase activity of CPR was performed under steady-state turnover conditions in 270 mM potassium phosphate buffer, pH 7.7 containing 100 µM NADPH, 500 µM potassium ferricyanide, and CPR concentrations of 0, 2.5, 5.0, 7.5, and 10 nM. Ferricyanide reduction was measured at 420 nm with $\Delta\varepsilon = 1.04\ mM^{-1}cm^{-1}$ [28].

Anaerobic reductive and oxidative titrations: Anaerobic reductive and oxidative titrations of the CPR variants were performed using sodium dithionite and potassium ferricyanide, respectively, in 270 mM potassium phosphate buffer, pH 7.7. Sodium dithionite and potassium ferricyanide solutions were made anaerobic by bubbling extensively with purified argon. CPR samples, typically 1.0 mL at 20 µM, were placed in a specially designed sealable titration cuvette and made anaerobic by completing several alternating gas exchange cycles with argon and a partial vacuum (water aspirator). Reductive titrations were performed by adding substoichiometric amounts (typically in 1 µL volumes) of anaerobic sodium dithionite using a special gas-tight Hamilton syringe assembly attached to the cuvette. Oxidative titrations were performed by first reducing the CPR sample with a slight excess of sodium dithionite followed by the addition of substoichiometric amounts of anaerobic potassium ferricyanide as described above. After each aliquot of titrant was added, the sample was gently but thoroughly mixed, and allowed to achieve equilibrium by monitoring the spectral changes until no further changes were

observed. A final spectrum between 300 and 700 nm was obtained and saved before the next addition of the titrant. For these experiments, oxidized flavin was measured at 455 nm and formation of the flavin semiquinone was measured at 580 nm. Both the reductive and oxidative titration procedures were used to titrate the WT, G141T, and G141del variants of CPR, however the results of these two reaction types are very comparable. The oxidative protocol was used for the G141A variant.

Pre-steady state kinetic analyses: Both the oxidative and reductive half-reactions for each CPR variant were performed on a Hi-Tech Scientific SF-61 stopped flow spectrophotometer which mixes equal volumes of two reactants with a mixing time (or sometimes referred to as the "dead time") of approximately 1.5 msec. After mixing, the flow is abruptly stopped and the absorbance changes at a specified wavelength are recorded and plotted as a function of time by the instrument software. For the reductive half-reaction, a 40 μM solution of CPR in 50 mM potassium phosphate, pH 7.0 in one syringe was mixed with 40, 200, or 400 μM NADPH in the same buffer in the second driving syringe (all concentration are reported as the pre-mixing concentration). All solutions were made anaerobic by extensive bubbling with argon except for the CPR solution for which only the buffer was sparged with argon before a small volume of a concentrated stock of the CPR variant was added (to avoid surface denaturation). These conditions represent the basic reductive half-reactions, however, competitive binding experiments were also performed in which 0, 40, 80, 200 or 400 μM $NADP^+$ was added to the solutions containing the NADPH (again at 40-400 μM). Reduction was monitored at 450 nm to record the loss of the oxidized flavin and at 590 nm to observe the formation of the flavin in the semiquinone state.

Similarly, the oxidative half-reaction of CPR was determined in 100 mM potassium phosphate, pH 7.0, again with all solutions made anaerobic by extensive argon bubbling. For these experiments, 10 µM CPR was mixed with solutions containing 10 µM NADPH and 10, 20, 40, 80 or 160 µM cytochrome c. It was assumed (and established separately) that the NADPH would very rapidly reduce the CPR prior to its transferring electrons to the cytochrome. This greatly simplified the experiment in that the CPR need not be retained in the reduced state for extensive periods of time, which is often difficult to achieve. The reduction of cytochrome c was measured at 550 nm.

Kinetics modeling of reductive and oxidative half-reactions: Data from the oxidative and reductive half-reactions were analyzed using KinTek® Global KinTek Explorer software.

Results and Discussion

Purification of G141A CPR: Over-expression of the soluble recombinant form of G141A CPR was achieved through the induction by IPTG of the BL21 (DE3) Rosetta strain of *E. coli* transformed with the pT7-7/G141A CPR plasmid. The expressed holoprotein was purified from the cell extracts using affinity chromatography based on the $NADP^+$ analog, 2', 5'-ADP as evidenced by the elution of yellow-colored protein fractions by the soluble competing ligand 2'(3')-AMP. To determine the purity of the G141A CPR protein obtained from the column, SDS-PAGE was performed. The samples represented on the gel are the combined fractions eluded from the affinity column, which showed considerable flavin content. The results of the SDS-PAGE gel demonstrated that the protein obtained was >99% pure (see Figure 10). This level of purity of G141A CPR clearly demonstrates the efficiency of this one-step affinity chromatographic procedure and was certainly sufficient to use for analytical experiments with no further purification steps being required.

Analysis of the flavin content of G141A, G141del, and WT CPR variants: High performance liquid chromatography (HPLC) analyses were performed to determine the flavin content of each CPR variety. Previously, it had been shown in flavocytochrome P450BM-3 that some alterations to the FMN binding loop can actually prevent or weaken the binding of the FMN cofactor [22]. This is of concern due to the fact that lack of a FMN cofactor can inhibit electron transport in CPR, resulting in non-functional enzymes.

Reverse phase HPLC analyses was performed as described in "Materials and Methods". Separation and retention times were established by injecting 2.0 nmol standards of FAD and

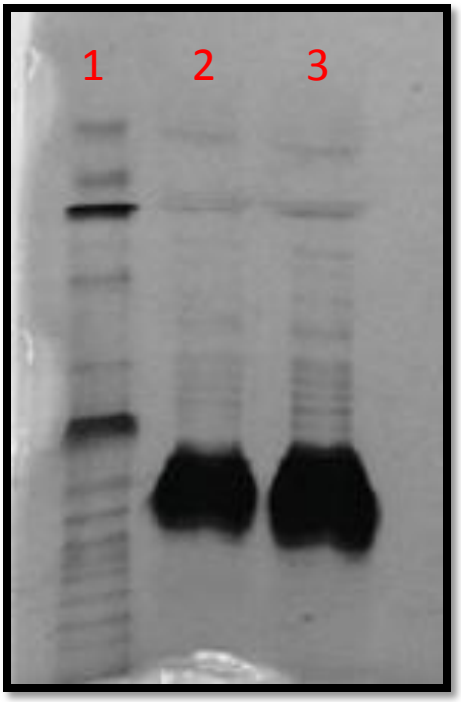

Figure 10- This is a photograph of the SDS-PAGE gel of purified G141A CPR. Lane 1 has the Benchmark® Protein Ladder (Invitrogen). Lane 2 has 10 µL of the G141A CPR stock solution added. Lane has 15 µL of the G141A CPR stock solution added.

FMN prior to the analysis of the experimental samples. Flavin elution was monitored at 450 nm and the relative peak height (or peak areas) was established for that amount of flavin cofactor. (Note that standard curves over the concentration range used in this study had been previously established in this laboratory.) Comparing peak heights/areas of the CPR samples to the standards allowed for approximation of flavin content. Experimental samples were prepared as followed. Aliquots containing 2.0 nmol of G141A CPR or other CPR variants were boiled for ten minutes to denature the protein and release flavin cofactors. The boiled samples were cooled and centrifuged to remove any denatured protein precipitate that might have formed. An exact volume of the clarified supernated CPR was injected onto the HPLC column and chromatography performed. Two peaks were observed that corresponded to the retention times for the FAD and FMN standards. Quantitation by peak height showed that 1.89 nmol of FAD were present in the sample, but only 0.855 nmol of FMN was present, with a FMN:FAD ratio of 0.45 (see Figure 11a). This was interpreted to mean that only 45% of CPR in the sample was fully constituted with both cofactors. This experiment was repeated for WT CPR and the results showed a FMN: FAD ratio of 0.93 or 93% of FMN retention. From these results, it was fairly clear that the substituted alanine residue caused enough biochemical changes to effect the binding of the FMN, but as expected the FAD cofactor, bound to a separate domain, is unaffected by the Glycine-141 alteration. So, either during the normal growth and expression conditions G141A CPR does not assume a structure for the FMN-binding domain that can efficiently acquire stoichiometric amounts of the FMN cofactor or during the purification process of G141A CPR FMN cofactor is lost. In an effort to resolve this issue, a study was conducted to attempt to reconstitute the purified G141A CPR with exogenously added FMN

cofactor. For these studies, the enzyme was incubated in 5-fold excess added free FMN followed by a solvent exchange to remove non-bound FMN, and HPLC analysis was repeated. This treatment resulted in a FMN: FAD ratio of 0.82 (see Figure 11b), representing an improvement in the level of bound FMN cofactor. These results suggest that the lower FMN:FAD ratio in untreated G141A CPR is likely the result of the loss during purification of a somewhat more weakly bound FMN cofactor in this variant. The fact that the enzyme can be significantly reconstituted further suggests that the FMN domain is folding properly during expression. The effectiveness of the FMN incubation in reconstituting enzyme led to a change in lab protocol so that all CPR variants, prior to kinetic or redox analysis, are first incubated in excess FMN. G141del CPR was also analyzed by HPLC after a FMN incubation to determine a FMN: FAD ratio of 0.69, which is less than G141A or WT CPR. This result which could be expected considering the shorter less flexible FMN-binding loop appears more like BMR (the reductase portion of flavocytochrome P450BM-3) and the recombinant BMR has FMN:FAD ratios of between 0.56-0.65 showing a relatively low FMN retention compared to WT CPR [unpublished HPLC results from the Swenson lab].

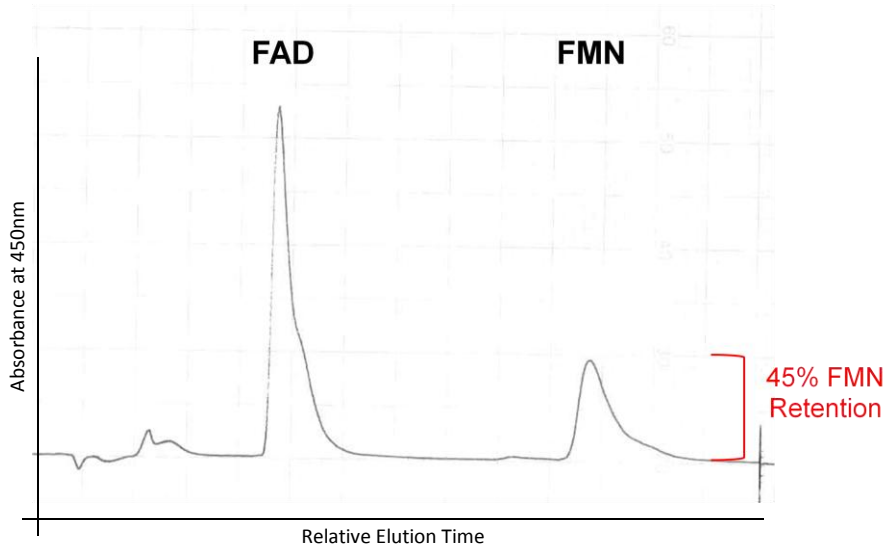

Figure 11a- This chart represents the HPLC flavin analysis results of G141A CPR at 450nm without free FMN incubation. The ratio of FMN:FAD was 0.45 showing only 45% of FMN retention in the protein

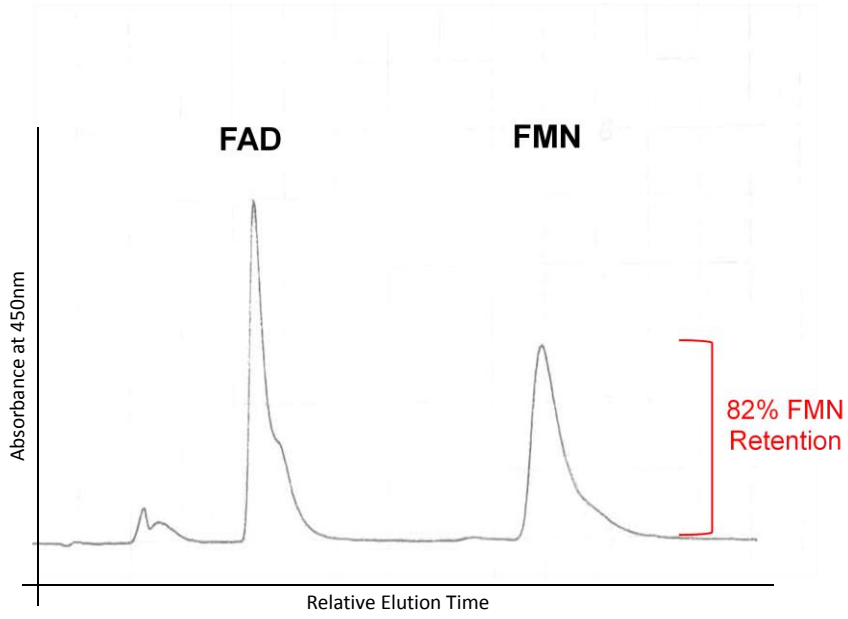

Figure 11b- This chart represents the HPLC flavin analysis results of G141A CPR at 450nm with 5-fold excess free FMN incubation. The ratio of FMN:FAD was 0.82 showing only 82% of FMN retention in the protein.

Steady-state turnover assay of G141A CPR with NADPH and Cytochrome c: The purified G141A CPR was characterized by the evaluation of its steady-state turnover (SSTO) activity using NADPH as the physiological electron donor and cytochrome c as the terminal electron acceptor. It is important to note that although cytochrome c is not the true redox partner for CPR, this cytochrome is routinely used and widely accepted as a good measure of cytochrome reductase activity because of the stability of the reduced form and the ease of use experimentally [16,27]. Generally speaking, this experiment will observe the movement of electrons from the bound NADPH reductant to the FAD cofactor then the FMN cofactor and finally to the cytochrome c acceptor. This reduction of cytochrome c is measured at 550 nm and as stated the $\Delta\varepsilon = 21\ mM^{-1}cm^{-1}$ (this value represents the difference in absorbance between oxidized cytochrome c with $\Delta\varepsilon = 8.9\ mM^{-1}cm^{-1}$ and reduced cytochrome c with $\Delta\varepsilon = 29.9\ mM^{-1}cm^{-1}$). Five different trials of this reaction were performed, which differed in the concentration of G141A CPR in the reaction cuvette. The assay buffer was always 270 mM potassium phosphate, pH 7.7 and in each trial the NADPH and cytochrome c concentrations were 100 µM and 65 µM, respectively. The concentration of G141A CPR was varied between trials and was 0, 2.5, 5.0, 7.5, or 10 nM in the reaction cuvette, but the assay at each CPR concentration was performed in triplicate. For these SSTO assays, the reactants, NADPH and cytochrome c, are in fairly high excess compared to CPR. However, because both are consumed during the assay, the initial reaction velocity of cytochrome c reduction is measured for only the first 180 seconds of reaction. These initial velocities (ΔAU/s) are converted to nmol/min of cytochrome c reduced which is compared to the nmol of CPR in the reaction cuvette to determine the overall turnover number in

nmol/min/nmol (min^{-1}). This number was determined graphically by linearly comparing the turnover number at each concentration of G141A CPR and fitting the data (see Figure 12).

The cytochrome c reductase activity of G141A CPR was measured for two primary reasons: (1) if the protein was folded incorrectly, lost the ability to bind a flavin cofactor, and/or was inactive for some other reason; these problems would result in serious effects on functional activity and (2) the turnover number for WT CPR (obtained from literature and experimentally by M. Wohlever), G141T (experimentally obtained by M. Wohlever), and G141del CPR (experimentally obtained by A. McKenna) had been established (see Figure 13); allowing for easy comparison of relative activities. It was determined that our expressed and purified G141A CPR was functional with a turnover number of 4600 ± 450 min^{-1} (see Figure 12). Additionally, we have shown that the turnover number for G141A CPR is 118% of that rate of WT CPR, determined to be 3900 min^{-1}. This result was a bit unexpected, but student t-tests showed that the increased activity for G141A, compared to WT, was not statistically significant. The other CPR with substitutions for the Glycine-141 residue only had 72% (G141T = 2800min^{-1}) and 44% (G141del = 1700 min^{-1}) the activity of WT CPR (see Figure 13 for the data table). It was assumed that the activity of the G141A CPR variety would also be less than that of WT CPR considering the methyl side-chain would have some effect on the conformational change of the FMN-binding loop and consequently on the stability of the FMNsq. However, as previously noted, experiments in which the conserved glycine in the flavodoxin of *C. beijerinckii* was substituted for alanine showed very little effect to overall redox, activity, and structural properties of the protein [20].

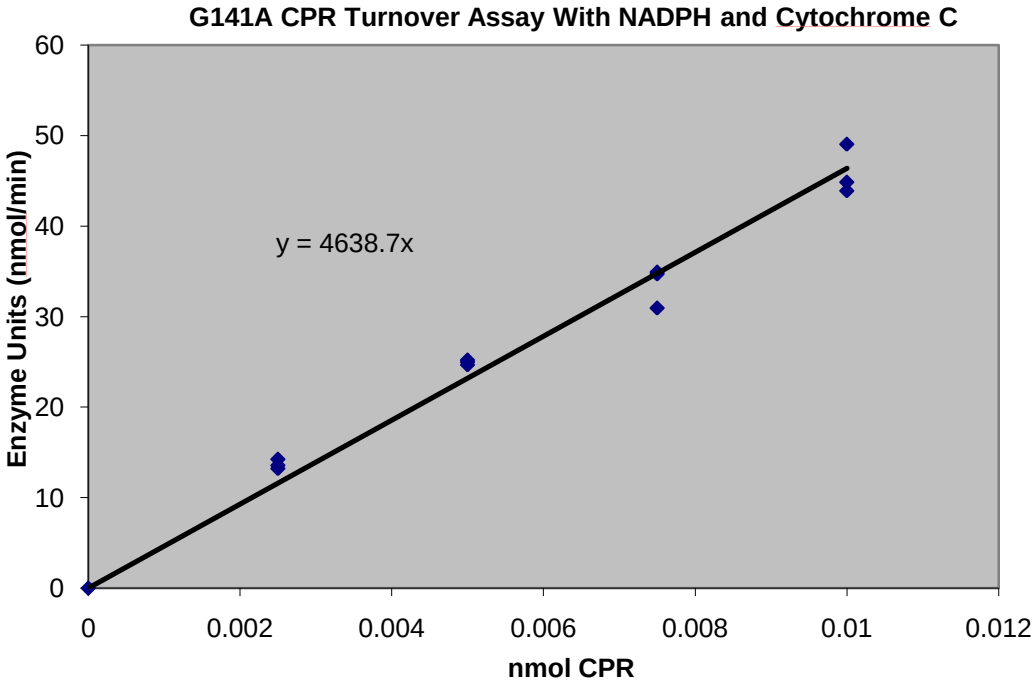

Figure 12- This is the graphical analysis and linear fit of the cytochrome c reductase activity of G141A CPR. Fitting the triplicate trials of this SSTO experiment at each of the different G141A CPR concentrations gives slope, which represents a specific activity of 4638.7 nmol/min/nmol; which with calculated error is represented as 4600 ± 450 min^{-1}.

Cytochrome c reductase activity of CPR varieties

Protein Sample	Turnover Number (nmol/min/nmol)	Percent Activity of Wild-Type
WT CPR (lit.)	3900	--
WT CPR	3900 ± 100	100%
G141A CPR	4600 ± 450[1]	118%
G141T CPR	2800 ± 300[2]	72%
G141del CPR	1700 ± 420[3]	44%

Student t-test: [1] p = 0.058 (not statistically different from WT); [2] p = 0.0038; and [3] p = 0.0009.

Figure 13- This figure represents the experimentally obtained values of cytochrome c dependent SSTO activity of a number of CPR varieties.

FAD-dependent electron transferase assay with ferricyanide: The cytochrome c reductase assay measures the entire electron transport process from NADPH to the cytochrome c proceeding through both the FAD and FMN cofactors. However, utilizing a potassium ferricyanide reductase assay allows for the measurement of the transfer of electrons from NADPH to the FAD cofactor and finally to a ferricyanide molecule [16]. This electron transfer activity functionally removes the participation of the FMN cofactor and more directly monitors CPR's ability to accept the electrons from the hydride transfer of NADPH. Like the cytochrome c reductase assay, ferricyanide activity assays were performed in SSTO conditions with excess reactants. The concentrations of NADPH and ferricyanide were 100 μM and 500 μM in the reaction cuvette, respectively. The concentration of G141A CPR was varied between experimental trials and was 0, 2.5, 5.0, 7.5, or 10 nM. The assay was performed in triplicate at each CPR concentration. This assay measures enzyme activity by observing the initial rate of decrease of absorbance at 420 nm, which represents loss of oxidized ferricyanide ($\Delta\varepsilon$ = 1.04 $mM^{-1}cm^{-1}$). These initial rates (ΔAU/s) are converted to nmol/min of ferricyanide reduced which again is compared to the nmol of CPR in the reaction cuvette to determine the overall turnover number to be 5700 ± 500 min^{-1} (nmol/min/nmol). This number was determined graphically by linearly comparing the turnover number at each concentration of G141A CPR and fitting the data by linear regression analysis (see Figure 14). The SSTO value for the ferricyanide reductase activity for WT, G141T and G141del CPR have been determined under similar conditions which allows for comparison with G141A CPR data (each CPR variant's specific activity obtained by the

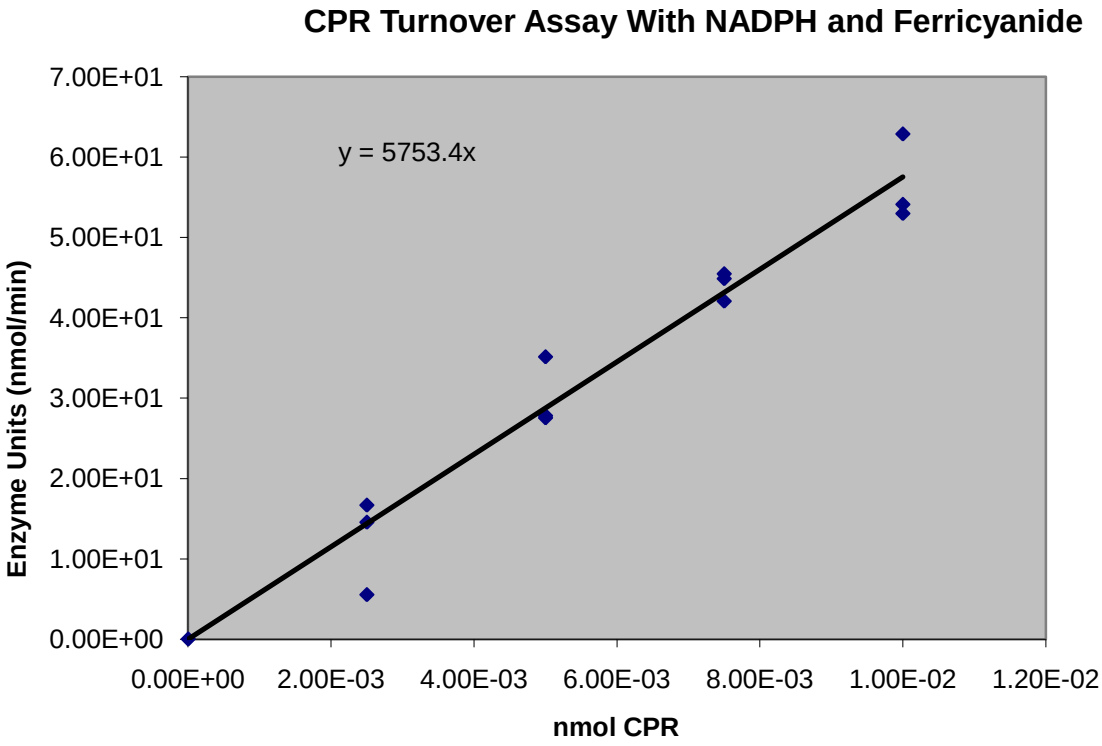

Figure 14- This is the graphical analysis and linear fit of the ferricyanide reductase activity of G141A CPR. Fitting the triplicate trials of this SSTO experiment at each of the different G141A CPR concentrations gives slope, which represents specific activity, of 5753.4 nmol/min/nmol; which with calculated error is represented as 5700 ± 500 min^{-1}.

Ferricyanide FAD dependent reductase activity of CPR varieties

Protein Sample	Turnover Number (nmol/min/nmol)	Percent Activity of Wild-Type
WT CPR (lit.)	7800	--
WT CPR	6600 ± 700	100%
G141A CPR	5700 ± 500[1]	86%
G141T CPR	4000 ± 800[2]	61%
G141del CPR	4100 ± 240[3]	62%

Student t-test: [1] p = 0.144 (not statistically different from WT); [2] p = 0.0133; and [3] p = 0.0043

Figure 15- This figure represents the experimentally obtained values of ferricyanide (FAD) dependent SSTO activity of a number of CPR varieties.

same experimenter as cytochrome c reductase values). The results show that all Glycine-141 mutant variants have lower activities than WT CPR. Compared to WT CPR, G141A has 86% activity (which by student t-test was shown not to be statistically different from WT CPR), G141T has 61% activity, and G141del CPR has 62% activity (see Figure 15). The changes in ferricyanide reductase activity do seem to have a correspondence to the size of the Glycine-141 alteration. The minimal sidechain of alanine has a smaller effect than the β-branched threonine or the residue deletion. These findings are interesting considering the target of this assay is the FAD-binding domain, which is identical for WT, G141A, G141T, and G141del CPR. Therefore, it was expected that ferricyanide reductase activity between the variants should be very similar, but it was not. This phenomenon has been observed previously in our lab. While the cause is not know with any certainty, a possible explanation may be related to the idea that in the CPR enzyme there is a substantial amount of domain-domain interaction and movement accompanying each step of the electron transfer process [6,10,13,15]. It seems plausible that the alterations to the Glycine-141 residue and the changed redox properties of the FMN cofactor and binding domain could be having an effect on the properties of the FAD-binding domain through changes in these interactions. Thus, our variants may, for the first time, be suggesting a role of the FMN domain in the regulation of electron transfer to and from the FAD, which is seemingly contrary to the basic premise offered in the literature. The observation that ferricyanide, with NADPH present, could be reduced by the FAD domain was based on the retention of this activity in CPR in which the FMN cofactor has been removed and by recombinant forms of the isolated FAD-binding domain alone [15, unpublished work from this laboratory]. Further research will be necessary to clarify this issue, however.

Anaerobic oxidative titration of G141A CPR with ferricyanide: The sequential spectrochemical titration of flavoproteins with substoichiometric amounts of chemical reductants or oxidants under anaerobic conditions is a well established means of establishing the formation, identity, and relative thermodynamic stabilization of the know redox states of the bound flavin cofactors. Each redox state has a distinct UV-visible absorbance spectrum which can be effectively monitored during the titration. Typically the reductive and oxidative processes are equivalent and freely reversible thermodynamically in the reductases and related flavoproteins. Furthermore, the accumulation of nearly stoichiometric levels of the "blue" neutral semiquinone state for both the FAD and the FMN cofactors, the so called "disemiquinoid state" is a distinctive "hallmark" feature of WT CPR [6, 28, 30]. Thus, the anaerobic oxidative titration of G141A CPR was performed to evaluate the relative stability of each of the redox states of the flavin cofactors in this variant. Because the focus of this study was on the role of Glycine-141 in the stabilization of the one-electron reduced state of the FMN cofactor, emphasis was placed on monitoring the formation and stability of the "blue" neutral semiquinone as it is formed as G141A CPR is being oxidized. Similar titrations have performed in both the reductive and oxidative directions for WT CPR, G141T CPR, and G141del FBD; so the relative amounts of semiquinone formed can be easily compared [30]. It should be noted that the reductive titration was attempted for the G141A CPR variant, but was not successful due to the difficulty in removing all traces of molecular oxygen from the protein solution. However, because of the reversibility of the process, similar results can (and have for the other variants) be obtained by first reducing the G141A CPR with sodium dithionite (which also destroys any residual oxygen in the solution) followed by the step-wise re-oxidation of the reductase with the addition of

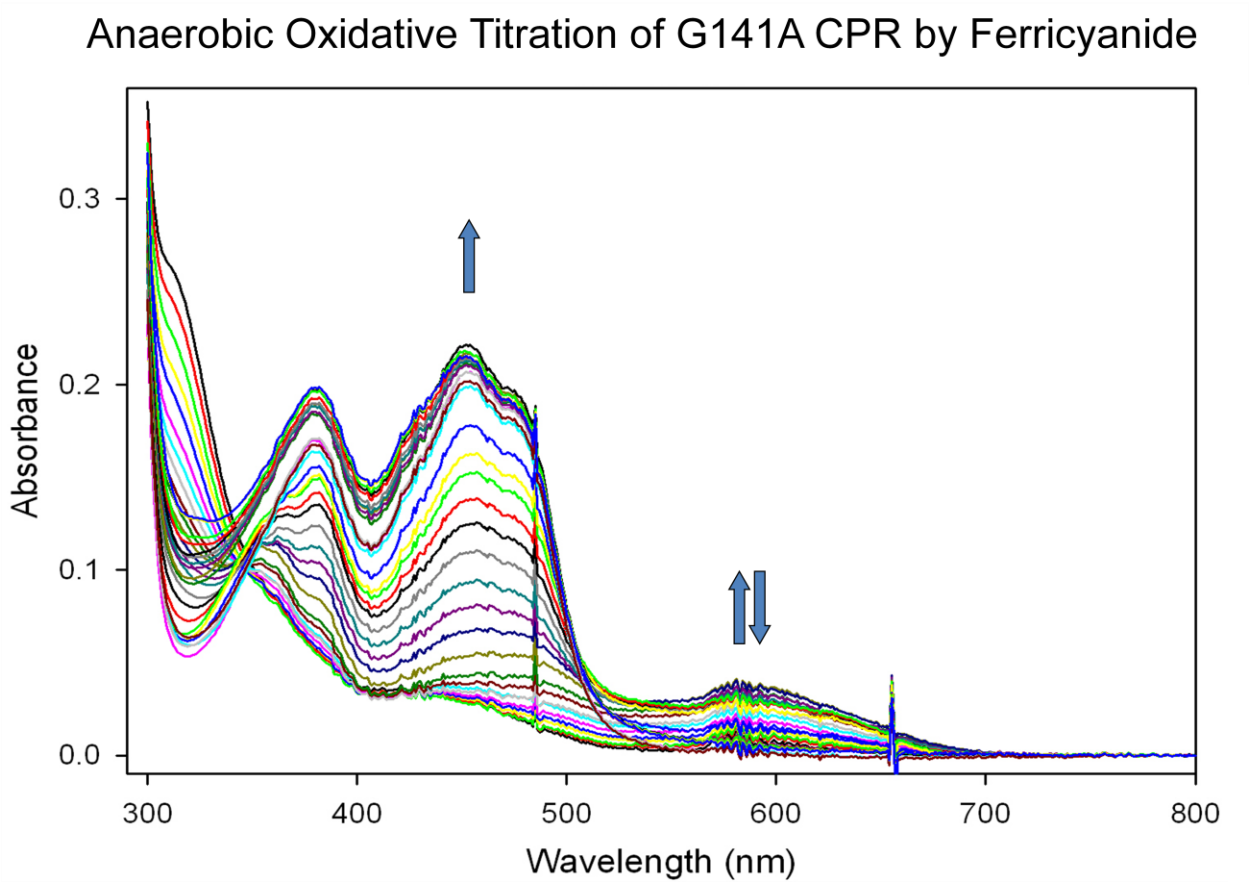

Figure 16- This series of spectrum shows the gradual anaerobic oxidation of G141A CPR. The 20 µM sample of G141A CPR was first fully reduced by 2.0 mM sodium dithionite and then oxidized stepwise by 1.0 µL additions of 0.5 mM potassium ferricyanide. Each different colored line represents the system at equilibrium after oxidant addition. Arrows at 580 nm show the formation and subsequent loss of the semiquinone species. The arrow at 455 nm shows the gradual gain of oxidized flavin.

small volumes (1 µL) of an anaerobic potassium ferricyanide solution. Once the system reached equilibrium after ferricyanide addition, as indicated by stable UV-visible absorbance spectra, a full spectrum of the reaction cuvette was recorded (see Figure 16). The observed changes in absorbance at 455 nm and 580 nm represents the formation of oxidized and semiquinone flavin, respectively. From the spectral path, the order of events can be seen: (1) as electron equivalents are removed from the G141A CPR system there is an initial increase in absorbance at 580 nm indicating the formation of the "blue" neutral semiquinone radical, (2) then as greater than two electron equivalents are removed you begin to see a loss of absorbance at 580 nm and, simultaneously, a gain of absorbance at 455 nm illustrating the presence of fully oxidized flavin, and (3) finally there is complete loss of absorbance at 580 nm when absorbance at 455 nm reaches its highest value.

The results for this experiment become pertinent when the amount of semiquinone formed by G141A CPR is directly compared to the amount of semiquinone formed with WT CPR. A similar anaerobic reductive titration was performed with WT CPR [30] which was observed to form about 90% of the disemiquinoid species expected when comparing experimental absorbance change at 580 nm absorbance to the calculated absorbance change based on the molar extinction coefficient of FMNsq and FADsq at 580 nm. The spectral changes occurring during the titrations for the G141A and WT CPR enzymes were compared by aligning traces on a 455 nm vs. 580 nm chart for both reactions (see Figure 17). The result shows that G141A CPR forms only about 80% of the semiquinone that WT CPR does. Because CPR contains two flavin cofactors, FAD and FMN, both of which are capable of forming the neutral semiquinone state, it is not possible with absolute certainty to know which flavin is displaying a

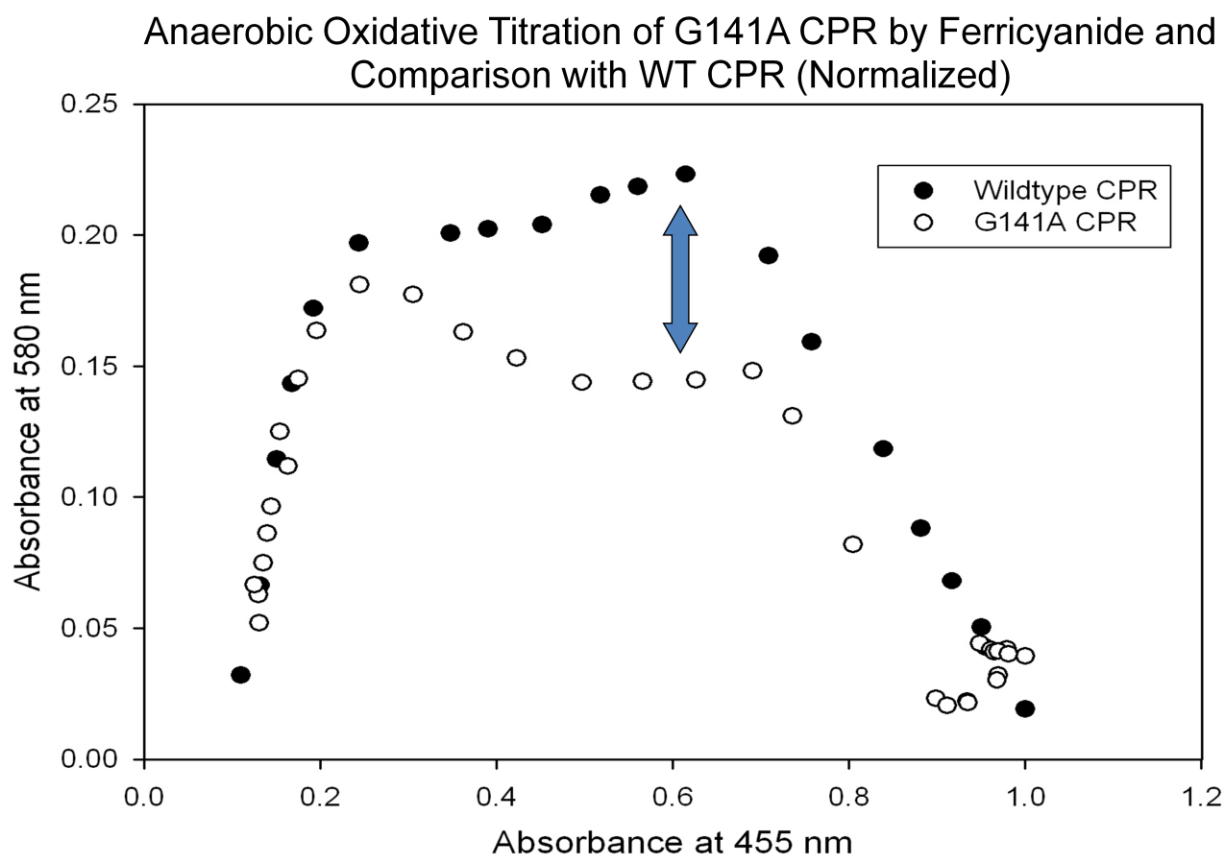

Figure 17- This 455 nm vs. 580 nm plot compares the anaerobic oxidative titration of G141A CPR with the anaerobic reductive titration of WT CPR. Specifically this plot is useful in comparing the formation of flavin SQ (580 nm) as it compared to the total oxidation of flavin (455 nm). The double headed arrow shows the disparity of semiquinone formation between WT and G141A CPR. Values for G141A CPR were normalized to WT CPR due to differences in initial protein concentration. WT CPR data calculated from reference 30.

lesser semiquinone stability. However, it is very reasonable to assume that since the only distinction between these two enzymes is the alteration in the FMN-binding loop and that a similar alteration in the flavodoxin homolog also disrupts the FMN radical, the difference in accumulation of the neutral semiquinone is associated with the destabilization of the FMN semiquinone state in response to the G141A residue substitution.

To further make a case, the G141A CPR oxidative titration has been compared with the reductive titration of the G141T CPR variant [performed by M.Wohlever]. G141T CPR accumulated even less semiquinone than G141A CPR and compared to WT CPR, there is only about 73% semiquinone formation in G141T relative to WT (see Figure 18). Anaerobic reductive experiments with sodium dithionite have also been performed on the purified isolated recombinant G141T FMN-binding domain itself (designated FBD). These results showed that compared to WT FBD, G141T stabilized the formation of only about 30% the neutral FMNsq. This gives support to the conclusion that the loss of absorbance at 580nm seen in G141T and G141A CPR assays corresponds to the destabilization of the FMNsq, not the FADsq. These results are also consistent with similar modifications within the bacterial flavodoxin (the model for my studies) which only contains the single FMN cofactor [20]. Finally, similar preliminary experiments have been conducted with the G141del FBD and the results from this showed virtually no (<10%) formation of the FMNsq compared to WT FBD. Collectively, these experiments demonstrate in the FMN-binding domain of CPR that the nature of the Glycine-141 alterations, like those seen in the *C. beijerinckii* flavodoxin experiments [20], can result in the disruption of FMN-binding loop and its conformation changes which affect the hydrogen

bonding with the N(5)H of FMNsq and its stability. The consequences of this disruption on the electron transferring activity of CPR were addressed next.

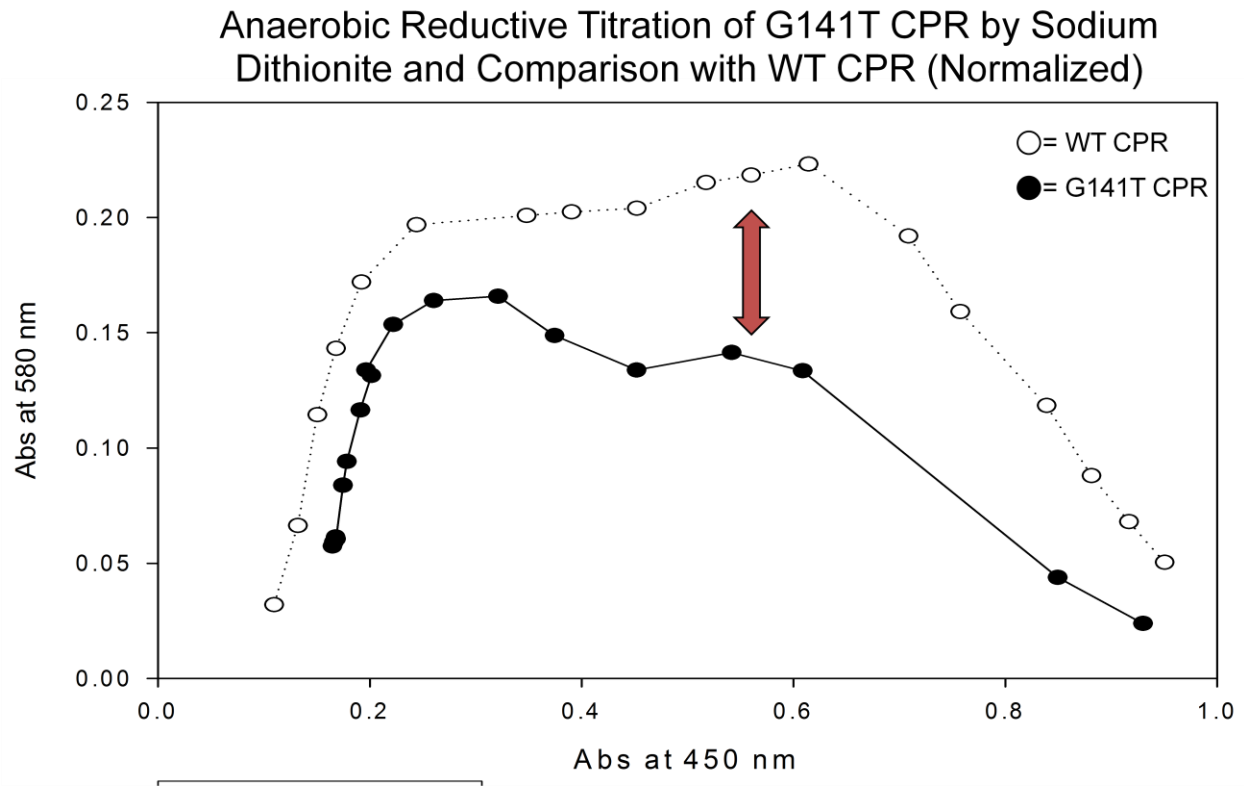

Figure 18- This 450 nm vs. 580 nm plot compares the anaerobic reductive titration of G141T CPR with the anaerobic reductive titration of WT CPR. Specifically this plot is useful in comparing the formation of flavin semiquinone (580 nm) as it compared to the total oxidation of flavin (455 nm). The double headed arrow shows the disparity of SQ formation between WT and G141T CPR. Values for G141T CPR were normalized to WT CPR due to differences in initial protein concentration. WT CPR data calculated from reference 30.

Reductive half-reaction of WT, G141A, G141T and G141del CPR: The anaerobic reductive and oxidative titrations demonstrated that the stability of the FMNsq is directly related to the disruption caused by the size and structure of the sidechain substitutions introduced for Glycine-141 or its total deletion; meaning that alanine introduced the smallest change at the position of the glycine residue and resulted in the smallest alteration in FMNsq stabilization, whereas the more drastic deletion of the glycine residue itself caused the largest change in the accumulation of the FMNsq. Similarly, cytochrome c reductase assays demonstrated that there were differences in rate of steady-state turnover activity between WT, G141T and G141del CPR variants but less so for G141A. However, there are many mechanistic steps associated with the overall reductase activity. Any one or a combination of several may represent the rate-limiting step(s) in this process. Furthermore, it was somewhat surprising given the generally accepted role of the FMNsq state in cytochrome reduction that its loss of stability and lack of accumulation in the G141del variant did not affect cytochrome reduction in a more substantial manner. Why is this? Thus, the next step in this project was to examine how and to what extent the loss of stability of the FMNsq caused by the Glycine-141 alterations specifically affects the electron transfer in the mutant CPR variants. To do this, pre-steady state turnover assays were performed using a Hi-Tech Scientific SF-61 stopped-flow spectrophotometer. This instrument allows for a reaction to be monitored within the first 1.5 milliseconds of mixing two solutions and is therefore a valuable tool in characterizing the rapidly occurring electron-transfer reactions of CPR. Additionally, the use of pre-steady state kinetics allowed us to dissect the overall electron transfer performed by CPR into two smaller reactions: (1) the reductive half-reaction (RHR) that consist of electrons moving from NADPH to CPR and between the flavin

cofactors and (2) the oxidative half-reaction (OHR) that consist of electron moving from their respective cofactors in CPR to cytochrome c as the terminal electron acceptor.

As was previously stated, the RHR observes the transfer of electrons from a bound NADPH to CPR through the following proposed mechanism shown in Figure 19. The first step is the binding of NADPH, which is assumed to be very fast even at stoichiometric levels (and subsequently confirmed by the kinetic data). Secondly, NADPH transfers a hydride to the FAD of CPR, which will be shown to be the rate limiting step. Finally, and also very quickly, the FADhq transfers a single electron to FMNox forming the disemiquinoid (FADsq and FMNsq) form of CPR. Therefore, this simple mechanism should result in spectrophotometric changes that occur as a single exponential phases involving the loss of absorbance at 450 nm and a gain of absorbance at 590 nm, reflecting the loss of oxidized flavin and the formation of the disemiquinoid state. Both these absorbance changes should occur at the rate of hydride transfer if this step is truly rate limiting. This is the model shown in Figure 19.

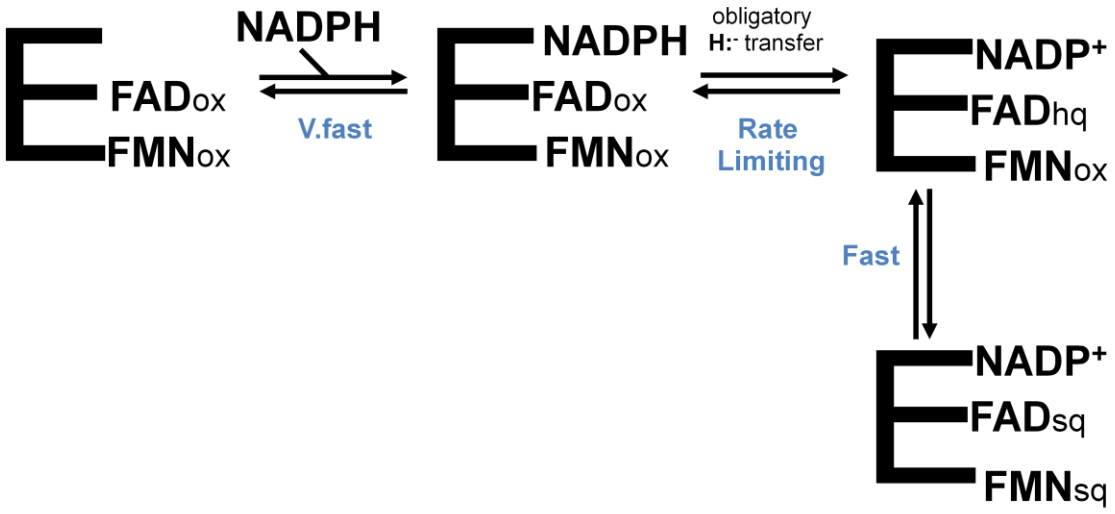

Figure 19- This is a cartoon of two electron reduction of CPR. Note the rate limiting hydride transfer step.

Reductive half-reaction of WT CPR: The first set of experiments performed involved observing the course of the RHR of all CPR variants as a function of the concentration of the NADPH concentration. For these experiments, the concentration of CPR was 40 µM for all trials and the concentration of NADPH was 40, 200, or 400 µM. (Note: Throughout these sections describing the stopped-flow experiments, the reported concentrations of the reactants are those before mixing. The final concentrations within the stopped-flow spectrophotometer observation cell will be half the concentration listed due to solution mixing in the reaction chamber of the instrument.) For each different concentration of NADPH, the experiment was performed in triplicate and the reactions observed at either 450 nm or 590 nm. The triplicate reaction traces were then combined into average reaction traces. For fitting and comparison, the 450 nm and

590 nm data was normalized to begin at zero and were plotted together (see Figure 20a-c). As can be seen, the RHR reaction traces for 40, 200, and 400 µM NADPH were not a single phase of reduction as might have been anticipated for the simple reductive mechanism outlined above. Furthermore, the initial loss of absorbance at 450nm (reduction of the FAD) corresponded with the increase in absorbance at 590nm (the formation of the disemiquinoid state). This observation is consistent with the reduction of the FAD being the rate limiting step with the formation of the disemiquinoid state then subsequently occurring at a faster rate. However, again, this mechanism does not predict the bi- or triphasic kinetic characteristics observed on these conditions. What is the cause? The appearance of a biphasic reduction of WT CPR was not entirely unexpected as Shen *et al*. showed that the RHR can proceed through two phases with excess NADPH added, when measuring change in absorbance at 452 nm and 585 nm [16,19]. However, at this point our identification of multiple phases was based on cursory inspection of the traces, therefore, to specifically identify and determine values for these rates the data was transferred into the SigmaPlot graphical plotting program for iterative fitting. Global fits of the 450 nm and the 590 nm data were performed on the averages traces for the 40, 200, and 400 µM NADPH trials. Initially, a single and then a double exponential equation were used to fit the data (exponential fits have been used to fit CPR RHRs both in this lab and in the literature [19]), but satisfactory fits were only achieved when using a triple exponential, 7 parameter fit (see Equation 3, 4, and 5).

(3) $y = y_0 + ae^{-bx} + ce^{-dx} + ge^{-hx}$ (this is the generic SigmaPlot equation)

(4) $A_{450} = y_0 + A_1^{-k_{obs1}t} + A_2^{-k_{obs2}t} + A_3^{-k_{obs3}t}$

(5) $A_{590} = y_0 + A_1^{-k_{obs1}t} + A_2^{-k_{obs2}t} + A_3^{-k_{obs3}t}$

In equations 4 and 5, y_0 represents final absorbance; A_1, A_2, and A_3 represent relative amplitude values; and $k_{obs}1$, $k_{obs}2$, and $k_{obs}3$ represent the observed rate constants (referred to as K1, K2 and K3 in this thesis). All of these values can be seen in the table in Figure 20d.

The presence of a triphasic reduction was unseen in previous reductive half-reactive studies of CPR [16,19], so the third phase could not really be compared, but the first two rates could be compared to literature values. Gutierrez *et al.* showed that, under identical buffer conditions, the RHR of human CPR was biphasic and at stoichiometric NADPH had values of K1 = 20 s^{-1} and K2 = 3.0 s^{-1} [13] and at 20-fold molar excess NADPH had values of K1 = 20 s^{-1} and K2 = 3.5 s^{-1} [19]. Our experimental WT CPR at stoichiometric NADPH had values of K1 = 42.6 s^{-1} and K2 = 5.72 s^{-1}, at 5-fold molar excess NADPH had values of K1 = 30.6 s^{-1} and K2 = 7.62s^{-1}, and at 10-fold molar excess NADPH had values of K1 = 27.5 s^{-1} and K2 = 6.0 s^{-1}. The values are quite close and possible explanations for the small differences could be: (1) variation between activities of the rat liver CPR we used and the human CPR they used, (2) differences in the experimental conditions , and (3) lower concentration of CPR (we had a 20 µM post-mix volume and human CPR was at 10 µM post mix). From these data, we can see that the values of K1, K2, and K3 are very similar despite the increasing concentrations of NADPH added (however, relative absorbance changes do vary). This demonstrates that the electron transfer observed likely derives from rate limiting steps that are independent of NADPH concentration and reliant more on CPR concentration. Had the binding of NADPH been rate limiting, one would expect that one or both of the observed rates would increase with increasing NADPH concentration. Thus, the very rapid rate of NADPH binding, as proposed above in our simple mechanism of Figure 19, was confirmed and supports the earlier assertion that hydride transfer reflects the

first observed rate limiting step. Another aspect of this reaction that is interesting, besides the multiple phases, is that the A2 value at 590 nm for the 40 μM trial that represents an increase in absorbance and, therefore, an increase in the amount of semiquinone being formed. Contrastingly, the A2 value at both trials of excess NADPH reflects a loss of absorbance at 590 nm and a loss of the semiquinone state. The loss of semiquinone at excess NADPH is due, presumably, to the addition of more than two electrons into CPR from another NADPH, taking the flavins to the fully reduced, hydroquinone state [13,19]. There does appear to be a third phase present in the RHR, however, for WT CPR (and for the rest of the CPR variants) the third phase is occurring after the 1.0 sec time point with a rate that is about three orders of magnitude slower than the rate of reduction and the turnover number from the SSTO assays. Thus, this phase most likely is not catalytically relevant and there is even some data to suggest that this phase is an artifact of re-oxidation of CPR by atmospheric oxygen not removed during argon sparging (unpublished Swenson lab data). Additionally, as will be shown in the kinetics, this phase usually does not represent a large or fast absorbance change, compared to the first two rates (particularly at stoichiometric NADPH). Therefore, this third phase, although represented in fitting, will not be discussed in detail in this thesis.

Wt CPR

20a.

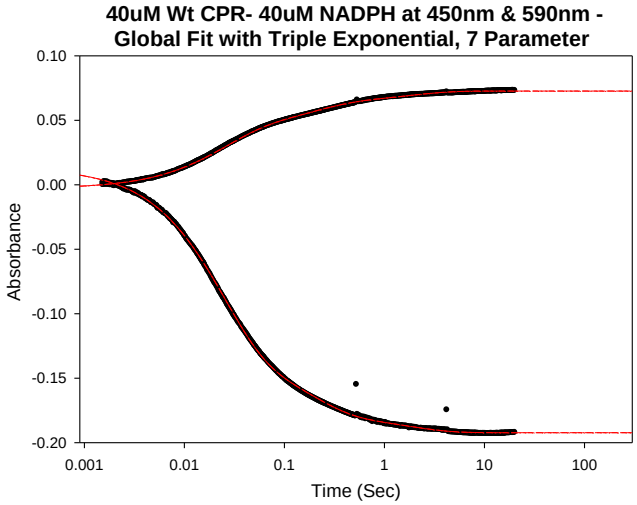

20b.

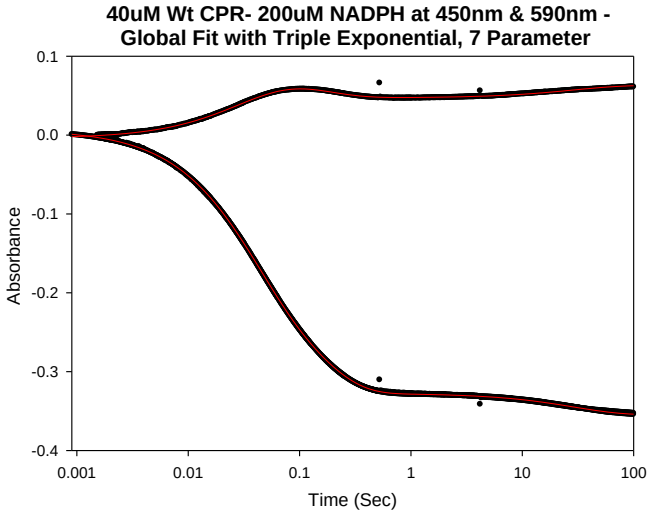

20c.

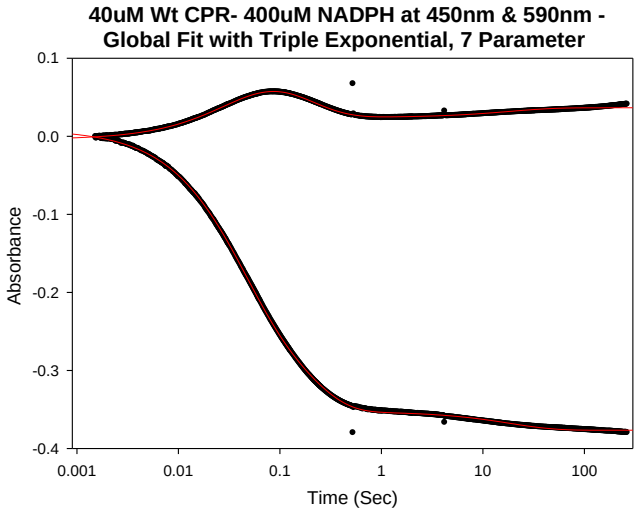

20d.

Wild-Type CPR

	40 uM NADPH		**200 uM NADPH**		**400 uM NADPH**	
	450nm	***590nm***	***450nm***	***590nm***	***450nm***	***590nm***
A1	0.143	-0.044	0.179	-0.0841	0.208	-0.0996
K1	**42.6**		**30.6**		**27.5**	
A2	0.0481	-0.0217	0.156	0.0329	0.153	0.0715
K2	**5.72**		**7.62**		**6.00**	
A3	0.014	-0.0099	0.0272	-0.016	0.0238	-0.0125
K3	**0.587**		**0.0345**		**0.054**	

Figure 20- The thick black lines are the averaged reductive half-reaction traces between 40 µM WT CPR and 40 µM (20a), 200 µM (20b) and 400 µM (20c) NADPH measured at 450 nm and 590 nm. The 590 nm trace is the upper trace and 450 nm is the lower trace for all graphs. The thin red line on each graph represents the triple exponential, 7 parameter fit to the data and the related rates and relative absorbance values can be seen in the table in 20d.

Reductive half-reaction of G141A CPR: The RHR of G141A CPR was evaluated using the same experimental approach and analyses as for the WT CPR. The triplicate stopped-flow reaction traces at 40, 200, and 400 μM NADPH for both 450 nm and 590 nm were averaged and these combined traces were transferred to SigmaPlot for curve fitting and analysis (see Figure 21a-c). Like that for WT CPR, the kinetic traces for the RHR of G141A CPR for each NADPH concentration was best fit to a triple exponential, 7 parameter equation and the observed rates and relative absorbance changes can be seen in the table in Figure 21d. The kinetic parameters obtained for G141A were very similar to that of WT CPR with the general comment that the reaction was slightly slower (especially at stoichiometric NADPH). Considering how minor an alteration the alanine substitution represents, the similarity to the WT CPR was expected. Minor differences were observed for the K2 and K3 values for the trials with stoichiometric NADPH. The G141A K2 value of 2.95 s^{-1} is just a little less than half the 5.72 s^{-1} rate observed for WT and the K3 value is very small at 0.0048 for G141A, which is not even a hundredth of the 0.587 value observed in WT CPR. Although these values are not especially different, it is possible that this step involves the FMNsq and therefore the G141A alteration.

G141A CPR

21a-

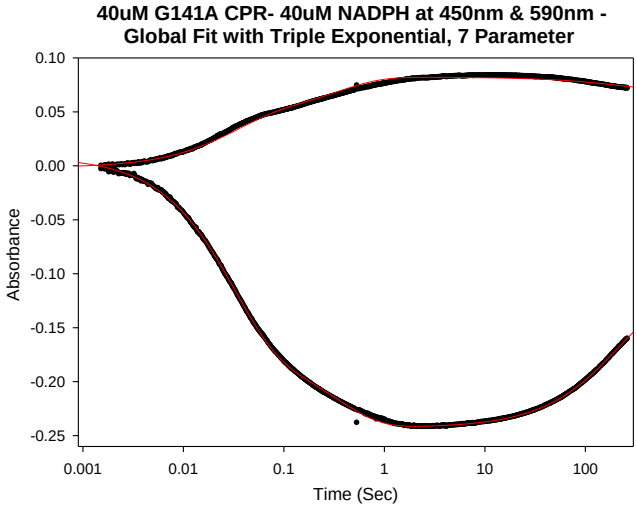

21b-

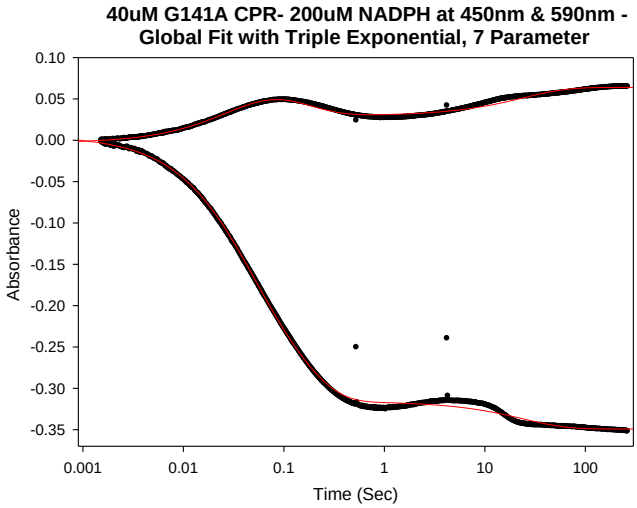

21c-

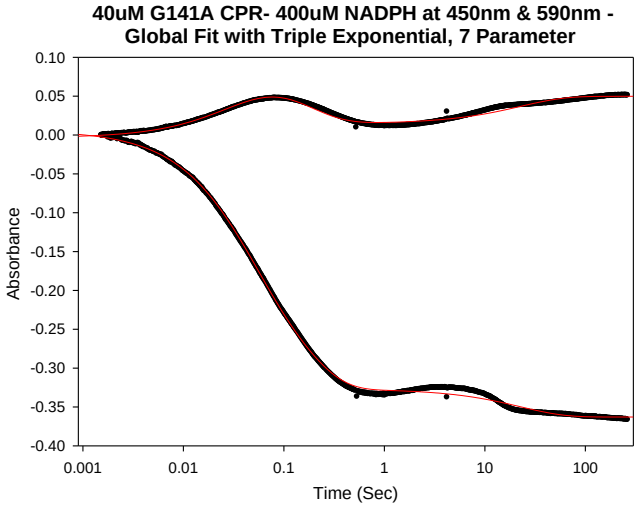

G141A CPR

	40 uM NADPH		200 uM NADPH		400 uM NADPH	
	450nm	***590nm***	***450nm***	***590nm***	***450nm***	***590nm***
A1	0.179	-0.0471	0.150	-0.0830	0.157	-0.0968
K1	**32.6**		**29.7**		**27.6**	
A2	0.0720	-0.0367	0.172	0.0502	0.176	0.0788
K2	**2.95**		**7.73**		**7.07**	
A3	-0.116	0.0119	0.0332	-0.0342	0.0359	-0.0352
K3	**0.0048**		**0.0416**		**0.0442**	

Figure 21- The thick black lines are the averaged reductive half-reaction traces between 40 µM G141A CPR and 40 µM (21a), 200 µM (21b) and 400 µM (21c) NADPH measured at 450 nm and 590 nm. The 590 nm trace is the upper trace and 450 nm is the lower trace for all graphs. The thin red line on each graph represents the triple exponential, 7 parameter fit to the data and the related rates and relative absorbance values can be seen in the table in 21d.

Reductive half-reaction of G141T CPR: The RHR for G141T CPR was also similarly evaluated. The triplicates of reaction traces at 40, 200, and 400 μM NADPH at both 450 nm and 590 nm were averaged and these combined traces (see Figure 22a-c) were again transferred to SigmaPlot for fitting to a triple exponential, 7 parameter equation (see table in Figure 22d). Comparison of the reaction traces and the rate constants from the fit show that, like G141A CPR, the derived rates for each of the three phases observed for the RHR of G141T CPR were very similar to that of WT CPR. In the trial with stoichiometric NADPH, the K1 values are very close at 42.6 and 43.1 s^{-1} for WT and G141T, respectively; however, the K2 and K3 values of 2.84 and 0.0210 s^{-1} are lower for G141T than for WT CPR (5.72 and 0.587 s^{-1}). Although the differences in K2 and K3 are again not especially substantial, they represent a continued trend from the G141A CPR data. In contrast to G141A, the K1 and K2 values for G141T CPR increase in the reactions with excess NADPH. To reiterate an important point obtained from analyses, the time courses for the RHR's of WT, G141A, and G141T CPR were observed to be quite similar but with minor changes to the apparent rates observed for the second and third phases, *i.e.* K2 and K3.

G141T CPR

22a-

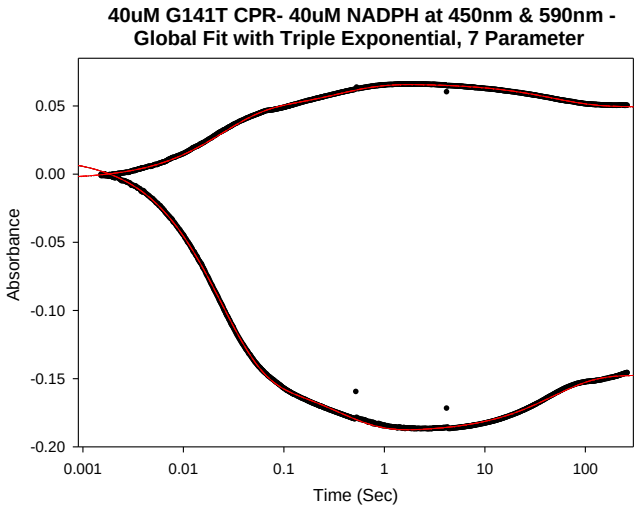

22b-

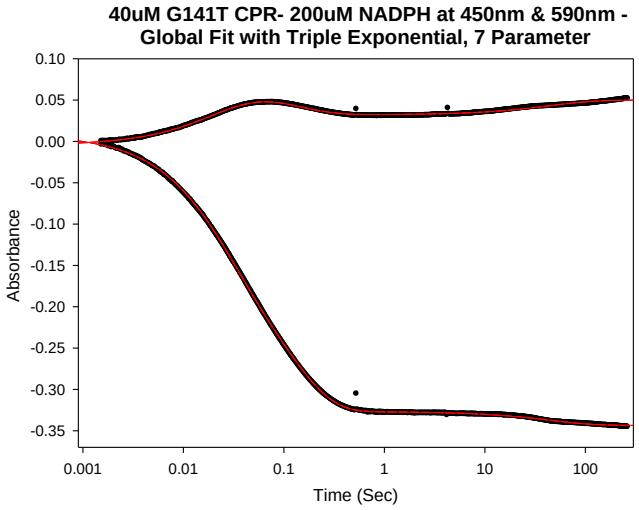

22c-

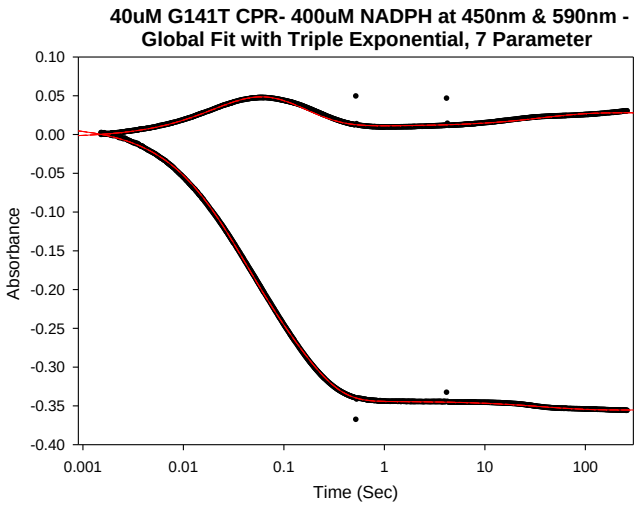

22d-

G141T CPR

	40 uM NADPH		200 uM NADPH		400 uM NADPH	
	450nm	***590nm***	***450nm***	***590nm***	***450nm***	***590nm***
A1	0.163	-0.0499	0.144	-0.0712	0.158	-0.0867
K1	**43.1**		**44.5**		**38.2**	
A2	0.0389	-0.0202	0.191	0.0346	0.198	0.0721
K2	**2.84**		**8.69**		**7.30**	
A3	-0.0416	0.0170	0.0167	-0.0177	0.0112	-0.0173
K3	**0.0210**		**0.0221**		**0.0264**	

Figure 22- The thick black lines are the averaged reductive half-reaction traces between 40 µM G141T CPR and 40 µM (22a), 200 µM (22b) and 400 µM (22c) NADPH measured at 450 nm and 590 nm. The 590 nm trace is the upper trace and 450 nm is the lower trace for all graphs. The thin red line on each graph represents the triple exponential, 7 parameter fit to the data and the related rates and relative absorbance values can be seen in the table in 22d.

Reductive half-reaction of G141del CPR: The averaged time courses RHR for the G141del CPR variant at 40, 200, and 400 μM NADPH at both 450 nm and 590 nm (see Figure 23a-c) were again best fit to a triple exponential, 7 parameter equation (see table in Figure 23d). A striking difference was noted for the reaction profile for this variant at the stoichiometric amount NADPH, especially at 590 nm, compared to the others. At 590 nm for the other variants, there are two major phases associated with the formation of the semiquinone state: (1) the major and most rapid phase represented by K1 and (2) slower and minor phase represented by K2. In contrast, G141del CPR has the initial phase of semiquinone formation just like the other CPR variants, however, the K2 represents a rapid loss of absorbance at 590 nm. This observation indicates that the disemiquinoid species of G141del CPR, which is being formed (K1 = 69.8 s^{-1}), is rapidly lost (K2 = 16.3 s^{-1}). This transient formation of the semiquinone is unique to G141del, but these results were not wholly unexpected since the anaerobic redox titrations of G141del FBD showed very little stable formation (<10%) of the neutral semiquinone state. Additionally, in all RHR's the K1 of G141del CPR is larger than the WT CPR, however, in excess NADPH the K2, A2 and K3, A3 values are essentially the same for WT CPR and the reaction traces are similar looking as well.

The two differences found in the RHR's for G141del CPR are particularly interesting when compared to those of wild-type BMR (BM-3's diflavin reductase domain). Recall that the FMN-binding loop of G141del resembles that of BM-3 in that it is missing the conserved glycine and is shorter and less flexible than the binding loop of WT CPR. With this in mind, the observed rates of K1 for WT BMR is >700 s^{-1} in excess NADPH according to Munro *et al.* (and in this lab numbers ~300-400 s^{-1} are obtained) and the semiquinone formation in BMR is only transient

just as it is in G141del CPR [12,24]. BMR's rate of K1 for stoichiometric amounts of NADPH was 159 s^{-1} at 590 nm and also there was also only transient semiquinone formation [Unpublished Swenson Lab data obtained by myself]. The reaction traces for G141del CPR are mostly similar to WT CPR, however especially at stoichiometric NADPH, G141del shows characteristic of WT BMR RHRs. The unique nature of the rapid loss of the disemiquinoid state by G141del CPR will be explored in depth later in this thesis.

G141del CPR

23a-

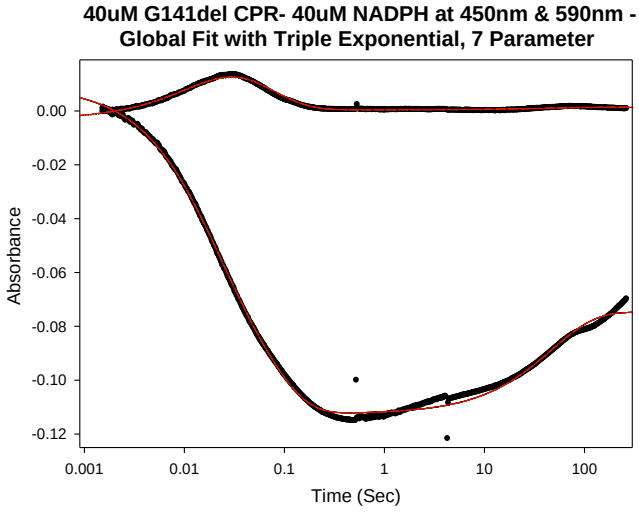

23b-

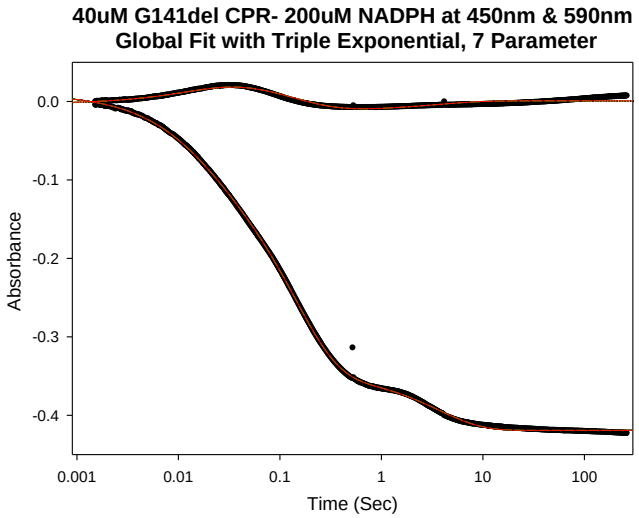

23c-

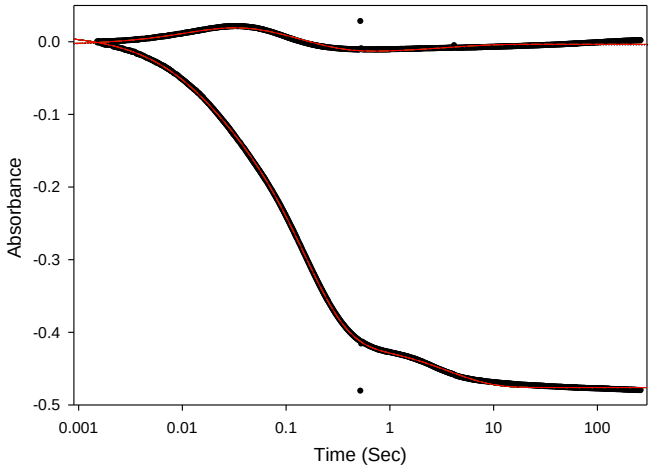

23d-

G141del CPR

	40 uM NADPH		**200 uM NADPH**		**400 uM NADPH**	
	450nm	***590nm***	***450nm***	***590nm***	***450nm***	***590nm***
A1	0.0530	-0.0291	0.0815	-0.0339	0.078	-0.0362
K1	**69.8**		**65.6**		**72.6**	
A2	0.0687	0.0257	0.276	0.0429	0.347	0.0473
K2	**16.3**		**7.20**		**6.86**	
A3	-0.0378	-0.0010	0.0709	-0.0125	0.0618	-0.0119
K3	**0.0212**		**0.275**		**0.2743**	

Figure 23- The thick black lines are the averaged reductive half-reaction traces between 40 µM G141del CPR and 40 µM (23a), 200 µM (23b) and 400 µM (23c) NADPH measured at 450 nm and 590 nm. The 590 nm trace is the upper trace and 450 nm is the lower trace for all graphs. The thin red line on each graph represents the triple exponential, 7 parameter fit to the data and the related rates and relative absorbance values can be seen in the table in 23d.

Reductive half-reaction of WT CPR with competitive inhibition of $NADP^+$: The above described results point to some significant differences in the mechanism of electron transfer and distribution over the course of the RHR, especially for the G141del variant. However, as discussed at beginning of this section, the reactions traces being multiphasic do not conform to the simple reaction mechanism shown in Figure 19. In order to interpret the observed changes in response to the Glycine-141 alterations, a series of experiments were performed to explore the basis for multiple phases of reduction seen in all the CPR variants, with a particular interest in WT CPR. Although the second phase of reduction seen at 450 nm and 590 nm for stoichiometric NADPH at WT CPR was different from the expected results, the second phase seen in excess NADPH has been explained. Previously published stopped-flow spectrophotometric studies at excess NADPH attributed the second phase of reduction to the release of $NADP^+$, subsequent binding of a second NADPH molecule, and finally a transfer of an additional hydride to CPR taking the both flavins from the semiquinone state to the hydroquinone state [13,19]. Our reaction time courses at the higher concentrations of NADPH in excess of the reductase, *i.e.* 200 and 400 μM NADPH, support this conclusion in WT CPR, with a second phase corresponding to loss of absorbance at 590 nm and loss of absorbance at 450 nm. However, our results for the trials using stoichiometric amounts of NADPH also contain a second phase of reduction that is related to a loss of absorbance at 450 nm (loss of oxidized flavin), but an unexpected continuation of the increase in the absorbance at 590 nm (formation of the semiquinone). Because this second phase seems to be occurring at a similar rate at all NADPH concentrations (see Figure 20d), it is tempting to speculate that this phase is associated

with the release of $NADP^+$ and subsequent effects on the rate of distribution of the electrons between the two flavin cofactors.

To test this hypothesis that the second phase is related to $NADP^+$ binding and/or release, a stopped-flow experiment was performed in which 40 μM of WT CPR was reacted with 40 μM NADPH with increasing concentrations of $NADP^+$(40, 200, or 400 μM). The expected result, if there is competitive binding, is that rates (K1, K2 and K3) should decrease as $NADP^+$ concentration increases. The results conform to the expectations and as in previous RHRs, the 450 nm and 590 nm absorbance data were again fit to a triple exponential, seven parameter rate equation (see Figure 24). The rates show a steady decrease as the $NADP^+$ concentration increases as follows: K1 = 42.6, 17.6, 6.03, 2.40 s^{-1}; K2 = 5.72, 1.45, 0.755, 0.33 s^{-1}; and K3 = 0.587, 0.0016, 0.0015, 0.002 s^{-1} (these values are for 0, 40, 200, and 400 μM $NADP^+$, respectively). Note that there is an exception to decreasing rate with K3 values, but again these values were almost too slow to be catalytically relevant. The decrease in the rate for the first phase (K1) was anticipated as this phase has been attributed to the hydride transfer from NADPH to the FAD. It seems very reasonable that $NADP^+$ would compete for the NADPH binding site. It has been shown that the adenosine moiety of the NADPH molecule is the primary binding component and this allows for binding of the similar molecules 2',5'-ADP [13] and $NADP^+$ [6,15] to CPR. Therefore, it seems likely that $NADP^+$, which is at increasing concentration as the reaction proceeds, present in the reaction solution could be competing with NADPH binding and, consequently, altering the progressive rate of further reduction of the flavins.

Following this experiment, we realized that although the observed rates were inversely related to the concentration of $NADP^+$, this did not technically show that competitive binding was causing the decreased rates. A second explanation is that the $NADP^+$ is binding tightly to WT CPR and forming a non-functional version of the enzyme, not that $NADP^+$ is just occupying the binding site of NADPH. To provide further support for the competitive binding hypothesis, a second set of stopped-flow spectrophotometric studies were performed, but in this set 40 µM WT CPR was reacted with 200 µM $NADP^+$ with increasing concentrations of NADPH: 40, 200, or 400 µM. The premise was that if competitive binding was in play then increasing the concentration of NADPH in the reaction solution should make NADPH binding more likely, effectively decreasing the chances of $NADP^+$ occupying the binding site and increasing the rate of WT CPR reduction. Again, similar triphasic reaction time courses were obtained (see Figure 25). However, in the presence of $NADP^+$, the increasing concentration of NADPH increased the observed rates as follows: K1 = 4.63, 7.46, 14.5 s^{-1}; K2 = 0.548, 3.10, 6.43 s^{-1}; and K3 = 0.0024, 0.0159, 0.022 s^{-1} (these values are for 40, 200, and 400 µM NADPH, respectively). Thus, these results are consistent with a competition between NADPH and its oxidation product $NADP^+$ which, again, can easily be rationalized for the first and fastest phase associated with hydride transfer.

40, 200, & 400 uM NADP + 40 uM NADPH shot against 40 uM WT CPR

	40 uM NADP		200 uM NADP		400 uM NADP	
	450nm	*590nm*	*450nm*	*590nm*	*450nm*	*590nm*
A1	0.100	-0.0338	0.0926	-0.0349	0.081	-0.0302
K1	**17.8**		**6.03**		**2.4**	
A2	0.0613	-0.0216	0.0777	-0.0267	0.085	-0.0325
K2	**1.45**		**0.755**		**0.33**	
A3	-0.100	-0.0156	-0.0645	-0.0189	-0.0181	-0.0156
K3	**0.0015**		**0.0016**		**0.002**	

Figure 24- This table represents the reductive half-reaction of WT CPR with stoichiometric NADPH in the presence of increasing amounts of $NADP^+$. As a reference, the rate values for the stoichiometric reductive half-reaction of WT CPR without $NADP^+$ are K1 = 42.6, K2= 5.72, and K3 = 0.587.

40uM WT CPR + 200uM NADP shot against 40, 200, and 400 uM NADPH

	40 uM NADPH		200 uM NADPH		400 uM NADPH	
	450nm	*590nm*	*450nm*	*590nm*	*450nm*	*590nm*
A1	0.137	-0.0485	0.280	-0.084	0.112	-0.0931
K1	**4.63**		**7.46**		**14.5**	
A2	0.0711	-0.0282	0.0536	-0.0036	0.262	0.0247
K2	**0.548**		**3.10**		**6.43**	
A3	-0.0998	-0.0179	0.0575	-0.0245	0.0593	-0.037
K3	**0.0024**		**0.0159**		**0.022**	

Figure 25- This table represents the reductive half-reaction of WT CPR with 200 µM $NADP^+$ in the presence of increasing amounts of NADPH. As a reference, the rate values for the stoichiometric reductive half-reaction of WT CPR without $NADP^+$ are K1 = 42.6, K2= 5.72, and K3 = 0.587.

However, competitive binding does not fully explain the second or third phase of reduction present in WT CPR at stoichiometric NAPDH. These phases would seem to occur after the initial reduction of the FAD and more so with the second phase which seems to be associated with the redistribution of the two electrons between the two flavin cofactors as the disemiquinoid species is formed. Therefore, an even more complex mechanism must be developed to explain these portions of the reaction trace of the RHR. Nonetheless, these experiments just discussed (as seen in the kinetic modeling) provided an important step in the mechanism of electron transfer in WT CPR. An expanded mechanism and efforts to fit the data to this mechanism will be discussed in detail below.

Reductive half-reaction of G141A, G141T and G141del CPR with competitive inhibition of $NADP^+$: Similar studies of competitive binding in the WT CPR were performed with G141A, G141T and G141del CPR. The results were very similar in that increasing the amount of $NADP^+$ in RHR experiments was found to decrease all observed rates of reduction. One observation of interest is that during an experiment of 40 μM G141del CPR with 80 μM NADPH and increasing concentrations of $NADP^+$ (40, 200, or 400 μM) the overall data could not be globally fit because although the absorbance changes at 590 nm appeared the same as the stoichiometric reaction, the absorbance change showed that a second round of reduction was occurring with G141del. This turnover (a second round or reduction) was unseen in identical experiment performed on G141A and G141T CPR. At the time this observation was unremarkable, but as will be shown in the kinetic modeling results, this information lends itself to support the unique flavin reduction characteristics of G141del CPR.

Kinetic modeling of the reductive half-reaction in CPR: As mentioned, a simple model of electron transfer shown in Figure 19 in CPR with stoichiometric NADPH cannot adequately explain the multiphasic results obtained for the RHR. This model does not account for the release of the oxidation product $NADP^+$ and 1) the possibility for competitive binding between NADPH and $NADP^+$ and 2) the effect of $NADP^+$ either being bound to or released differentially from the various redox states of the CPR enzyme during the course of the reaction. Our next task was to devise a mechanism based on the redox states observed for FAD and FMN that was capable of fitting the RHR absorbance data at 450 nm and 590 nm for all CPR variants, especially at stoichiometric levels of NADPH. As an exceptional aid in this process, the KinTek® Global Kintek Explorer software was employed. This very sophisticated software program (kindly loaned to us by Dr. Zucai Suo) provides the flexibility of formulating often complex reaction mechanisms which then uses integration algorithms to simulate the reaction time course of the reaction. The program allows one to plot the time course for the formation and conversion of every reaction intermediate involved. By applying known extinction coefficients for each species, in this case at 450 nm and 590 nm, a simulated time course can be calculated for both wavelengths. But, most importantly, the program can be used to establish the individual microscopic rate constants for each step of the proposed model that are consistent with the reaction time course. The program also allows for the simultaneous "global fitting" of multiple data sets generated for the same enzyme, but under different conditions such as various substrate concentration and, in our case, in the presence of different concentrations of $NADP^+$. Thus, this powerful program very effectively allows us to acquaint our kinetic data to specific biochemical steps. The specific goals of these modeling studies was to: (1) determine what was

causing the second phase of reduction in all CPR variants and (2) find out what was causing the disparity between the semiquinone formation in G141del CPR and the other variants. To achieve these goals we first had to build a mechanism that could fit the reaction traces for WT, G141A, G141T and G141del CPR variants and then we could compare the microscopic rate constants to identify the differences in electron transfer between the variants.

Throughout the process of modeling reactions, we tried to keep the kinetic model as simple as possible and additions made to the model always had a basis in either our own experimentation or conclusions made from literature sources. The growth of our model went through four iterations: (1) Minimal Model, (2) Moderate Model Mk.I, (3) Moderate Model Mk.II, and (4) the Full Model (see Figure 26). We began with the minimal model of electron transfer representing the simplest version and the general mechanism of two electron transfer into and within CPR and, as previously mentioned (Figure 19 and 26a), this model could not fit the data. The mechanism was made more complex by adding the release of $NADP^+$ from the FADhq/FMNox and the FADsq/FMNsq redox states to generate the Moderate Model Mk.I. The idea that the enzyme character changes with or without $NADP^+$ relates back to the fact that binding/release of $NADP^+$ causes conformational changes in CPR which effect activity [6,10,15]. Additionally, the release of $NADP^+$ from WT CPR creating two functional forms of the reduced enzyme in kinetics studies has been hypothesized by *Gutierrez et al.* [19]. The Moderate Model Mk.II incorporated the competitive binding of $NADP^+$ (released from CPR after hydride transfer) to the NADPH-binding site. The evidence for this step came from our experimentation described in the section, "*Reductive half-reaction of WT CPR with competitive inhibition of*

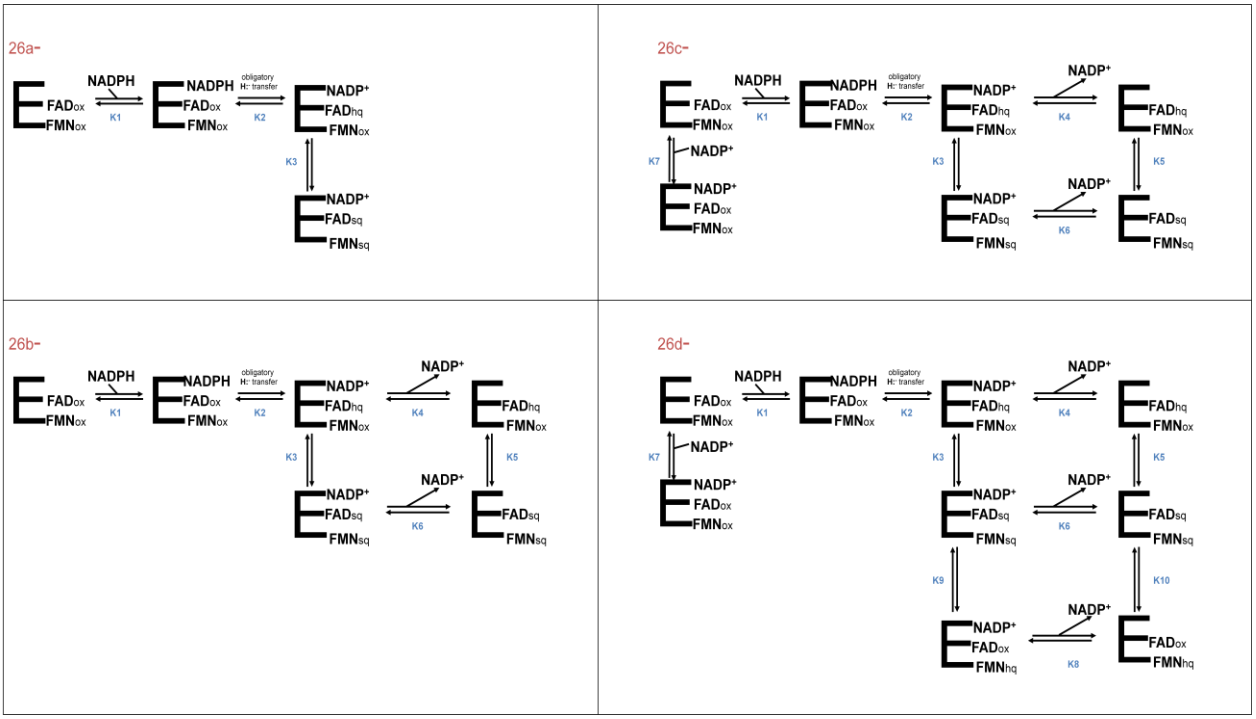

26e- The Full Model

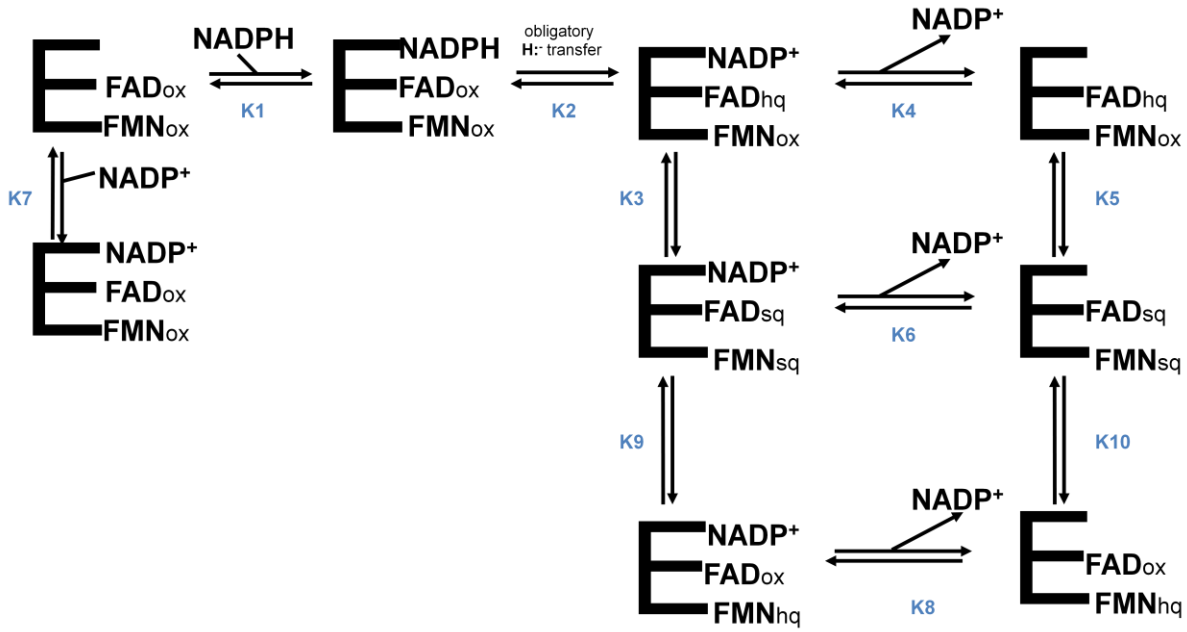

Figure 26- These four represent the four models of the reductive half-reaction created, including the Minimal Model (a), the Moderate Model Mk.I (b), the Moderate Model Mk.II (c), and the Full Model (d). The Full Model (expanded in 26e) is the mechanism which best represents the electron transfer in WT, G141A, G141T, and G141del CPR.

$NADP^+$." However, despite the additions to the model, the fits to the WT CPR reaction traces at 450 nm and 590 nm were unsatisfactory. The addition of the FADox/FMNhq redox species with and without the bound $NADP^+$ in the Full Model gave us a model that quite adequately fit the time courses for the reductive half-reaction for the WT CPR (and the other CPR variants as well) for all of the reaction condition studies (see Figure 26e, for a larger view of the Full Mechanism). The formation of the FADox/FMNhq was added after the consideration that in many diflavin reductases (BM-3 for example) the disemiquinoid species is formed only transiently before both electrons derived from the NADPH travel to and accumulate on the FMN cofactor. It seemed likely that in CPR there might not be full stabilization of the disemiquinoid species and an eventual formation of the FADox/FMNhq. This was certainly likely to be the case for the G141del variant where the disemiquinoid was only formed transiently (see reaction trace 23a at 590 nm).

The Full Model was used to perform a global fit to the reaction time courses at 450 nm and 590 nm at stoichiometric amounts of NADPH for WT CPR. The fit to this data had very little error and there was only a small difference between the experimentally obtained molar extinction coefficients from the Full Model and the initially calculated extinction coefficients based on literature values. After this initial fitting, the acquired microscopic rate constants were used as a starting point for the global fitting of the half-reactions of WT CPR with stoichiometric levels of NADPH and 0, 40, and 200 μM $NADP^+$ (see Figure 27, 28). The Full Mechanism was again found to accurately fit all three half-reaction trials. In addition, the K_d values calculated from the appropriate forward and reverse microscopic rate constants for those steps involving nucleotide binding were quite comparable to literature values. The calculated K_{eq} values for the

other steps were also reasonable. Thus, the global fitting of all of the data for the WT CPR to this mechanism was very gratifying and provides substantial confidence in the devised mechanism. Furthermore, conclusions can be drawn from the microscopic rate constants obtained from the fitting. First, the rate k2+ corresponds to the rate of hydride transfer and has a value of 43 s^{-1}, which is very close to the observed rate of 42.6 s^{-1} attributed to hydride transfer. Additionally, the second order rate constant for NADPH binding, k1+, of 85.6 uM^{-1} s^{-1} combined with the initial concentration of the NADPH generates rates that are, in fact, much higher than hydride transfer as proposed from the absence of a NADPH concentration dependence for this initial reductive phase. Second, K3+, which represents the transfer of one electron from the FAD to FMN to form the disemiquinoid species was shown to be 124 s^{-1} from the fitting, which is also faster than hydride transfer, again consistent with hydride transfer being the rate limiting step and explains why the formation of the disemiquinoid species is concomitant with hydride transfer. Thirdly, it became very clear, through the essential nature of the $NADP^+$ competitive binding step (step K7 in the model) and the ability of the model to fit the $NADP^+$ addition trials, that $NADP^+$ competitively binding with NADPH does play a role in the overall rate of reduction in WT CPR and in particular the second phase. Finally, and perhaps one of the most important revelations is that the second and third phases of the reduction observed in the RHR cannot be attributed specifically to any single microscopic rate constant. After many iterations of fitting and observation of species formation within the KinTek program it has become clear that the observed rates of the second and third phase are the combination of several microscopic rates.

Wt CPR and Stoich NADPH and various $NADP^+$- Global fit of 450 + 590 data

Kintek Global Fit Data

Rate	K1	K2	K3	K4	K5	K6	K7	K8	K9	K10
K+	85.6	43	124	12.9	0.532	32.3	39.6	0.0717	125	190
K-	229	0.17	53.7	0.109	0.399	0.155	58.2	0.01	62.6	134
Kd (uM)	2.7			118.3		208.4	1.47	7.2		
Lit. Kd (uM)	6.5	-	-	-	-	-	0.76	-	-	-
Keq (uM)		252.9	2.3		1.3				2.0	1.4

Molar Extinction Coefficients ($\mu M^{-1} cm^{-1}$)

	FADox/FMNox	FADhq/FMNox	FADsq/FMNsq	FADox/FMNhq
Initially Calculated:				
450nm:	0.0204	0.0124	0.0059	0.0124
590nm:	0	0	0.0092	0
Experimentally Obtained:				
0uM $NADP^+$ to 40uM NADPH				
450nm:	0.0021	0.0133	0.0059	0.0133
590nm:	0	0	0.0102	0
40uM $NADP^+$ to 40uM NADPH				
450nm:	0.0205	0.0154	0.0065	0.0154
590nm:	0	0	0.0078	0
200uM $NADP^+$ to 40uM NADPH				
450nm:	0.0204	0.0138	0.0068	0.0138
590nm:	0	0	0.0094	0

Figure 27a. The top chart shows the microscopic rate constants that were obtained from fitting the WT CPR reductive half-reactions with differing concentrations of $NADP^+$. The bottom chart shows the molar extinction coefficients obtained from fitting the experimental data.

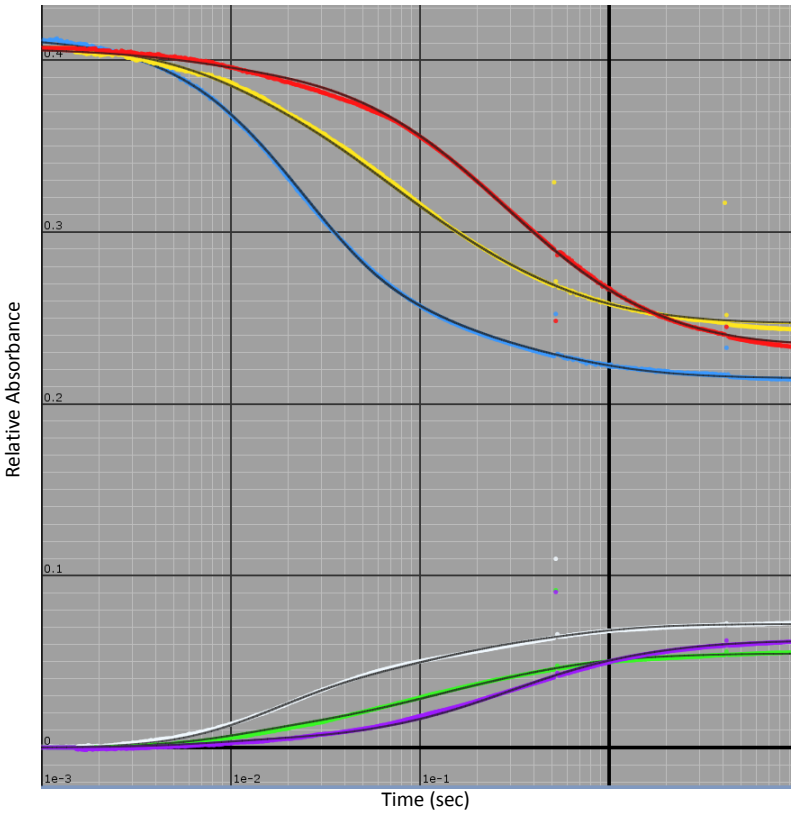

Figure 27b. This data reflects the global fitting of the WT CPR data with and without $NADP^+$ added. The blue and white lines represent the 450 nm and 590 nm reaction traces, respectively, for the 0 µM $NADP^+$ RHR. The yellow and green lines represent the 450 nm and 590 nm reaction traces, respectively, for the 40 µM $NADP^+$ RHR. The red and purple lines represent the 450 nm and 590 nm reaction traces, respectively, for the 200 µM $NADP^+$ RHR.

Global fit of reductive half-reactions of Glycine-141 variants to the initial reduction steps within the Full Model: The Full Model (Figure 26e) was used in the globally fitting of the reaction time courses at 450 nm and 590 nm for the RHR's for each of the G141A, G141T, and G141del CPR variants with the stoichiometric amounts of NADPH as the reductant as done for WT CPR. With a few very notable exceptions, most often for the G141del variant, the microscopic rate constants, K_d values, K_{eq} values, and experimentally obtained molar extinction coefficients were nearly always very similar to those of WT CPR. A summary of all rate constants and parameters obtained from the fitting process are summarized along with graphical fitting results for each variant in Figures 28-30. Much like WT CPR, many of the same conclusions can be drawn from the microscopic rate constants and the overall mechanism. In this section, those parameters that are part of the initial reduction steps will be summarized with a separate discussion later for those differences noted primarily for the G141del variant.

The value for the microscopic rate constant k2+ (representing hydride transfer) has a value of 55.7 s^{-1} and 66.2 s^{-1} for the G141A and G141T variants, respectively. Both values conform reasonably well to the observed rate for the first phase of reduction which was 32.6 s^{-1} and 43.1 s^{-1} for each variant, respectively. The k2+ values for both variants are perhaps slightly higher than that obtained for the WT enzyme (43 s^{-1}). As with WT, this rate constant does remain lower than the product of the second order rate constant k1+ and the initial NADPH concentration as well as k3+ associated with the formation of the disemiquinoid species, again indicating that this step is rate limiting in both variants. Perhaps of significance, the k2+ value for the G141del variant was somewhat smaller (11.8 s^{-1}) suggesting that this alteration may

have some influence on this reductive step. The k3+ values for all three variants are similar to that of WT.

Secondly, the K_d value calculated from k7+ and k7- is low (~1.5-1.8 μM) and in the same range as that calculated for NADPH (from k1+ and k1-) for both the G141A and G141T variants. Both the K_d values (for the binding of NADPH and $NADP^+$) compare favorably with literature values determined by other methods although the K_d calculated for $NADP^+$ for the G141del variant tended to be somewhat higher. Nevertheless, these observations are consistent with the presence of the competitive binding of $NADP^+$ to the initial oxidized state of reductase, supporting the importance of including this process in the interpretation of the overall electron transfer mechanism. The similarity for these aspects of the electron transfer mechanism is expected considering they involve the FAD-binding domain which is identical for all CPR variants and well separated from the Glycine-141 alteration occurring in the separate FMN-binding domain. Finally, as was the case for the WT CPR, the second and third slower observed phases of reduction time course appear to be the combination of several microscopic rate constants in all three variants. Thus, this minor modification resulted in only relatively small changes, if any, to the microscopic rate constants derived for each step in this mechanism.

G141A CPR and Stoich NADPH- Global fit of 450nm + 590nm data.

Kintek Global Fit Data

Rate	K1	K2	K3	K4	K5	K6	K7	K8	K9	K10
k+	85.6	43	124	12.9	0.532	32.3	39.6	0.0717	125	190
k-	229	0.17	53.7	0.109	0.399	0.155	58.2	0.01	62.6	134
Kd (uM)	2.7			118.3		208.4	1.47	7.2		
Lit. Kd (uM)	6.5	-	-	-	-	-	0.76	-	-	-
Keq (uM)		252.9	2.3		1.3				2.0	1.4

Molar Extinction Coefficients (µM-1cm-1)

	FADox/FMNox	FADhq/FMNox	FADsq/FMNsq	FADox/FMNhq
Initially Calculated:				
450nm:	0.0204	0.0124	0.0059	0.0124
590nm:	0	0	0.0092	0
Experimentally Obtained:				
0uM $NADP^+$ to 40uM NADPH				
450nm:	0.0203	0.0120	0.0059	0.0120
590nm:	0	0	0.0095	0

Figure 28a- The top chart shows the microscopic rate constants that were obtained from fitting the G141A CPR reductive half-reaction performed with stoichiometric NADPH. The bottom chart shows the molar extinction coefficients obtained from fitting the experimental data.

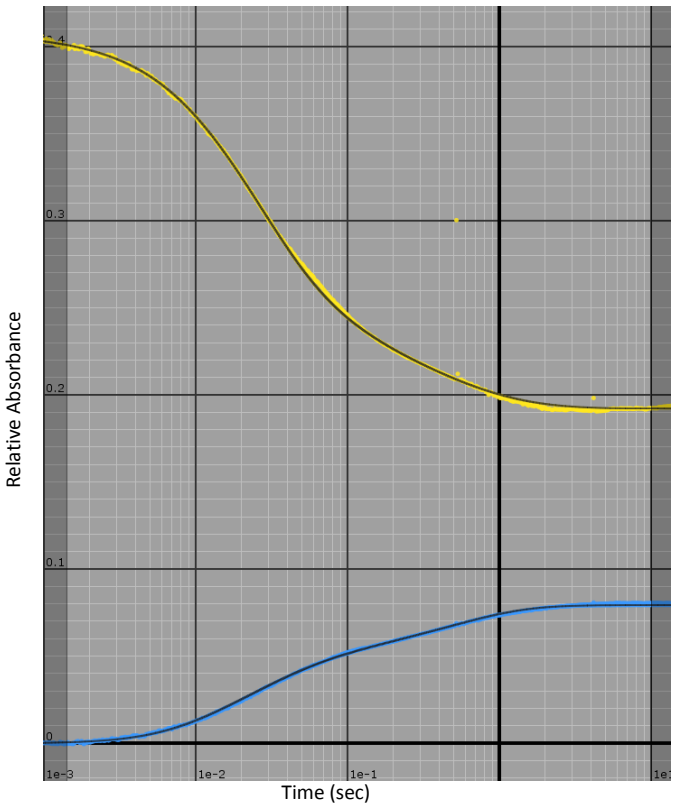

Figure 28b. This data reflects the global fitting of the G141A CPR data without $NADP^+$ added. The yellow and blue lines represent the 450 nm and 590 nm reaction traces, respectively, for the RHR with stoichiometric amounts of NADPH.

G141T CPR and Stoich NADPH- Global fit of 450nm + 590nm data

Kintek Global Fit Data

Rate	K1	K2	K3	K4	K5	K6	K7	K8	K9	K10
k+	129	66.2	131	7.88	1.4	12	35.8	0.397	151	178
k-	848	2.99	62.8	1.82	1.03	0.0187	66.2	0.024	106	115
Kd (uM)	6.6			4.3		641.7	1.85	16.5		
Lit. Kd (uM)	6.5	-	-	-	-	-	0.76	-	-	-
Keq (uM)		22.1	2.1		1.4				1.4	1.5

Molar Extinction Coefficients (µM-1cm-1)

	FADox/FMNox	FADhq/FMNox	FADsq/FMNsq	FADox/FMNhq
Initially Calculated:				
450nm:	0.0204	0.0124	0.0059	0.0124
590nm:	0	0	0.0092	0
Experimentally Obtained:				
0uM $NADP^+$ to 40uM NADPH				
450nm:	0.0203	0.0120	0.0059	0.0120
590nm:	0	0	0.0095	0

Figure 29a- The top chart shows the microscopic rate constants that were obtained from fitting the G141T CPR reductive half-reaction performed with stoichiometric NADPH. The bottom chart shows the molar extinction coefficients obtained from fitting the experimental data.

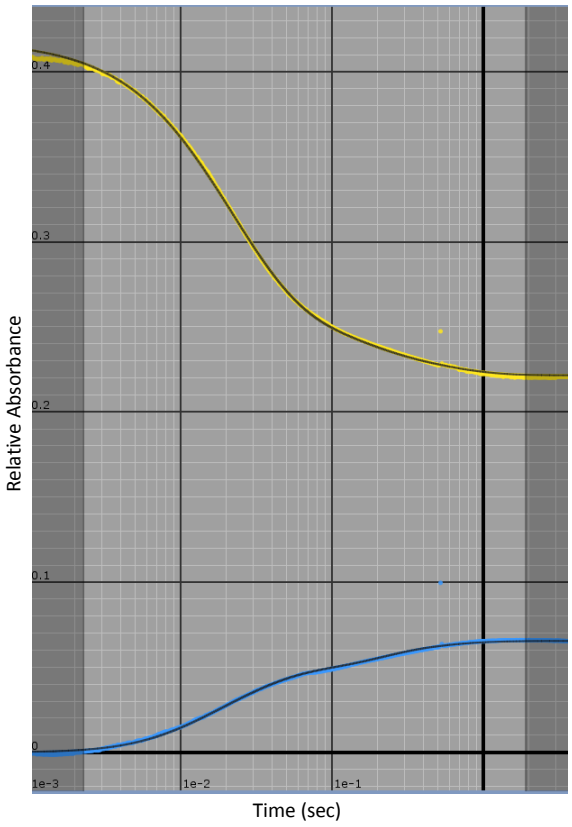

Figure 29b. This data reflects the global fitting of the G141T CPR data without $NADP^+$ added. The yellow and blue lines represent the 450 nm and 590 nm reaction traces, respectively, for the RHR with stoichiometric amounts of NADPH.

G141del CPR and Stoich NADPH- Global fit of 450nm + 590nm data

Kintek Global Fit Data

Rate	K1	K2	K3	K4	K5	K6	K7	K8	K9	K10
k+	64.5	11.8	81	11.9	1.06	365	15.5	0.00829	2.78	238
k-	320	0.653	37.6	1.03	0.864	12.9	101	0.00234	1.25	0.341
Kd (uM)	5.0			11.6		28.3	6.52	3.5427		
Lit. Kd (uM)	6.5	-	-	-	-	-	0.76	-	-	-
Keq (uM)		18.1	2.2		1.2269				2.2	697.9

Molar Extinction Coefficients (µM-1cm-1)

	FADox/FMNox	FADhq/FMNox	FADsq/FMNsq	FADox/FMNhq
Initially Calculated:				
450nm:	0.0204	0.0124	0.0059	0.0124
590nm:	0	0	0.0092	0
Experimentally Obtained:				
0uM $NADP^+$ to 40uM NADPH				
450nm:	0.0204	0.0147	0.0061	0.0147
590nm:	0	0	0.0101	

Figure 30a- The top chart shows the microscopic rate constants that were obtained from fitting the G141del CPR reductive half-reaction performed with stoichiometric NADPH. The bottom chart shows the molar extinction coefficients obtained from fitting the experimental data.

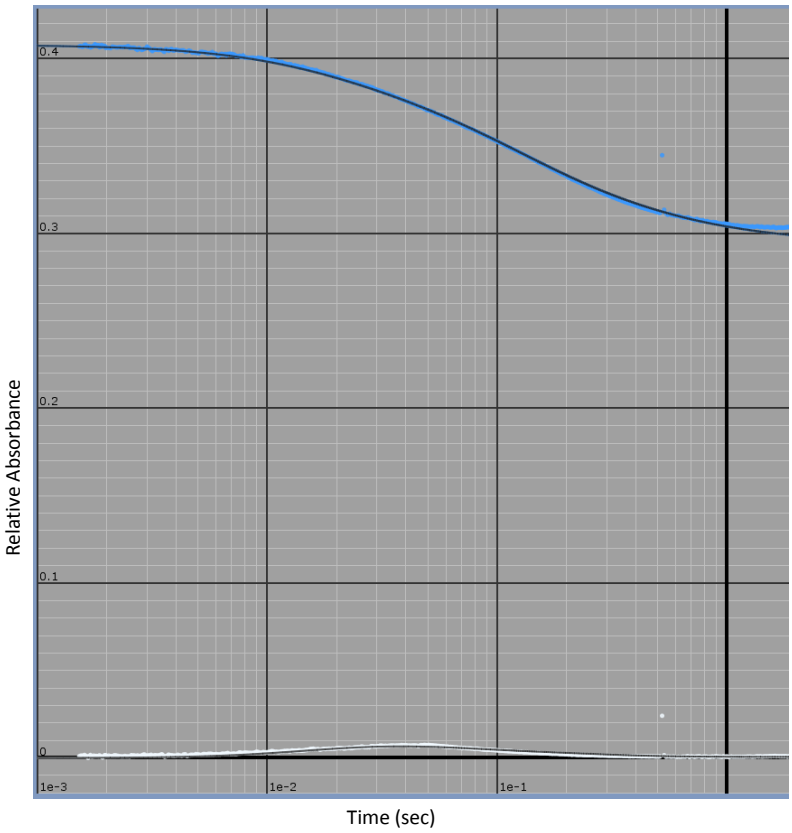

Figure 30b. This data reflects the global of the G141del CPR data without $NADP^+$ added. The yellow and white lines represent the 450 nm and 590 nm reaction traces, respectively, for the RHR with stoichiometric amounts of NADPH.

Analysis of the reliability of the microscopic rate constants obtained from the global fitting: Before proceeding to a more detailed discussion regarding the differences observed for primarily the G141del variant, it is important to establish for the reader the relative reliability of the microscopic rate constants and parameters obtained from the mechanistic global fitting analyses. This process was deemed to be essential in order to gain confidence in the values for comparisons within the variants and in the final mechanistic interpretations. The results of these analyses are represented by the collection of the microscopic rate constants into a color-coded table of results shown in Figure 31. The amount of error or flexibility of each set of rate constants was analyzed by determining the range of values for each constant that was allowed while retaining an accurate fitting of the reaction traces for each CPR variant. The table is color coded to illustrate the relative "flexibility" or variability that could be accommodated for each microscopic rate constants. The relatively inflexible values (yellow) cannot be altered without significantly increasing the error in the data fit, the moderately flexible (orange) rates can accommodate a small range without affecting the data fitting, and the very flexible rates (pink) allow large variation in the values. (Note that the values shown for the moderately and very flexible values are those obtained from the best fit of the data). Essentially, the flexibility of the rates serves as a benchmark for the degree of confidence and mechanistic importance that can be placed on those values. The inflexible rates were taken to be more integral to the mechanism considering their specificity and the significant effect of their change. Conversely, the very flexible rate constants, which can vary many orders of magnitudes, cannot be conclusively related to any interpretations on the effect of the glycine alterations on the

mechanism of electron transfer due to the fact that changing their rate has little effect on fitting the absorbance data.

Therefore, with the reliability reflective in these flexibility "indices" in mind, the comparison of WT, G141A, and G141T CPR, led to some significant conclusions for the reductive half-reaction. Primarily, the values obtained for the microscopic rate constants K1, K2, K3, and K6 are relatively reliable ("inflexible") and the examination of these rate constants suggest that in WT, G141A, and G141T the disemiquinoid state (the FADsq/FMNsq species with or without the bound $NADP^+$) is the favored redox state. Following the rapid hydride transfer reflected in the rate constants K1 and K2, the formation of the disemiquinoid state reflected in K3. The K6 value indicates that the forward reaction representing the eventual loss of the bound $NADP^+$ is favored in these reductases. Additionally, the equilibrium constants derived from the K9 and K10 values for these CPR variants are all close to equilibrium value of 1, with a slight favor for the FADox/FMNhq state, illustrating that although a second electron transfer from FAD to FMN is possible in these varieties, the prevalent state is the FADsq/FMNsq. This interpretation of the electron transfer mechanism can be confirmed by two sources: (1) using the KinTek software to simulate the formation of each redox species employing the established kinetic constants and parameters substantiates that the FMNsq/FADsq species with and without bound $NADP^+$ is favored within a catalytically relevant timeframe, (2) the RHR with stoichiometric NADPH levels indicate that the reaction ends with the stable formation of predominately the FMNsq/FADsq species (high stable absorbance at 590 nm at the end of the time courses) and (3) the anaerobic redox titrations of WT, G141A, and G141T CPR show significant and stable semiquinone formation when two electron equivalents are added into each respective enzyme.

Global fit of the reductive half-reactions for the G141del CPR variant to all aspects of the Full Model: The RHR results obtained for the G141del CPR variant conformed very well to the Full Model just as for the other CPR variants (see Figure 30). As discussed, the similarity in the initial steps involving NADPH binding and hydride transfer was expected considering they involve the FAD-binding domain which should remain essentially unaltered in all CPR variants. However, the evaluation of the RHR with stoichiometric NADPH levels, specifically at 590 nm, shows a profound difference in the reaction time course compared to the other variants in that the disemiquinoid state of this form of the G141del reductase forms only transiently, being rapidly lost in the second observed phase. Examination of the microscopic rates of G141del CPR, especially within the reliability compilation shown in Figure 31 (but also in Figure 30), a unique profile of electron transfer became apparent. Three microscopic rates are markedly different between G141del and the other CPR variants (note that values for the CPR variants referred to here are averages of WT, G141A, and G141T CPR; this is done for ease of comparison). The first rate constant is k6+ which is very inflexible and displays a value of 365 s^{-1} in G141del, greater than ten-fold higher than the rate of average value of 27 s^{-1} of the other CPR variants. The second rate constant k9+, which has a value of 2.78 s^{-1}, is of interest because this value is 50-fold less than that for the WT, G141A and G141T variants (average of 132 s^{-1}). From the K9 value, we can conclude that there is little formation of the FADox/FMNhq form of the enzyme with the $NADP^+$ bound to the reductase. Finally, the K_{eq} calculated from the k10+ and k10- values for G141del is 698 (k10+: 238 s^{-1}/ k10-: 0.341 s^{-1}), a value strongly favoring the transfer of a second electron from FADsq to FMNsq to form the FADox/FMNhq species. The K_{eq} has a 1.4 average (k10+: 180 s^{-1}/ k10-: 130 s^{-1}) for WT, G141A, and G141T CPR showing only a minor favor

for the formation of FADox/FMNhq. Combining these differences it can be concluded that the electron transfer in G141del CPR forms the disemiquinoid state relatively quickly, releases the $NADP^+$ and then very quickly, and rather irreversibly, a second electron from the FADsq is transferred to the FMNsq causing the formation of the FADox/FMNhq. This preferred electron transfer pathway is highlighted by the orange-colored arrows in Figure 32. This mechanism, in which the disemiquinoid species is only transiently formed, is significantly different from the preferred, stable formation of the disemiquinoid state observed for the WT, G141A and G141T CPR variants. This mechanism of electron transfer can be confirmed primarily by three sources: (1) simulating the formation of each redox species using the KinTek software confirms that for a catalytically relevant timeframe that the majority species formed is the FMNox/FADhq without $NADP^+$, (2) the RHR for the G141del CPR in excess and stoichiometric NADPH show that before a second round of flavin reduction (shown by further decrease at 450 nm) takes place, the disemiquinoid species must first be converted to the FADox/FMNhq species (shown by loss of absorbance at 590 nm) in order that the fully oxidized FAD cofactor (FADox) can accept a second electron pair (as the hydride) as it must from NADPH, and (3) the anaerobic redox titration of the G141del FBD only shows only limited and transient disemiquinoid formation (<10%). The implications of these rather substantial differences for this variant will become apparent in the next section.

Figure 31- Microscopic Rate Constant Flexibility Table

Wt CPR and Stoich NADPH and various $NADP^+$- Global fit of 450 nm + 590 nm data

Kintek Global Fit Data

Rate	K1	K2	K3	K4	K5	K6	K7	K8	K9	K10
k+	85.6	43	124	12.9	0.532	32.3	39.6	0.0717	125	190
k-	229	0.17	53.7	0.109	0.399	0.155	58.2	0.01	62.6	134
Kd (uM)	2.7			118.3		208.4	1.47	7.2		
Lit. Kd (uM)	6.5	-	-	-	-	-	0.76	-	-	-
Keq (uM)		252.9	2.3		1.3				2.0	1.4

G141del CPR and Stoich NADPH- Global fit of 450 nm + 590nm data

Kintek Global Fit Data

Rate	K1	K2	K3	K4	K5	K6	K7	K8	K9	K10
k+	64.5	11.8	81	11.9	1.06	365	15.5	0.00829	2.78	238
k-	320	0.653	37.6	1.03	0.864	12.9	101	0.00234	1.25	0.341
Kd (uM)	5.0			11.6		28.3	6.52	3.5427		
Lit. Kd (uM)	6.5	-	-	-	-	-	0.76	-	-	-
Keq (uM)		18.1	2.2		1.23				2.2	697.9

G141A CPR and Stoich NADPH- Global fit of 450 nm + 590 nm data

Kintek Global Fit Data

Rate	K1	K2	K3	K4	K5	K6	K7	K8	K9	K10
k+	197	55.7	141	11.1	0.0309	37	32.2	0.0252	121	191
k-	1850	2.03	65.7	0.136	0.0223	0.0259	135	0.00162	91.8	143
Kd (uM)	9.4			81.6		1428.6	4.19	15.6		
Lit. Kd (uM)	6.5	-	-	-	-	-	0.76	-	-	-
Keq (uM)		27.4	2.1		1.4				1.3	1.3

G141T CPR and Stoich NADPH- Global fit of 450nm + 590nm data

Kintek Global Fit Data

Rate	K1	K2	K3	K4	K5	K6	K7	K8	K9	K10
k+	129	66.2	131	7.88	1.4	12	35.8	0.397	151	178
k-	848	2.99	62.8	1.82	1.03	0.0187	66.2	0.024	106	115
Kd (uM)	6.6			4.3		641.7	1.85	16.5		
Lit. Kd (uM)	6.5	-	-	-	-	-	0.76	-	-	-
Keq (uM)		22.1	2.1		1.4				1.4	1.5

→ (+) = Inflexible Microscopic Rate Constant
→ (++) = Moderately Flexible Microscopic Constant
→ (+++) = Very Flexible Microscopic Rate Constant

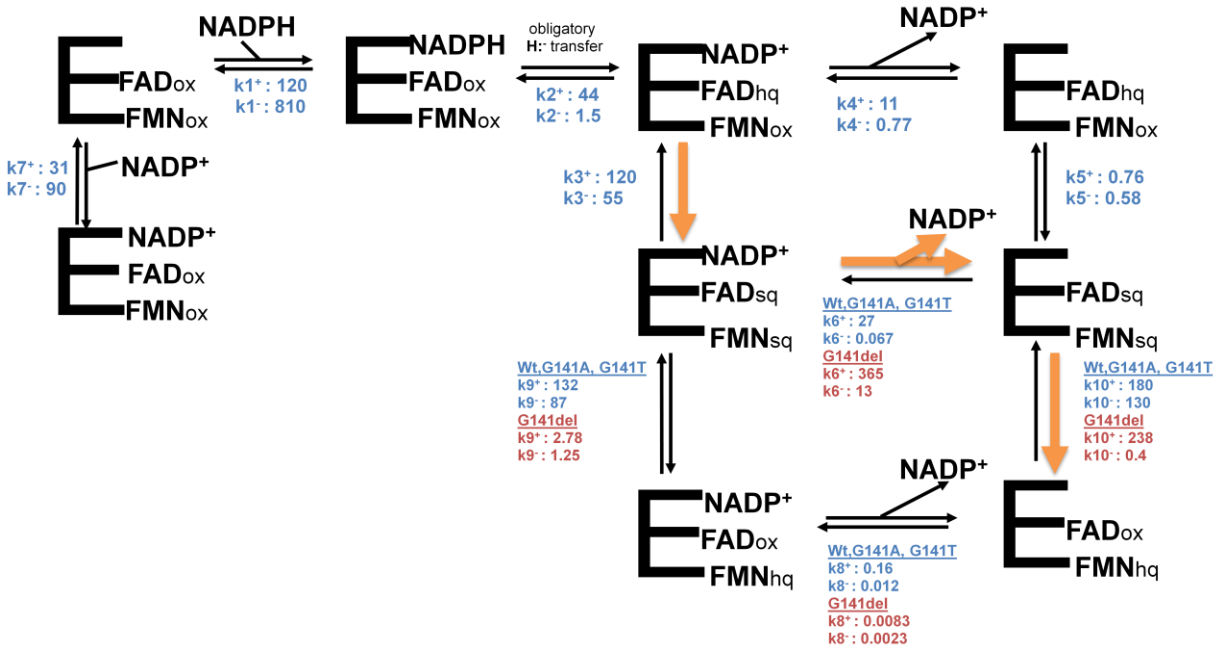

Figure 32- This is a cartoon of 2 electron reduction of the CPR variants. The microscopic rate constants for WT, G141A, and G141T CPR for K6, K8, K9 and K10 have been averaged due to the similarity of their electron transfer mechanism. Essentially, these proteins ultimately form the disemiquinoid form with or (more likely) without $NADP^+$. G141del CPR shows a different electron transfer mechanism, illustrated by the orange arrows. The rate constants K1, K2, K3, K4, K5, and K7 were similar between WT, G141A, G141T, and G141del and were averaged.

Oxidative Half-Reaction of WT CPR: The model for the RHR in CPR allowed for the determination of the mechanism of electron entrance into the enzyme and flow of electrons to and between the flavin cofactors. This mechanism, however, only accounts for a portion of the turnover of CPR. In an effort to complete our understanding of the entire electron transfer process for CPR, the oxidative half-reaction (OHR) was evaluated for the CPR variants. The OHR is of importance, especially in our investigation, because the FMN cofactor has been shown to be the electron donor to the final cytochrome acceptor in diflavin reductases. In particular, there is strong evidence to suggest that the FMNsq is the redox state that allows for transfer of electron out of CPR. In fact, it has been suggested that the reductase is inhibited when "over-reduced", a state in which the FMNhq is formed [6,15,18]. The primary goal of the OHR experiments were to determine the effect the Glycine-141 alterations had on the transport of electrons to cytochrome c acceptor in order to complete our understanding of this enzyme's overall steady-state turnover activity.

The OHR was first performed with WT CPR and our primary focus was on the two electron transport process under stoichiometric concentrations of NADPH. It has been shown in previous experiments in this lab that the rate of reduction of CPR by NADPH is fast compared to the transfer of electron to cytochrome c (which is the rate limiting step). This observation greatly simplifies the experiment because CPR does not have to be pre-reduced and maintained in a reduced state for extended periods of time, a feat that is difficult technically. It was possible then, to premix the cytochrome c with NADPH in one of the stopped-flow syringes and cytochrome reduction is only initiated when oxidized CPR is rapidly added through the stopped-flow instrument. For each trial, about 10 μM of WT CPR was reacted with a solution of 10 μM

NADPH and increasing concentrations of cytochrome c: 10, 20, 40, 80, and 160 µM. In this lab and the literature [18], previous experiments with excess CPR have shown that the OHR follows a monophasic, first order reaction demonstrating Michaelis-Menten kinetics. The proposed mechanism depicted in Figure 34 shows that the after binding occurs between reduced CPR and oxidized cytochrome c a single electron is transferred from CPR to cytochrome c, reducing it and causing an absorbance change at 550 nm. Therefore, under pseudo-first order conditions (when the cytochrome is in excess) a monophasic reaction, relating to this electron transfer is expected. Multiple concentrations of cytochrome c were used to assess the relationship between concentration and the rate of reduction and as a means to estimate the maximal rate achievable under saturating conditions. The experiment was performed in triplicate for each different concentration of cytochrome c and the reactions were monitored at 550 nm which reflects the change in absorbance between oxidized and reduced cytochrome c. The triplicate reaction traces were then combined into average reaction traces. For fitting and comparison, the 550 nm data was normalized to begin at zero and were plotted together (see Figure 33a). Upon first inspection, the reaction traces do appear to be monophasic with the apparent rate of cytochrome reduction increasing with the increasing concentration of cytochrome c (see Figure 33a). To specifically identify and assign a rate to this phase, the data was transferred into the SigmaPlot graphical plotting program for iterative fitting. A fairly satisfactory fit, especially for the OHRs with higher cytochrome c concentrations, was achieved using a single exponential, three parameter fit (see Equation 6 and 7).

(6) $y = y_0 + ae^{-bx}$ (this is the generic SigmaPlot equation)

(7) $A_{550} = y_0 + A_1^{-k_{obs1}t}$

33a-

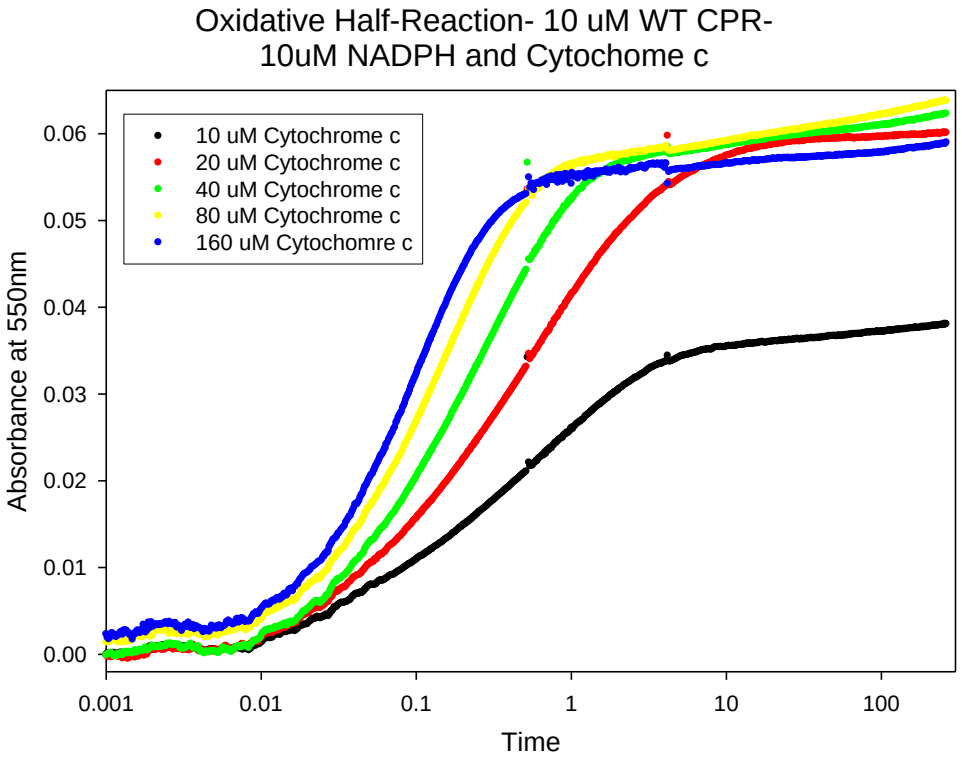

33b-

OHR of WT CPR with Stoich. NADPH + Cyt C - 1 Exponential Fit

10 uM Cyt C +10 uM NADPH	A1	K1	y_o
550 nm:	-0.0416	**1.91**	0.211
20 uM Cyt C +10 uM NADPH	A1	K1	y_o
550 nm:	-0.0714	**1.72**	0.301
40 uM Cyt C +10 uM NADPH	A1	K1	y_o
550 nm:	-0.0712	**3.66**	0.410
80 uM Cyt C +10 uM NADPH	A1	K1	y_o
550 nm:	-0.0693	**5.72**	0.557
160 uM Cyt C +10 uM NADPH	A1	K1	y_o
550 nm:	-0.0659	**8.54**	0.860

Figure 33- (a) The OHR reaction traces at 550 nm for the various cytochrome c concentrations. (b) The values from a single exponential, three parameter fit.

In equation 7, y_0 represents final absorbance; A_1 represent relative amplitude values; and $k_{obs}1$ represent the observed rate constants (referred to as K1). All of these values are shown in the table in Figure 33b. The apparent rates for 10, 20, 40, 80, and 160 µM were 1.91, 1.72, 3.66, 5.72, and 8.54 s^{-1}. These data were plotted (Figure 33c) and fit to a Michaelis-Menten hyperbolic fit (see Equation 8 and 9)

(8) Y = (a*x)/(b+x) (this is the generic SigmaPlot equation)

(9) $K_i = (K_{max}*[\text{cytochrome c}])/(K_d+[\text{cytochrome c}])$

where K_{max} is the maximum rate and K_d is the dissociation of cytochrome c. The values obtained for WT CPR were 15.1 s^{-1} and 63.1 µM for K_{max} and K_d respectively, and compared to the literature values our K_{max} was very close to the 14 s^{-1}, however the K_d was about two fold higher than the 37 µM obtained by *Grunau et al.* (see Figure 33c) [15]. However, the literature values were obtained under different experimental conditions and with human CPR, both of which could affect the relative K_d. In addition to the analysis of rates, the absorbance changes of these reactions (obtained from absorbance values from the single exponential fit) were considered. It was expected that the two-electron reduced WT CPR in disemiquinoid state could reduce a stoichiometric equivalent of cytochrome c, meaning only a single electron, from the FMNsq would be transferred to a single bound cytochrome c. To determine if this was the case, absorbance changes at 550 nm were analyzed to establish the amount to cytochrome c actually reduced in the reaction. We observed that for WT CPR the amount of reduced cytochrome c that was formed was 57%, 80%, 78%, 73%, and 68% of the calculated amount expected for one

cytochrome reduced per CPR molecule at 10, 20, 40, 80, and 160 µM cytochrome c respectively, (see figure 33d).

33c-

Single Turnover Stopped Flow Experiment with WT CPR

Single Exp. Fit Data- Michaelis Menten Fit $K_i = (K_{max}*[S])/(K_d+[S])$

K_{max} = 15.1 +/- 2.56 s^{-1} K_d= 63.1 +/- 19.2 uM

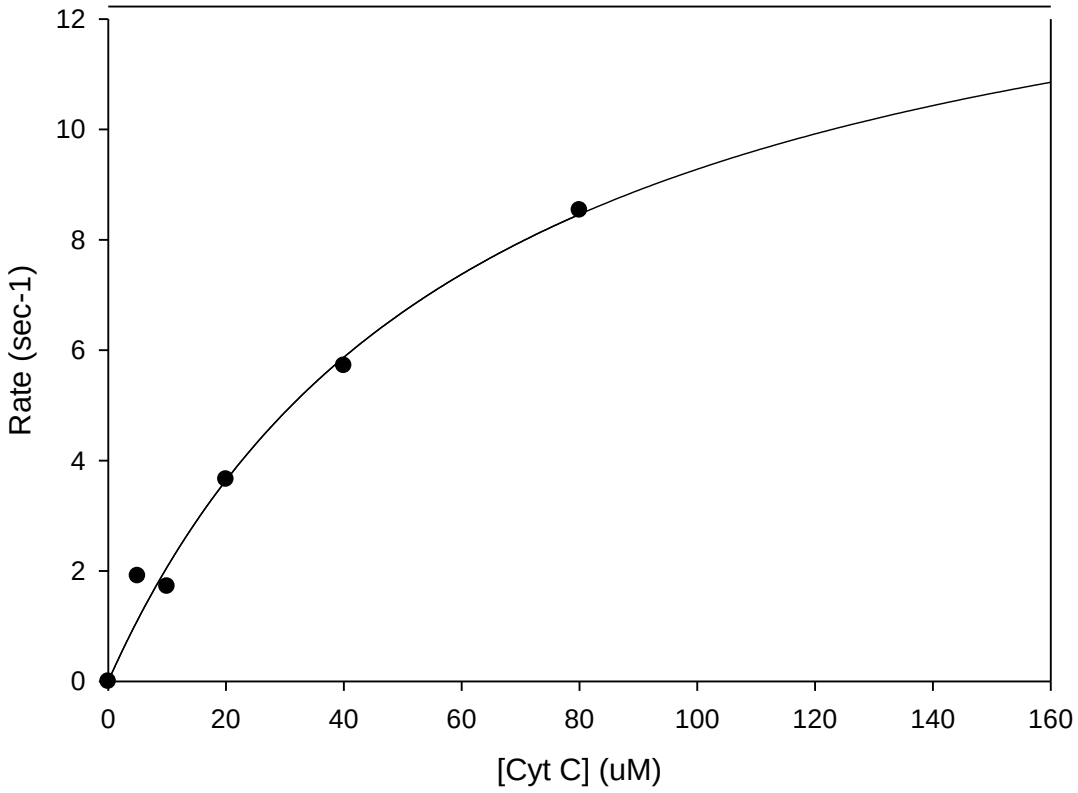

33d-

Oxidative Half-Reaction of WT CPR

	Amount of Cyt C Reduced (uM)	Percent Reduction Relative to Stoich. Cyt C Reduction
10 uM Cyt C +10 uM NADPH	2.83	57%
20 uM Cyt C +10 uM NADPH	4.73	80%
40 uM Cyt C +10 uM NADPH	4.65	78%
80 uM Cyt C +10 uM NADPH	4.34	73%
160 uM Cyt C +10 uM NADPH	4.04	68%
		[WT CPR]- 11.88uM

Figure 33- (c) A Michaelis-Menten hyperbolic fit of the OHR data. (d) Relative amounts of cytochrome c reduced.

While this type of analysis provides a reasonable estimate of the process, it must be noted that at the low concentrations of cytochrome c, the experimental conditions do not conform to pseudo-first order conditions given the proposed reaction shown in Figure 34. In fact, the fits of the stopped-flow data at the low concentrations were not fit exactly by a single exponential. However, as expected, as concentrations got higher and in greater excess to the reductase the fits substantially improved. At low concentrations of cytochrome c, the cytochrome c and WT CPR concentrations had an effect on the rate of binding and therefore the rate of reduction, making the OHR a second order rate function depending on cytochrome c and WT CPR (r_{obs} = k[CytC][CPR]). However, at high enough concentrations of cytochrome c [40,

80, and 160 μM] this value functionally becomes a constant due to the relatively minute concentration change in the OHR. Therefore, the function becomes pseudo-first order where the rate depends only on the concentration of WT CPR (r_{obs} = k'[CPR]). Use of multiple exponential fits can obviously improve the fit to the data, but such an approach in not validated by the proposed mechanism or the nature of the system under study so this approach, although tried, was justifiably abandoned. Instead, KinTek kinetics modeling was again used to elucidate the full mechanism of electron transfer in the OHR and these efforts will be discussed later in this thesis.

Oxidative Half-Reaction of G141A CPR: The OHR of G141A CPR was evaluated using the same experimental approach and analyses as for the WT CPR. The triplicate stopped-flow reaction traces at 10, 20, 40, 80, and 160 μM NADPH monitored at 550 nm were averaged and these combined traces were transferred to SigmaPlot for curve fitting and analysis (see Figure 35a-b). Like that for WT CPR, the kinetic traces for the OHR of G141A CPR were observed to be monophasic at each cytochrome c concentration. Each could be fit well to a single exponential, 3 parameter equation and the observed rates and relative absorbance changes summarized in the table in Figure 35b. The observed apparent rates obtained from the iterative fitting were generally slower than those of WT CPR at each relative concentrations of cytochrome c. The values obtained were 1.56, 1.29, 2.52, 3.39, and 5.94 s^{-1} for 10, 20, 40, 80, and 160 μM respectively. Thus, increased reduction rates were again observed with increasing cytochrome c concentrations and could be fit to a hyperbolic Michaelis-Menten function. The derived K_{max} value (10.7 s^{-1}) was lower than that obtained for WT CPR (15.1 s^{-1}). K_d for G141A was 69.5 μM which was similar to that of 63.1 μM for WT CPR (see Figure 35c). This data suggest that not the

electron transfer rate for the G141A variant was somewhat slower than for WT CPR. This demonstration of more activity in WT is also apparent when observing the amount of cytochrome c reduced in G141A CPR (see figure 35d). G141A has a maximum reduction of 4.44 µM of cytochrome c representing only a 54% reduction of the expected stoichiometric cytochrome c, whereas WT CPR had 80% reduction.

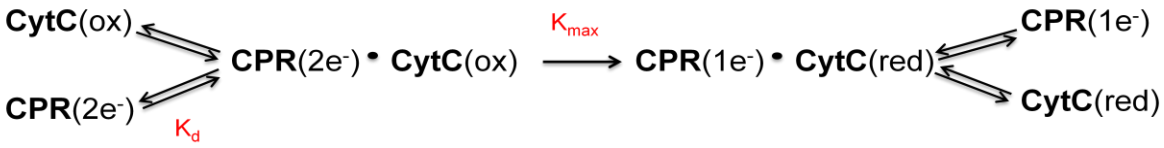

Figure 34- This equation represents the expected reaction for the OHR in which reduced CPR transfers a single electron to an oxidized cytochrome c. The observed rate should be a single exponential because the only observable absorbance change occurs as cytochrome c goes from oxidized to reduced form in the step with the K_{max} label.

35a

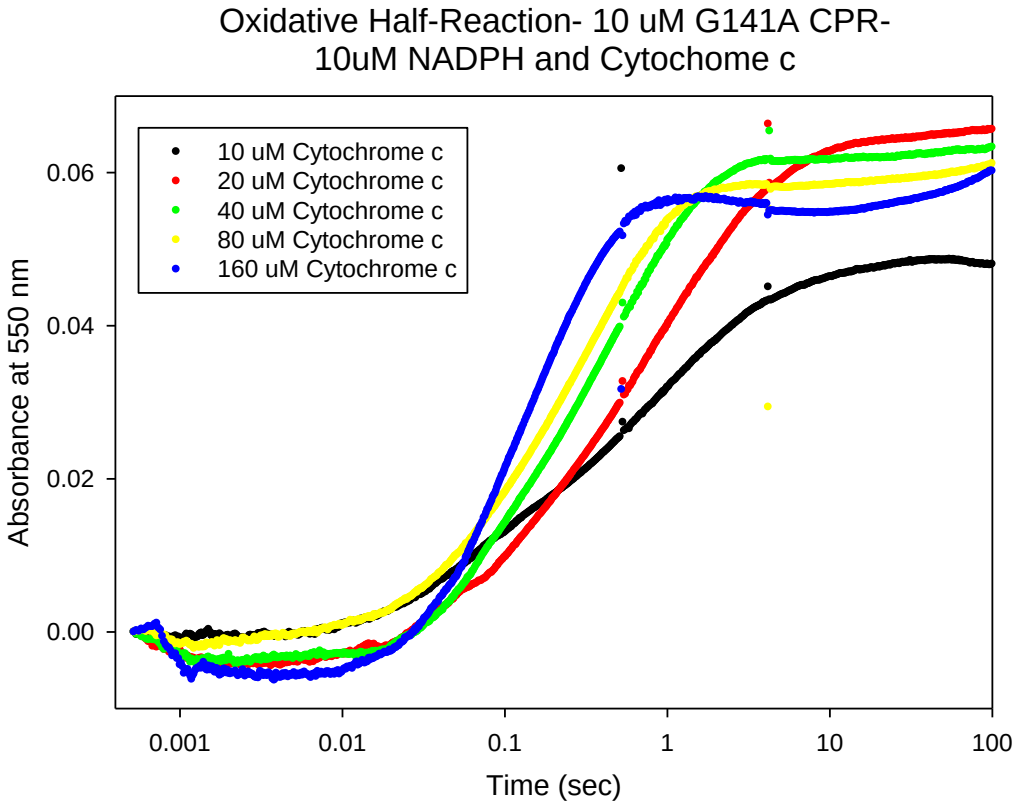

35b-

OHR of G141A CPR with Stoich. NADPH + Cyt C- 1 Exp Fit

10 uM Cyt C +10 uM NADPH	A1	K1	y_o
	-0.0446	**1.559**	0.2233
20 uM Cyt C +10 uM NADPH	A1	K1	y_o
	-0.067	**1.2913**	0.3143
40 uM Cyt C +10 uM NADPH	A1	K1	y_o
	-0.0693	**2.5172**	0.3849
80 uM Cyt C +10 uM NADPH	A1	K1	y_o
	-0.0622	**3.3892**	0.4194
160 uM Cyt C +10 uM NADPH	A1	K1	y_o
	-0.0703	**5.9404**	0.7389

35c-

Single Turnover Stopped Flow Experiment with G141A CPR

Single Exp. Fit Data- Michaelis Menten Fit $K_i = (K_{max}*[S])/(K_d+[S])$

K_{max} = 10.7 +/- 3.30 s^{-1} K_d= 69.5 +/- 37.4 uM

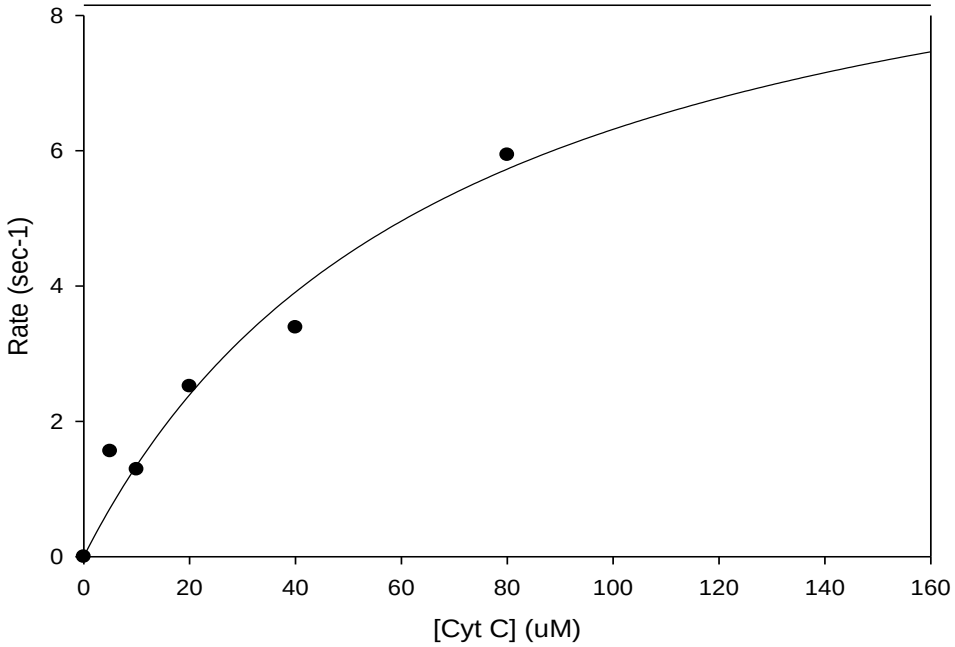

35d-

Oxidative Half-Reaction of G141A CPR

	Amount of Cyt C Reduced (uM)	Percent Reduction Relative to Stoich. Cyt C Reduction
10 uM Cyt C +10 uM NADPH	3.04	61%
20 uM Cyt C +10 uM NADPH	4.43	53%
40 uM Cyt C +10 uM NADPH	4.44	54%
80 uM Cyt C +10 uM NADPH	3.92	47%
160 uM Cyt C +10 uM NADPH	4.34	52%
		G141A CPR conc.- 16.58uM

Figure 35- (a) The OHR reaction traces at 550 nm for the various cytochrome c concentrations. (b) The values from a single exponential, three parameter fit. (c) A Michaelis-Menten hyperbolic fit of the OHR data. (d) Relative amounts of cytochrome c reduced.

Oxidative Half-Reaction of G141T CPR- The OHR for G141T CPR was evaluated similarly to G141A and WT CPR. Reaction traces along with the fitting to a single exponential, three parameter equation and analysis are shown in Figure 36a-b. Inspection of the overlaid reaction traces made it clear that G141T was behaving differently than WT or G141A CPR. Most striking was the larger absorbance increases observed at 550 nm for the 80 and 160 µM cytochrome c OHRs. The shape and extent of the reductive trace at 160 µM cytochrome c was clearly different from the others. The exact cause of the second increase occurring after 10 sec is not understood. This "phase" was not observed at any other cytochrome c concentrations for this variant or the others. It could be a spectrophotometric artifact, but this could not be confirmed. Nevertheless, this part of the reaction occurs at the relatively long timeframe and is likely to be catalytically irrelevant so it was ignored for the rest of the analysis. The rates obtained from iterative fitting were slower than those observed in WT and G141A CPR, being 1.59, 0.76, 2.57, and 3.90 s^{-1} at 10, 20, 40, and 80 µM cytochrome c, respectively, compared to 1.91, 1.72, 3.66 and 5.72 s^{-1} for WT. However, there is still direct relation between cytochrome c concentration and rate of reduction, so again a hyperbolic Michaelis-Menten fit was obtained (see 36c). Both the K_{max} and K_d values appear to be lower for G141T than for WT CPR (9.15 s^{-1} and 54.2 µM, respectively). However, these values contain substantial error because the actual data only define a portion of the fitted hyperbolic curve. Thus, while the results suggest a trend between the G141A and G141T CPR in the OHR, in which the rate of reduction decreases with the effect of the Glycine-141 substitution, any such conclusions must be considered tentative at this point.

However, the most striking difference that was noted for the G141T CPR variant compared to WT and G141A was the total amount of cytochrome c that was reduced at the higher concentration of the acceptor (see Figure 36d). At the 10 and 20 µM cytochrome c concentrations, the amount of cytochrome reduced was about 73% of what was calculated for the stoichiometric reduction by one electron, as was generally observed for the WT CPR. This was expected for a single round of reduction during this type of single-turnover experiment. However, at 40 and 80 µM cytochrome c, the level of reduction increased about two-fold to 158% and 151% of the expected reduction levels associated with a single electron transfer. These data suggest that some of the G141T CPR enzyme was able to donate both the electrons obtained from the initial reduction by NADPH to the cytochrome c, which is in excess of the reductase in these cases. It can be concluded, therefore, some other mechanism different from the simple model in figure 34 is happening and the Glycine-141 alteration is likely the root cause of this alternative electron transfer.

36a-

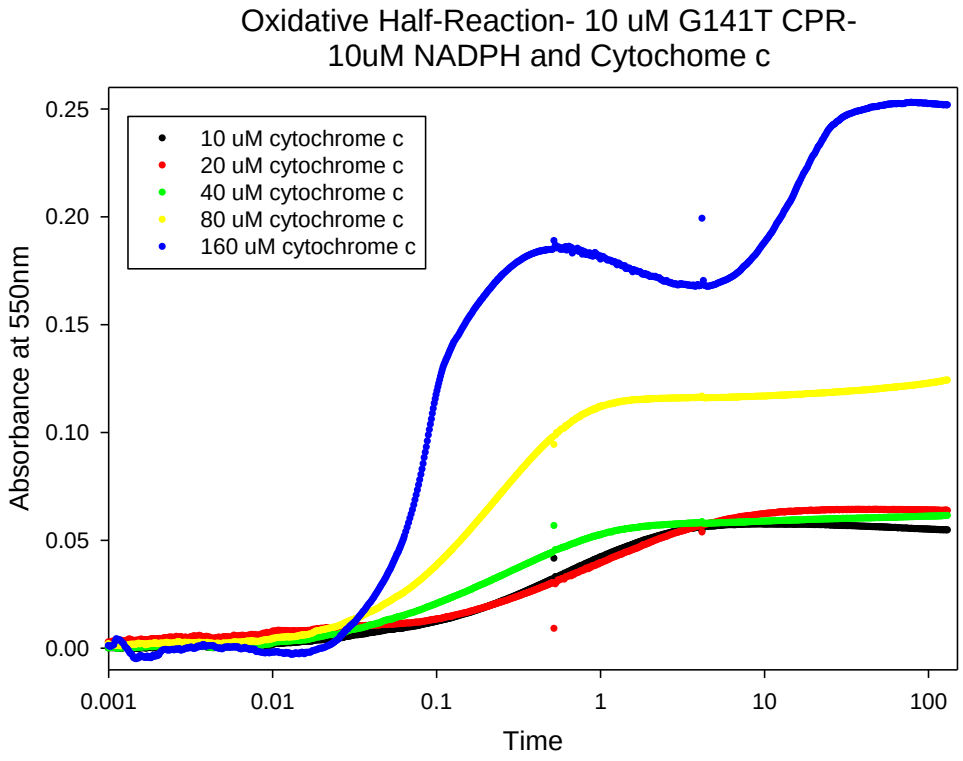

36b-

OHR of G141T CPR with Stoich. NADPH + Cyt C- 1 Exp. Fit

10 uM Cyt C +10 uM NADPH	A1	K1	y_o
550 nm:	-0.0524	**1.59**	0.113
20 uM Cyt C +10 uM NADPH	A1	K1	y_o
550 nm:	-0.0508	**0.76**	0.215
40 uM Cyt C +10 uM NADPH	A1	K1	y_o
550 nm:	-0.1181	**2.57**	0.342
80 uM Cyt C +10 uM NADPH	A1	K1	y_o
550 nm:	-0.1148	**3.90**	0.461

36c-

Single Turnover Stopped Flow Experiment with G141T CPR

Single Exp. Fit Data- Michaelis Menten Fit $K_i = (K_{max}*[S])/(K_d+[S])$

K_{max} = 9.15 +/- 7.45 s^{-1} K_d= 54.2 +/- 67.5 uM

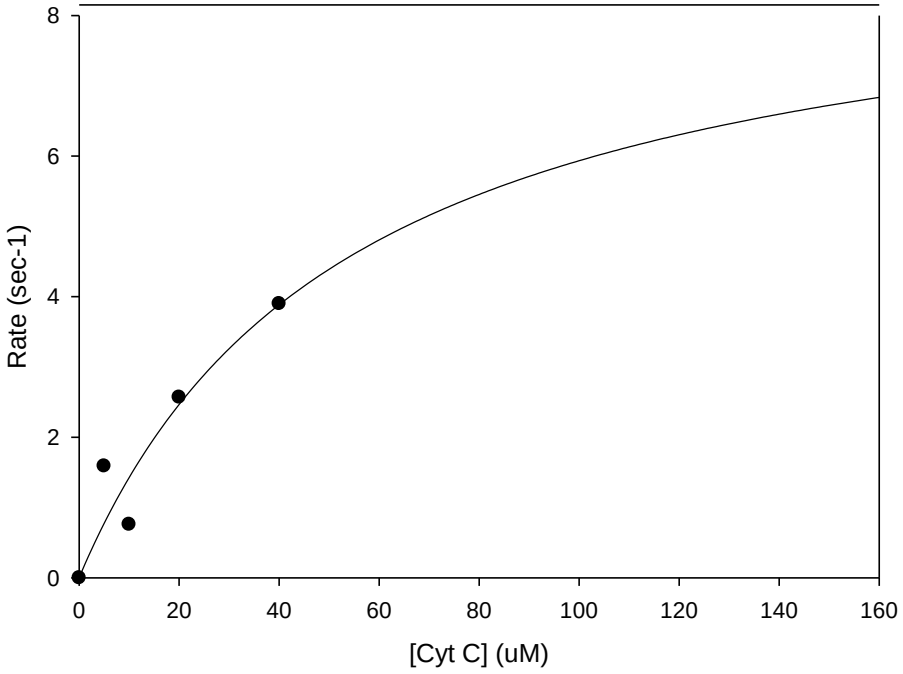

36d-

Oxidative Half-Reaction of G141T CPR

	Amount of Cyt C Reduced (uM)	Percent Reduction Relative to Stoich. Cyt C Reduction
10 uM Cyt C +10 uM NADPH	3.38	73%
20 uM Cyt C +10 uM NADPH	3.36	73%
40 uM Cyt C +10 uM NADPH	7.32	158%
80 uM Cyt C +10 uM NADPH	6.99	151%

WT CPR conc.- 9.62uM

Figure 36- (a) The OHR reaction traces at 550 nm for the various cytochrome c concentrations. (b) The values from a single exponential, three parameter fit. (c) A Michaelis-Menten hyperbolic fit of the OHR data. (d) Relative amounts of cytochrome c reduced.

Oxidative Half-Reaction of G141del CPR: The results obtained for the OHR for G141del CPR are shown in Figure 37a-b. Unlike for the other variants, both rate and extent of cytochrome c reduction changed with increasing cytochrome c concentrations, but there was no discernable correlation between these variables. However, the apparent rates of reduction,1.01, 0.90, 0.53, 0.47 and 1.12 s^{-1} for 10, 20, 40, 80, and 160 μM, respectively (Figure 37b), are substantially lower than those of WT at all concentrations. Understandably, these data could not be fit to a hyperbolic Michaelis-Menten. However, the amount of cytochrome c that was reduced by G141del CPR was of considerable interest to us. The amount of cytochrome c reduced was observed to be 39%, 105%, 298%, 301%, and 215% of that calculated for a single electron reduction process at 10, 20, 40, 80 and 160 μM respectively (see Figure 37c). These data strongly suggest that like G141T, G141del CPR is capable of transferring both electrons to two cytochrome c molecules. However, this conclusion must be tempered somewhat by some of the values being greater than the 200% expected in that case. The cause of the higher values is not known with certainty at this point. However, the results are intriguing enough to justify additional follow-up studies. If this observation can be substantiated, they suggest that electron transfer for this variant, like G141T, is proceeding through a different mechanism than WT CPR.

37a-

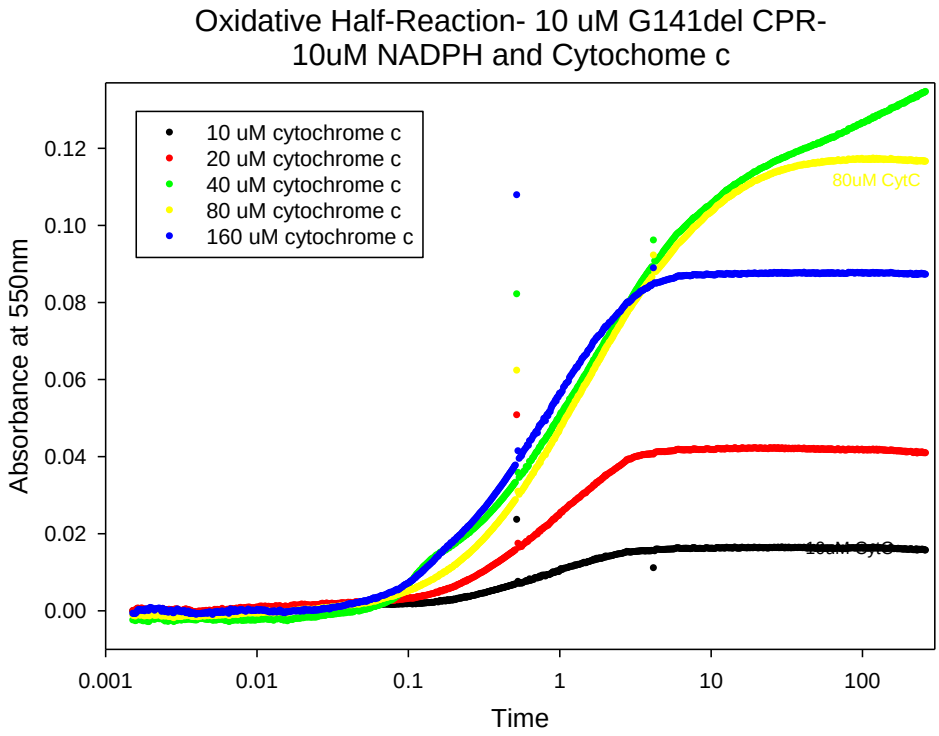

37b-

OHR of G141del with Stoich. NADPH + Cyt C- 1 Exp. Fit

10 uM Cyt C +10 uM NADPH	A1	K1	C
	-0.0209	**1.0169**	0.0708
20 uM Cyt C +10 uM NADPH	A1	K1	C
	-0.0574	**0.9033**	0.1729
40 uM Cyt C +10 uM NADPH	A1	K1	C
	-0.1471	**0.5338**	0.3717
80 uM Cyt C +10 uM NADPH	A1	K1	C
	-0.1528	**0.4698**	0.4723
160 uM Cyt C +10 uM NADPH	A1	K1	C
	-0.1121	**1.1212**	0.6392

37c-

Oxidative Half-Reaction of G141del CPR

	Amount of Cyt C Reduced (uM)	Percent Reduction Relative to Stoich. Cyt C Reduction
10 uM Cyt C +10 uM NADPH	1.29	39%
20 uM Cyt C +10 uM NADPH	3.44	105%
40 uM Cyt C +10 uM NADPH	9.75	298%
80 uM Cyt C +10 uM NADPH	9.84	301%
160 uM Cyt C +10 uM NADPH	7.02	215%
		G141del CPR conc.- 6.54uM

Figure 37- (a) The OHR reaction traces at 550 nm for the various cytochrome c concentrations. (b) The values from a single exponential, three parameter fit. (c) Relative amounts of cytochrome c reduced.

Kinetic modeling of the oxidative half-reaction in CPR: The primary fitting of the OHR data for all CPR variants made it clear that a neither a single exponential nor a double exponential equation could fit the OHR data for all the different concentrations of cytochrome c. This conclusion, in addition to the fact that Michaelis-Menten equation could not always provide a satisfactory fit to the data and the indication that more than a single electron transfer was possibly present in G141T and G141del CPR variants, led to the conclusion that the simple mechanism shown in figure 34 was not adequate to describe electron transfer from the flavin cofactors in CPR to the final cytochrome acceptor. It was decided to again utilize the KinTek® Global Kinetic Explorer software to develop models which could globally fit the absorbance data at 550 nm from the OHR at all concentrations of cytochrome c. Just as in the RHR, the established extinction coefficients for the different redox species of CPR and cytochrome c were used to generate relative absorbance data for the developed models and integration algorithms were used to globally fit the multiple reaction traces from each CPR variant. Consequently, microscopic rate constants were obtained which aided us in determining what other mechanistic steps might be occurring during the transfer of electrons between CPR and cytochrome c, if and how multiple electrons were transferred to cytochrome c for the G141T and G141del variants, and which aspects of the OHR mechanism might be affected by the glycine alterations.

Two kinetics models were developed to explain electron transfer in the OHR. Initial fitting was attempted with the simple model shown in Figure 34, but as expected the fits were unsatisfactory for all variants of CPR. From this point, two ideas were explored to create the final models that were developed. Primarily, we looked at competitive binding of a reduced cytochrome c to a reduced CPR enzyme, effectively generating an unproductive complex that

prevented reduction of other oxidized cytochrome c molecules. This step is certainly feasible in that one can easily imagine that either the oxidized or reduced forms of cytochrome c might have similar affinities for the reductase. Next, we looked at the ability of a single electron reduced CPR molecule to bind an oxidized cytochrome c molecule and eventually transfer the remaining electron, again, a step that is feasible biochemically. Two different models were eventually generated. The first model, called OHR Model Mk.I (Figure 38), was used to globally fit the WT CPR and the G141A CPR data and the second model, called OHR Model Mk.II (Figure 39), was able to globally fit G141T and G141del CPR OHR data.

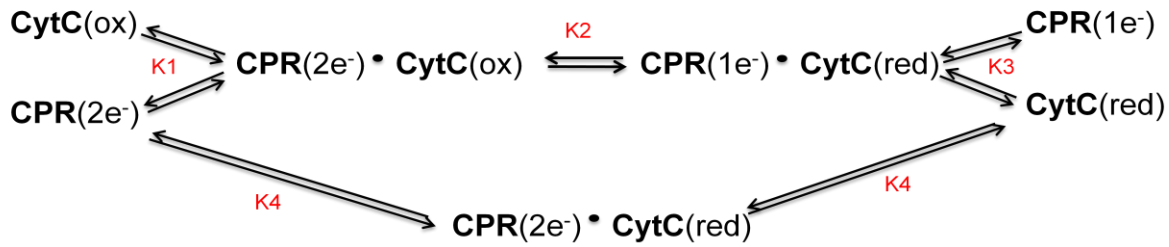

Figure 38- This is a cartoon of the OHR Model Mk.I for a two electron reduced CPR. Note that there are not two K4 values, rather K4 represents the formation of the complex with CPR(2e-) and CytC(red).

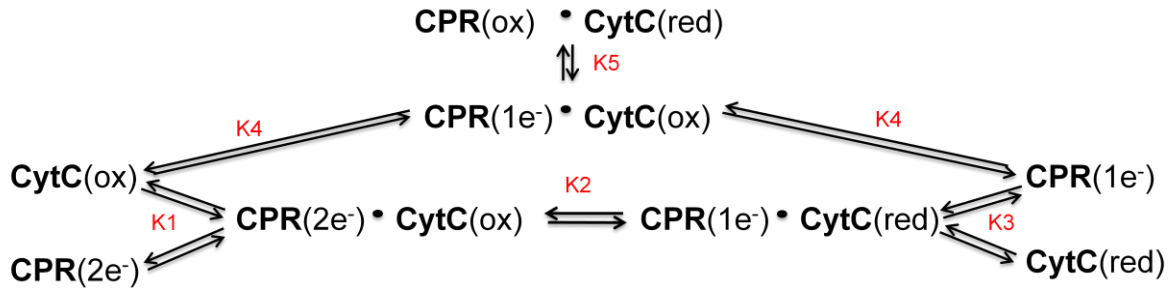

Figure 39- This is a cartoon of the OHR Model Mk.II for a two electron reduced CPR. Note that K4 represents the formation of the complex with CPR(2e-) and CytC(ox). This model includes two different electron transfer steps seen in rate constants K2 and K5.

Global fitting of WT and G141A to OHR Model Mk.I : The absorbance traces for WT and G141A CPR were very similar in both the observes rates and the fact that, even in excess cytochrome c, there was evidence for only a single electron transfer between FMN and the final electron acceptor. The similarity between these two variants was confirmed with the kinetic modeling. All OHR trials for each of these proteins could be globally fit to the OHR Model Mk.I. The only difference between this model and the simple mechanism shown in Figure 34 is the ability of reduced CPR to interact with reduced cytochrome c, however this single added step was sufficient to achieve accurate fitting (Figure 38).

The OHRs of WT CPR were the first to be globally fit (see Figures 40a-b). The results were not comparable to any of the other CPR variants, because none had been modeled at this point, however, the K_d for the reduced CPR: oxidized cytochrome complex and the forward rate constant k2+ could be evaluated against the K_d and $K_{max,}$ respectively, determined from the Michaelis-Menten fit of the WT CPR OHRs. The value of the K_d calculated from the model microscopic rate constants k1+ and k1- was 40.2 µM, which compares reasonably well to the K_d value of 63.1 µM obtained from the hyperbolic curve fitting previously described. Similarly the rate constant k2+ of 12 s^{-1} is very close to Michaelis-Menten K_{max} value of 15.1 s^{-1}. The other equilibrium of particular interest is K4 which generated a K_{eq} value of 1.01 suggesting that the binding of reduced WT CPR and reduced cytochrome c is not very prevalent.

40a-

Wt CPR and Stoich NADPH and various Cytochrome C - Global fit with OHR Model (Mk.I)

Kintek Global Fit Data					
Rate	K1	K2	K3	K4	
K+	4.5	12	15	6	
K-	181	1.3	0.825	6.03	
Kd (uM)	40.2		18.18	1.01	
Keq (uM)		9.2			
Molar Extinction Coefficients (µM-1cm-1)	CytCox	CPR (2e-)	CPR (2e-) +CytCox	CPR (1e-) + CytCred	CPR (1e-)
Initially Calculated Values:	0.0089	0.0087	0.0176	0.0344	0.0044
Experimentally Obtained:	0.0089	0.0087	0.0176	0.0344	0.0044

40b-

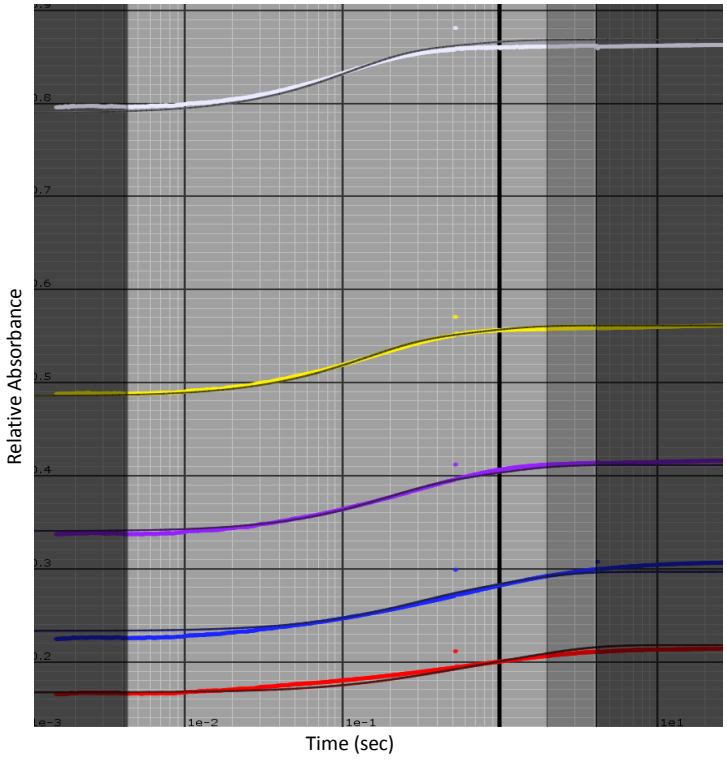

Figure 40- (a) These are the rate constant obtained from the global fitting of the WT CPR OHR absorbance traces at 550 nm. (b) This figure represents the global fit of the 10 (red), 20 (blue), 40 (purple), 80 (yellow) and 160 nm (white) data. The black lines are the data fits and the shaded regions on the edges represent data excluded from the global fit.

The OHR data for G141A CPR at 550 nm were also globally fit to the OHR Model Mk.I (see Figure 41a and 41b). Again to check the accuracy of the model the K_d for the K1 binding step and the rate constant k2+ were evaluated against the K_d and K_{max} values from the Michaelis-Menten fit for this variant. The value of the K_d from the model for the K1 step was calculated to be 39.9 µM, which again compares reasonably well to the Michaelis-Menten K_d value of 69.5 µM. The value for k2+ of 9.03 s^{-1} is also similar to K_{max} value of 10.7 s^{-1} derived from the hyperbolic curve fitting. Thus both analyses suggest that G141A CPR reduces cytochrome c somewhat less efficiently compared to WT. A reasonable biochemical explanation for this could be that the bulkier methyl sidechain of alanine substitution hinders the proper conformational changes needed for formation or positioning FMNsq (and this assertion is based on the redox titrations we performed showing lower FMNsq formation in this variant).

41a-

G141A CPR and Stoich NADPH and various Cytochrome C- Global fit with OHR (Mk.I)

Kintek Global Fit Data

Rate	K1	K2	K3	K4	
K+	3.06	9.03	23.1	119	
K-	122	0.182	7.14	31.7	
Kd (uM)	39.9		3.24	0.27	
Keq (uM)		49.6			
Molar Extinction Coefficients (µM-1cm-1)	CytCox	CPR (2e-)	CPR (2e-) +CytCox	CPR (1e-) + CytCred	CPR (1e-)
Initially Calculated Values:	0.0089	0.0087	0.0176	0.0344	0.0044
Experimentally Obtained:	0.0089	0.0087	0.0176	0.0344	0.0044

41b-

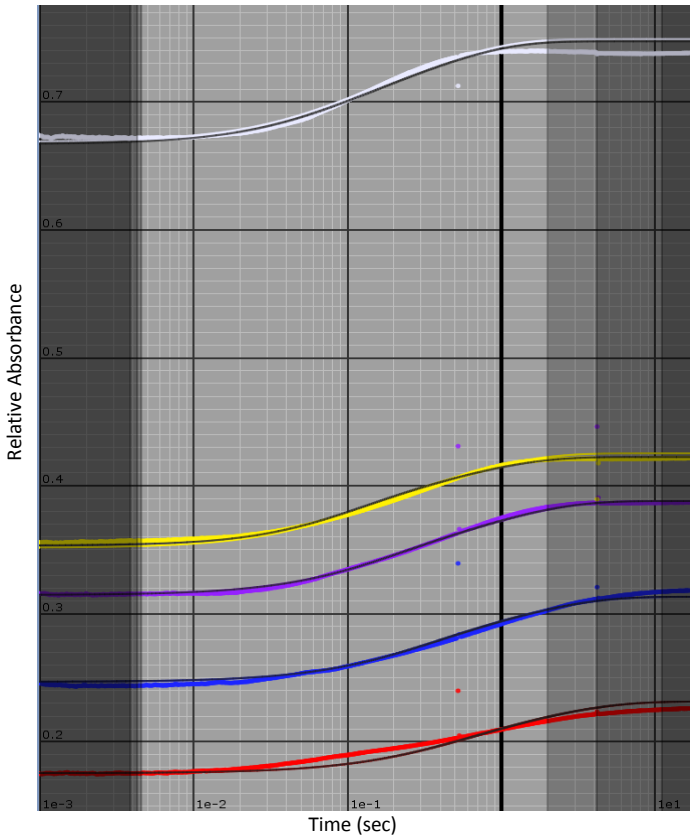

Figure 41- (a) These are the rate constant obtained from the global fitting of the G141A OHR absorbance traces at 550 nm. (b) This figure represents the global fit of the 10 (red), 20 (blue), 40 (purple), 80 (yellow) and 160 nm (white) data. The black lines are the data fits and the shaded regions on the edges represent data excluded from the global fit.

Global fitting of G141T and G141del CPR variants to OHR Model Mk.II - The larger amount of cytochrome c reduced by G141T and G141del CPR suggested that a second round of electron transfer to a second cytochrome c maybe occurring in these reductases. Accordingly, the observed rates of reduction for the different concentrations of cytochrome could not be fit well for G141T or G141del by the Michaelis-Menten equation. With these two observations, it is understandable that the mechanism of electron transfer in these two variants was more complicated than the basic equation in Figure 34. In fact, these data could not be adequately fit to the OHR Model Mk.I particularly at the low cytochrome c concentrations. Therefore, the OHR model Mk.II was then constructed to account for the two rounds of electron transfer that seems to be observed in these two variants.

The OHR data for G141T CPR were the first to be globally fit to the Mk.II model (see Figure 41a and 41b). Since a Michaelis-Menten hyperbolic fit was performed on the data, the K_d for K1 binding step and rate constant k2+ were evaluated against the K_d and K_{max}. The K_d for the K1 equilibrium was 109 µM which was about two fold higher than the K_d of 54.2 µM. So the correlation was less convincing than those of WT and G141A CPR, however, this does hint at relatively inefficient binding of oxidized cytochrome c. The k2+ value of 26.3 s^{-1} also was at least two-fold higher than the K_{max} of 9.15 s^{-1}. The K4 and K5 values for this Model do suggest that that the binding of an oxidized cytochrome c to a single electron reduced G141T CPR and the subsequent transfer of the electron from the FMNsq is possible. But the analysis of these rate constants and using KinTek software to simulate the formation of each species in the OHR indicated that the second electron transfer happens infrequently compared to the first electron transfer from a two electron reduced CPR molecule. The fitting for this mechanism does contain

a certain amount of error as can be seen by the difference in the experimentally obtained extinction coefficients at 550 nm for the fully reduced CPR species. In order to obtain satisfactory global fits, a certain amount of variation had to be allowed for these values and it is suspected that much of this error comes from the 10 and 20 µM cytochrome c OHRs where turnover activity by the enzyme is less likely.

42a.

G141T CPR and Stoich NADPH and various Cytochrome C- Global fit with OHR (Mk.II)

Kintek Individual Fit Data

Rate	K1	K2	K3	K4	K5
K+	0.453	26.3	38.3	1.1	4.82
K-	49.4	5.9	2.62	0.0497	36.1
Kd (uM)	109.1		14.62	0.05	
Keq (uM)		4.5			0.1

Molar Extinction Coefficients (µM-1cm-1)	CytCox	CPR 2e-	CPR 2e- +CytCox	CPR 1e- + CytCred	CPR 1e-	CytC Red	CPR 1e- + Cyt C Ox	CPR ox + CytC red
Initially Calculated Values:	0.0089	0.0087	0.0176	0.0344	0.0044	0.0299	0.0133	0.0299
Experimentally Obtained Values:	0.0089	10uM - 0.0066 20uM - 0.0141 40uM - 0.0033 80uM - 0.0062	0.0176	0.0344	0.0044	0.0299	0.0133	0.0299

42b.

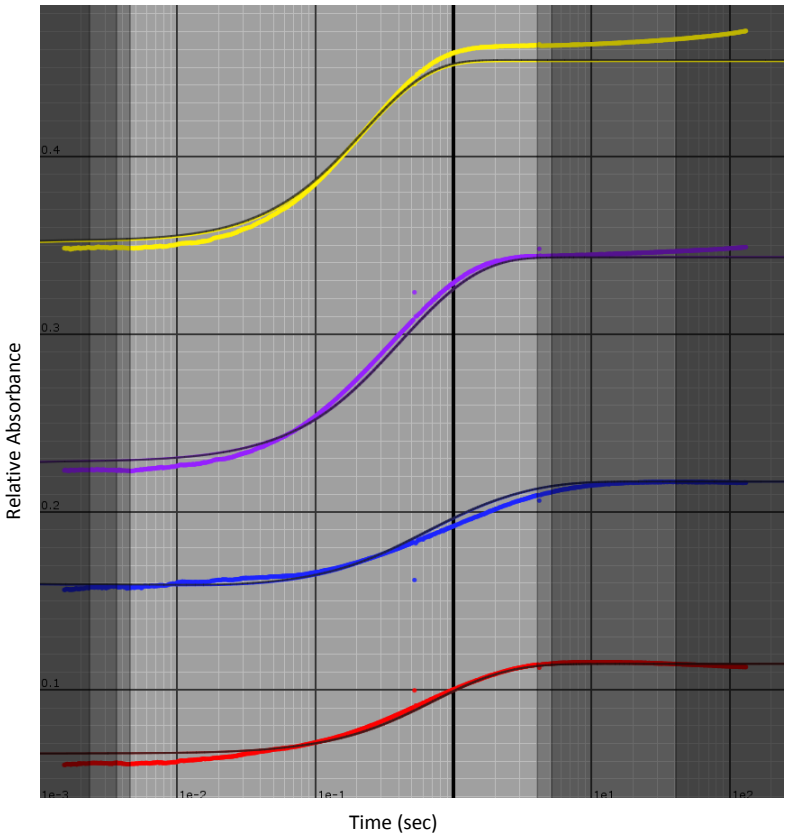

Figure 42- (a) These are the rate constant obtained from the global fitting of the G141T OHR absorbance traces at 550 nm. (b) This figure represents the global fit of the 10 (red), 20 (blue), 40 (purple), and 80 (yellow) data. The black lines are the data fits and the shaded regions on the edges represent data excluded from the global fit.

The OHR Model Mk.II was used to fit the OHR for G141del CPR (see Figure 42a and 42b). For this variant, the OHRs with 40, 80, and 160 μM cytochrome c all showed more than twice stoichiometric level of cytochrome c reduction as was discussed previously. The Model Mk.II takes into account the ability of G141del to transfer the second electron and consequently this model could more accurately fit the OHR time courses at all concentrations of cytochrome c. Because the Michaelis-Menten hyperbolic equation could fit the G141del OHR data, K_d and K_{max} values specific to the deletion variant could not be established for comparisons. An assessment to the other variants shows that the K_d of the K2 step for G141del (85.5 μM) is comparable to WT and G141A (40.2 and 39.9 μM, respectively) and most similar to G141T CPR (109 μM). The k2+ value is the slowest for any variant at 8.22 s^{-1} and this correlates well to the observed rates of reduction from single exponential fitting which were also the slowest for G141del. The most striking conclusion from the global fitting to the Mk.II mechanism comes from inspection of the K4 and K5 values and the comparison of these values for the G141T variant. The k4+ value for G141del is greater than three-fold higher than that of G141T, illustrating greater occurrence of binding between the single electron reduced enzyme and a cytochrome c. The K5-associated values represent the major difference between the G141T and G141del and explain the ability of this variant to reduce two equivalents of cytochrome c. The k5+ has a value of 396 s^{-1} which is 80-fold higher than G141T and K_{eq} value of 60.7 μM shows that not only is the second electron transferred very rapid after binding, but it is favored in the equilibrium. These conclusions suggest a possible connection between the RHR and the OHR. It was seen in the RHR that G141del, unlike the other CPR variants, favors the rapid transfer of both electrons to the FMN cofactor. Since the FMN cofactor is the donor of electrons to cytochrome c, the full

reduction of the FMN could support the transfer to two cytochrome c molecules without any additional inter-flavin electron transfers. However, in WT CPR the FMNsq is the electron donor and the transfer of a second electron is not favorable. This fact in mind, the glycine alteration destabilizes the FMNsq (as demonstrated by redox titrations) and in the case of G141del causes only transient formation of the FMNsq (seen in the RHRs), presumably allowing not only the full reduction of the FMN, but also efficient transfer of these two electrons to the cytochrome c. Fitting to the OHR model Mk.II shows this same phenomenon is seen in G141T CPR which also has a destabilized FMNsq. However, the smaller overall effect of bulkier sidechain of threonine (compared to the affect of the deletion of the glycine) represents a smaller propensity to transfer this second electron.

43a-

G141T CPR and Stoich NADPH and various Cytochrome C- Global fit with OHR (Mk.II)

Kintek Individual Fit Data

Rate	K1	K2	K3	K4	K5
K+	3.52	8.22	1.6	3.92	396
K-	301	2.06	7	0.512	6.52
Kd (uM)	85.5		0.23	0.13	
Keq (uM)		4.0			60.7

Molar Extinction Coefficients (µM-1cm-1)	CytCox	CPR 2e-	CPR 2e- +CytCox	CPR 1e- + CytCred	CPR 1e-	CytC Red	CPR 1e- + Cyt C Ox	CPR ox + CytC red
Initially Calculated Values:	0.0089	0.0087	0.0176	0.0344	0.0044	0.0299	0.0133	0.0299
Experimentally Obtained Values:	0.0089	10uM- 0.025 20uM- 0.0176 40uM - 0.0103 80uM - 0.0109 160uM- 0.026	0.0176	0.0344	0.0044	0.0299	0.0133	0.0299

43b-

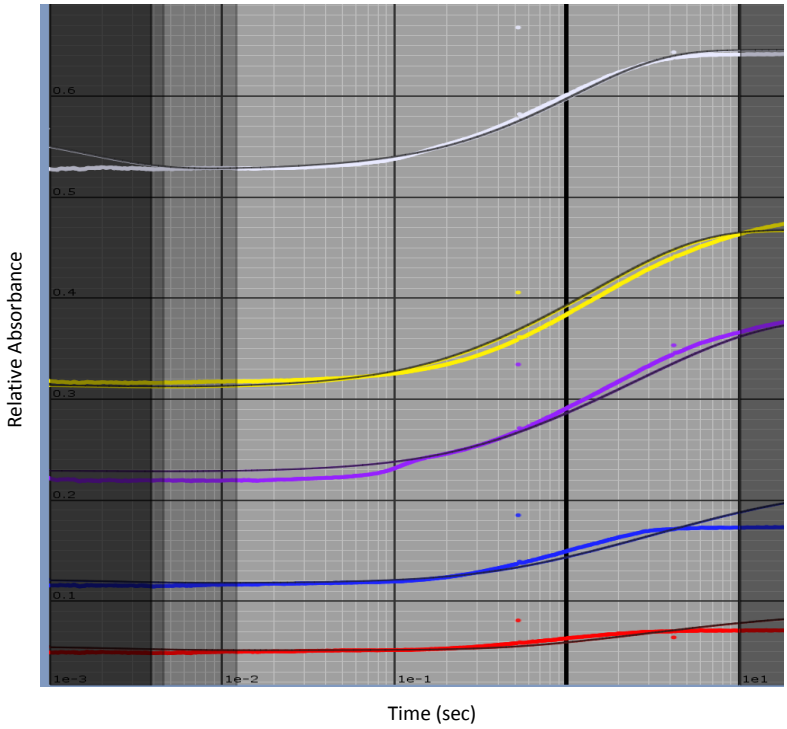

Figure 43- (a) These are the rate constant obtained from the global fitting of the G141del OHR absorbance traces at 550 nm. (b) This figure represents the global fit of the 10 (red), 20 (blue), 40 (purple), 80 (yellow) and 160 nm (white) data. The black lines are the data fits and the shaded regions on the edges represent data excluded from the global fit.

Summary and Conclusions

The majority of the specific analyses of the results of experiments performed in this thesis were discussed in the corresponding results sections. This section will serve as a summary of performed experiments, discussion of the most pertinent results, and examination of our conclusions in a broader context.

- Steady-state turnover assays of CPR with NADPH and cytochrome c showed significant differences between the cytochrome reductase activities of the CPR variants. WT CPR had an activity of 3900 s^{-1} and compared to this benchmark G141A CPR had 118% activity, G141T had 72% activity, and G141del CPR had 44% activity. The increased activity of G141A CPR was determined not to be statistically significant, however, the reduced activity of G141T and further reduced activity of G141del was attributed, at least in part, to the destabilization of the FMNsq by the glycine alterations because the FMNsq is generally thought to be the electron donor to the terminal cytochrome acceptor.
- The FAD-dependent ferricyanide reductase activity was observed to be altered in the glycine variants. Compared to WT all variants displayed decreased activity (86% for G141A, 61% for G141T, and 62% for G141del CPR. These results were perplexing because it is widely held in this field that ferricyanide reductase activity resides exclusively with the FAD-binding domain, which should remain unaltered in all CPR variants because the glycine alterations were introduced in the separate FMN-binding domain. These results, and other unpublished results from this laboratory, do suggest

that the FMN-binding domain might be exerting some influence on the transfer of electrons from NADPH to ferricyanide through the FAD cofactor, however. The molecular basis of this effect is not understood currently, but could benefit from further study using this group of CPR variants and others generated in this laboratory.

- Anaerobic redox titrations clearly demonstrated that the highly conserved glycine in the FMN-binding loop as identified by homology to other similar proteins affects the thermodynamic stability of the "blue" neutral FMNsq species. Accordingly, FMNsq stability appeared to directly correlate to the extent of alteration of the Glycine-141 residue. Relative to WT CPR, G141A had 80%, G141T had 72%, and the G141del FBD had basically undetectable (<10%) accumulation of neutral FMNsq. These results are consistent with previous studies in this laboratory on the bacterial flavodoxin. Those studies provide compelling evidence that the introduction of the sidechain, one even as modest as the methyl group of alanine, can influence the interaction made between the backbone carbonyl of the residue at this position (glycine in WT) and the N(5)H of the FMNsq. The FMN domain in CPR is similar in structure to the flavodoxin and, based on the results reported here, also likely stabilizes the neutral FMNsq in a similar manner. Because of the central role of the FMNsq species in electron transfer to cytochromes by this reductase, the focus of my research then became elucidating the specific mechanistic consequences of these differences in stability.
- The primary in depth study performed was the reductive half-reaction which observed transfer of electron for NADPH to the FAD and then between FAD and FMN. The absorbance data from these experiments showed a triphasic reduction for all variants of

CPR at stoichiometric and excess levels of NADPH. The third and slowest phase, involved only small absorbance changes and was deemed to be too slow to be catalytically pertinent, was discounted from further discussion. However, the two initial faster phases involved substantial absorbance changes and occurred in a timeframe to be of relevance. As was anticipated from the anaerobic titrations although using artificial electron donor/acceptors (dithionite and/or ferricyanide), the disemiquinoid species was seen to accumulate in these single-turnover experimental conditions with stoichiometric amounts of the added physiological electron donor NADPH for the WT, G141A, and G141T variants. In marked contrast, the G141del RHR at demonstrated only transient formation of the neutral disemiquinoid species presumable with both electrons derived from the NADPH ultimately residing in the FMN cofactor. These results are consistent with the absence of the accumulation of the neutral FMNsq during anaerobic titrations of the isolated FMN domain from this variant. The mechanistic implications of this observation were of significance during the evaluation of the OHR.

- To better understand the reaction traces and mechanism of the RHR and the disparity between G141del and the other variants, kinetics models were made to globally fit the absorbance traces and to eventually elucidate the electron transfer process. In particular, these modeling studies were found to be essential in explaining the enigmatic biphasic formation of the disemiquinoid species which could not be explained by a simple reduction mechanism. The first and major phase was clearly ascribed to the hydride transfer from NADPH to the FAD and the subsequent very rapid formation of

the disemiquinoid state. The second (and possibly third) phase could not be assigned to any one specific electron transfer step, but rather was described a combination of several microscopic rate constants relating a variety or electron transfers.

- Two different mechanisms of electron transfer mechanism for the RHR were established by comparison of the variants to WT CPR. The first mechanism showed that in WT, G141A, and G141T there was preferential formation of the disemiquinoid state, with or without the $NADP^+$ bound to the enzyme. In stark contrast, electron transfer in the G141del variant results in the ephemeral formation of the disemiquinoid before the $NADP^+$ is released and a second electron moves from FADsq to FMNsq, fully reducing the FMN cofactor. The difference in electron transfer here has to do with the very stable formation of the FMNsq, which in WT CPR appears to serve as a "road block", so to speak, for the transfer of a second electron to FMN. The G141del served as the contrasting model where loose binding to the inflexible peptide loop causes unstable FMNsq formation, allowing the FAD to immediately and rapidly transfer a second electron. G141A and G141T CPR, with their relative instability of FMNsq have mechanism somewhere in between those of WT and G141del CPR in which the majority of the time only a single electron transferred from FAD, but occasionally there is the opportunity to fully reduce FMN.
- The study of the oxidative half-reaction provided information on the second half of the steady-state turnover process associated with the cytochrome reductase activity of CPR. The expected result of this experiment for CPR was a single electron transfer from the FMNsq to a bound, oxidized cytochrome c, effectively reducing stoichiometric amounts

of cytochrome c as was observed for WT and G141A. However, G141T and G141del demonstrated the ability to reduce more than one equivalent of cytochrome through an additional round of the electron transfer utilizing the second and last electron derived from NADPH. Two separate mechanistic models were developed: (1) the Mk.I model which could globally fit the WT and G141A CPR data and revealed the possibility of competitive binding between reduced and oxidized cytochrome c on the FMN-binding domain of CPR and (2) the Mk.II model which was used in globally fitting the G141T and G141del OHR. The fitting to the Mk.II model accounted for the possibility of these enzymes (in their one electron reduced form) to bind and reduce a second cytochrome c. Although satisfactory fits were achieved using these mechanisms it does seem reasonable that in actuality the most correct mechanism would be better approximated with a combination the Mk.I and Mk.II models, where a huge number of chemical interactions are happening all at the same time. There was insufficient time to pursue this possibility.

- Completing analysis for the reductive and oxidative half-reactions has led us to think about likely connections between these two electron transfer processes. We began to hypothesize about how the unique RHR of G141del CPR could account for the ability of this enzyme to uncharacteristically transfer both of its electrons to cytochromes (this analysis would also apply, to a lesser degree to G141T CPR). Although the exact molecular mechanism of electron transfer is yet to be established for WT CPR, the available structural data provides a paradox. X-ray crystal structures of the reductase shows that the FMN-binding domain is closely associated with the FAD-binding domain

in a manner that places both flavin cofactors within van der Waals contact, a configuration ideal for efficient inter-flavin electron transfer. However, this conformation would seem to preclude access of the FMNsq to the cytochrome for electron transfer. This laboratory and others have hypothesized and are working to provide experiment support for a mechanistic model that involves the movement of the FMN-binding domain away from the FAD cofactor prior to transfer of electrons from the FMNsq to the cytochrome. Such a domain movement would be facilitated by the flexible polypeptide "hinge" region that connects the two domains. Indeed, there is experimental evidence for this movement, but this has yet to be linked with electron transfer and reductase activity in this enzyme. Given this model, the transfer of two electrons from WT CPR to two cytochrome molecules would then requires two domain movements. Furthermore, the thermodynamic stability of the two flavin semiquinone states in WT CPR may inhibit the process of the transfer of the second electron further, especially if domain movement is also involved. It is very intriguing to suggest that unlike the WT reductase the ability of G141del CPR, and perhaps to a lesser extent the G141T variant, to much more rapidly transfer the second electron from the FADsq to the FMNsq as demonstrated in this study and simulated and fit to the RHR Full Model (see k10+ values), could then allow for the formation of the FMNhq prior to domain movement. This FMNhq could then sequentially bind and transfer electrons to two cytochromes in a manner similar to the OHR Model Mk.II. We believe that this observation represents an important basis for a fundamental hypothesis regarding the details of electron transfer for this and perhaps other diflavin reductases. This

hypothesis, and many additional ones, represents questions currently being explored in this lab.

References

1. Porter, T.D., Kasper, C.B. (1986) NADPH-Cytochrome P-450 Oxidoreductase: Flavin Mononucleotide and Flavin Adenine Dinucleotide Domains Evolved from Different Flavoproteins. *Biochemistry. 25,* 1682-1687.
2. Porter, T.D. (1991) An unusual yet strongly conserved flavoprotein reductase in bacteria and mammals. *TIBS. 16,* 154-158.
3. Åström, A., DePierre, J.W. (1986) Rat-liver microsomal cytochrome P-450: purification, characterization, multiplicity and induction. *Biochimica et Biophysica Acta. 853,* 1-27.
4. Waxman, D.J., Chen, L. (1998) Methods of using cytochrome P450 reductase for the enhancement of P450-based anti-cancer gene therapy. *Patent:* Pub. No.: WO/1999/005299 International Application No.: PCT/US1998/015302
5. Guengerich, F.P. (2001) Common and Uncommon Cytochrome P450 Reactions Related to Metabolism and Chemical Toxicity. *Chemical Research in Toxicology. 14(6),* 611-650.
6. Murataliev, M.B., Feyereisen, R., Walker, F.A. (2004) Electron transfer in diflavin reductases. *Biochimica et Biophysica Acta. 1698,* 1-26.
7. Nelson, D.R., Zeldin, D.C., Hoffman, S.M.G., Maltais, L.J., Wain, H.M., Nerbert, D.W. (2004) Comparison of cytochrome P450 (CYP) genes from the mouse and human genomes, including nomenclature recommendations for genes, pseudogenes and alternative-splice variants. *Pharmacogenetics. 14,* 1-18.
8. Loeper, J., Descatoire, V., Maurice, M., Beaune, P., Belghiti, J., Houssin, D., Ballet, F., Feldmann, G., Guengerich, F.P., Pessayre, D. (1993) Cytochromes P-450 in human

hepatocyte plasma membrane: recognition by several autoantibodies. *Gastroenterology. 104(1),* 203-216.

9. Gutierrez, A., Grunau, A., Paine, M., Munro, A.W., Wolf, C.R., Roberts, G.C.K., Scrutton, N.S. (2003) Electron transfer in human cytochrome P450 reductase. *Biochemical Society Transactions. 31(3),* 497-501.
10. Wang, M., Roberts, D.L., Paschke, R., Shea, T.M., Masters, B.S.S., Kim, J.P. (1997) Three-dimensional structure of NADPH-cytochrome P450 reductase: Prototype for FMN- and FAD-containing enzymes. *Proc. Natl. Acad. Sci. USA. 94,* 8411-8416.
11. Roitel, O., Scrutton, N.S., Munro, A.W. (2003) Electron Transfer in Flavocytochrome P450 BM3: Kinetics of Flavin Reduction and Oxidation, the Role of Cysteine 999, and Relationships with Mammalian Cytochrome P450 Reductase. *Biochemistry. 42,* 10809-10821.
12. Munro, A.W., Daff, S., Coggins, J.R., Lindsay, J.G., Chapman, S.K. (1996) Probing electron transfer in flavocytochrome P-450 BM3 and its component domains. *Eur. J. Biochem. 239,* 403-409.
13. Grunau, A., Geraki, K., Grossman, J.G., Gutierrez, A. (2007) Conformational Dynamics and the Energetics of Protein-Ligand Interactions: Role of Interdomain Loop in Human Cytochrome P450 Reductase. *Biochemistry. 46,* 8244-8255.
14. Yaskukochi, Y., Peterson, J.A., Masters, B.S.S. (1979) NADPH-Cytochrome c (P-450) Reductase Spectrophotometric and Stopped Flow Kinetic Studies on the Formation of Reduced Flavoprotein Intermediates. *The Journal of Biological Chemistry. 254(15),* 7097-7104.

15. Grunau, A., Paine, M.J., Ladbury, J.E., Gutierrez, A. (2006) Global Effects of the Energetics of Coenzyme Binding: NADPH Controls the Protein Interaction Properties of Human Cytochrome P450 Reductase. *Biochemistry. 45,* 1421-1434.
16. Shen, A.L., Sem, D.S., Kasper, C.B. (1999) Mechanistic Studies on the Reductive Half-reaction of NADPH-Cytochrome P450 Oxidoreductase. *The Journal of Biological Chemistry. 274(9),* 5391-5398.
17. Massey, V., Palmer, G. (1966) On the Existence of Spectrally Distinct Classes of Flavoprotien Semiquinones. A New Method for the Quantitative Production of Flavoprotien Semiquinones. *Biochemistry. 5(10),* 3181-3189.
18. Murataliev, M.B., Feyereisen, R. (1999) Mechanism of cytochrome P450 reductase from the house fly: evidence for a FMN semiquinone as electron donor. *FEBS Letters. 453,* 201-204.
19. Gutierrez, A., Lian, L., Wolf, C.R., Scrutton, N.S., Roberts, G.C.K. (2001) Stopped-Flow Kinetic Studies of Flavin Reduction in Human Cytochrome P450 Reductase and Its Component Domains. *Biochemistry. 40,* 1964-1975.
20. Ludwig, M.L., Pattridge, K.A., Metzger, A.L., Dixon, M.M., Eren, M., Feng, Y., Swenson, R.P. (1997) Control of Oxidation-Reduction Potentials in Flavodoxin from *Clostridium beijerinckii:* The Role of Conformational Changes. *Biochemistry. 36,* 1259-1280.
21. O'Farrell, P.A., Walsh, M.A., McCarthy, A.A., Higgins, T.M., Voordouw, G., Mayhew, S.G. (1998) Modulation of the Redox Potentials of FMN in *Desulfovibrio vulgaris* Flavodoxin: Thermodynamics Properties and Crystal Structures of Glycine-61 Mutants. *Biochemistry. 37,* 8405-8416.

22. Chen, H.C., Swenson, R.P. (2008) Effect of the Insertion of a Glycine Residue into the Loop Spanning Residues 536-541 on the Semiquinone State and Redox Properties of the Flavin Mononucleotide-Binding Domain of Flavocytochrome P450BM-3 from *Bacillus megaterium. Biochemistry. 47,* 13788-13799.
23. Chang, F.C., Swenson, R.P. (1999) The Midpoint Potentials for the Oxidized-Semiquinone Couple for Gly57 Mutants of the *Clostridium beijerinckii* Flavodoxin Correlate with Changes in the Hydrogen-Bonding Interaction with the Proton on N(5) of the Reduced Flavin Mononucleotide Cofactor as Measured by NMR Chemical Shift Temperature Dependancies. *Biochemistry. 38,* 7168-7176.
24. Kasim, M., Chen, H.C., Swenson, R.P. (2009) Functional Characteristics of the *re*-Face Loop Spanning Residues 536-541 and Its Interactions with the Cofactor in the Flavin Mononucleotide-Binding Domain of Flavocytochrome P450 from *Bacillus megaterium. Biochemistry. 48,* 5131-5141.
25. Zhao, Q., Modi, S., Smith, G., Paine, M., McDonagh, P.D., Wolf, R.C., Tew, D., Lian, L.Y., Roberts, G.C.K., Driessen, H.P.C. (1999) Crystal structure of the FMN-binding domain of human cytochrome P450 reductase at 1.93 Å resolution. *Protein Science. 8,* 298-306.
26. Rock, D., Rock, D., Jones, J.P. (2001) Inexpensive Purification of the P450 Reductase and Other Proteins Using 2',5'-Adenosine Diphosphate Agarose Affinity Columns. *Protein Expression and Purification. 22,* 82-83.
27. Klein, M.L., Fulco, A.J. (1993) Critical Residues Involved in FMN Binding and Catalytic Activity in Cytochrome $P450_{BM-3}$. *The Journal of Biological Chemistry. 268(10),* 7553-7561.

28. Schellenberg, K.A., Hellerman, L. (1957) Oxidation of Reduced Diphosphopyridine Nucleotide. *Journal of Biological Chemistry. 220,* 547-556.
29. Marohnic, C.C., Panda, S.P., Martásek, P., Masters, B.S. (2006) Diminished FAD Binding in the Y459H and V492E Antley-Bixler Syndrome Mutants of Human Cytochrome P450 Reductase. *The Journal of Biological Chemistry. 281(47),* 35975-35982.
30. Munro, A.W., Noble, M.A., Robledo, L., Daff, S.N., Chapman, S.K. (2001) Determination of the Redox Properties of Human NADPH-Cytochrome P450 Reductase. *Biochemistry. 40,* 1956-1963.